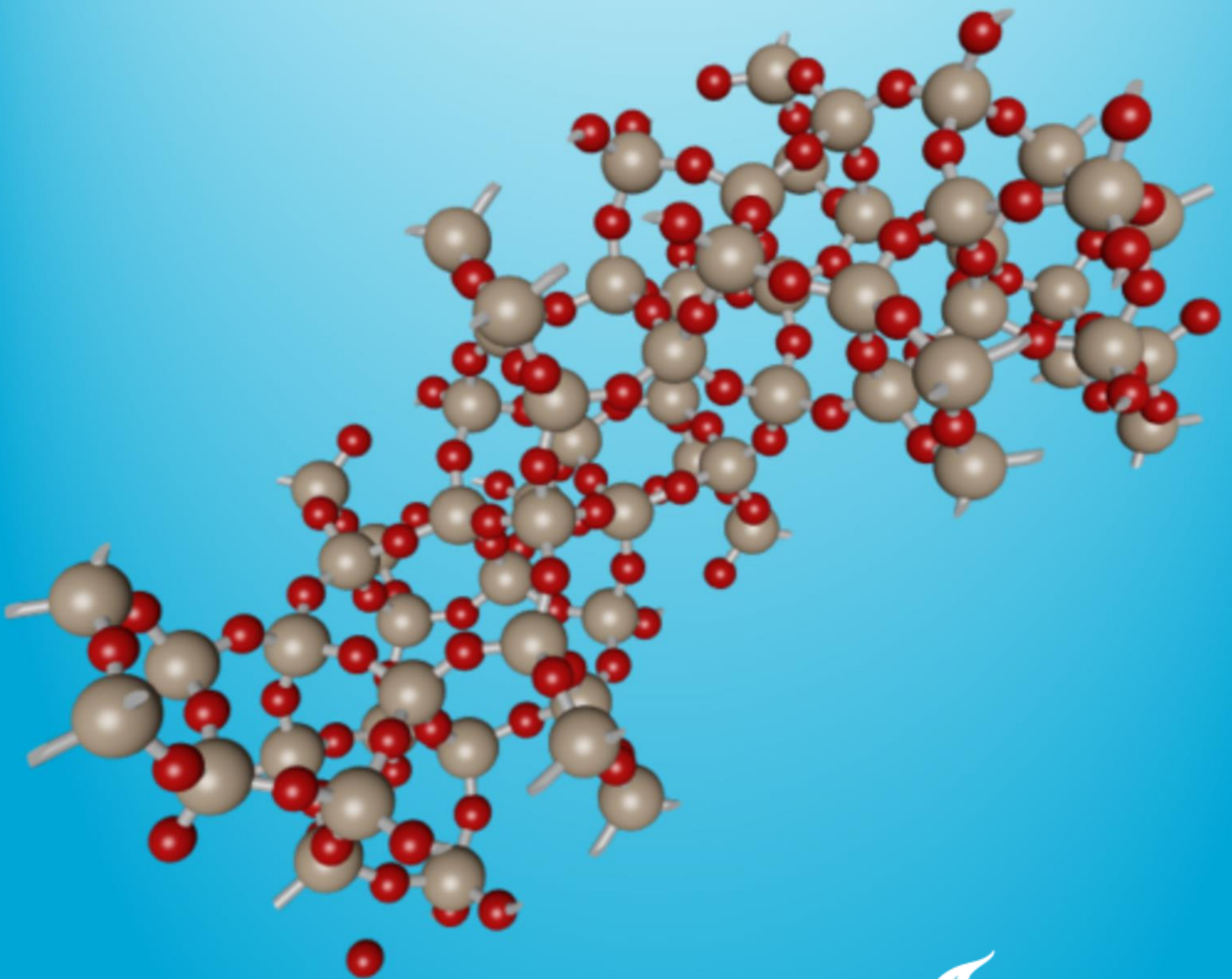# Challenging the oxygen infrastructure

Integrated Oxygen Production for Dutch Hospitals:
A Comprehensive Feasibility Study Using Pressure *Swing Adsorption*

Master Thesis
Liam Kleijwegt

TUDelft

Delft University of Technology

ME-EFPT Master Thesis
ME55035

Integrated Oxygen Production for Dutch Hospitals: A Comprehensive Feasibility Study Using Pressure Swing Adsorption

Author:
Liam Kleijwegt (4889061)

Supervisors:
Prof. dr. ir. Thijs Vlugt
Prof. dr. Maarten van der Elst

August 9, 2024

Abstract

Medical oxygen is crucial for effective treatment of patients, yet many low- and middle-income countries (LMICs) without a good healthcare infrastructure have been unable to provide sufficient oxygen therapy for years now. The COVID-19 pandemic highlighted the critical need for more oxygen, leading to supply shortages and rising prices even in developed countries. Currently, most medical oxygen is produced by a few large companies using centralized Cryogenic Air Separation Units (CAS). Pressure Swing Adsorption (PSA) offers a promising alternative, enabling local production of medical oxygen without reliance on suppliers. PSA leverages the pressure dependency of adsorption isotherms to selectively adsorb nitrogen, concentrating the oxygen.

This research has investigated the possibilities of designing a system that not only meets the specific oxygen demands of a Dutch hospital but also complies with the Dutch legal frameworks and forms an economically feasible case. A case study at Reinier de Graaf hospital (RdGG) in Delft used real oxygen consumption data. The applicable regulatory frameworks have been obtained by research in literature and with help of a representative at RdGG. For the technical design and optimisation, a numerical model of the PSA-cycle has been developed. This model is based on the Ideal Adsorption Solution Theory (IAST) and makes use of the Linear Driving Force model for adsorption kinetics. The model behaviour has been validated by experiments within a self-built, small-scale PSA-unit in the Process & Energy (P&E) lab. After this, the setup was scaled to hospital size within the model. A schematic PSA-plant has been designed based on the regulatory frameworks and system requirements which came from the numerical modelling. The economic viability has been addressed based on quotes, consumption data and electricity prices which were provided by RdGG.

Dutch regulations require hospitals to have three oxygen sources, each capable of independently providing the full design flow, with PSA units obligated to produce 93% oxygen concentration (± 3%) and meet strict impurity limits. To achieve the required oxygen purity, a vacuum pressure of 0.05 bar and an adsorption pressure of 6 bar with Oxysiv MDX zeolite are optimal. Depressurization should occur close to atmospheric pressure (1.05 bar) for efficiency. The adsorption column is most effective with a diameter-to-length ratio of 0.1 and a dimensionless time, t_c, of 9.56 seconds for maximum oxygen production. The dimensionless time represents the time it takes for the gas to pass through the length of the column based on its inlet velocity.

The PSA unit at RdGG must handle a normal demand of 10 Nm³/h and a peak demand of 80 Nm³/h for three consecutive days. The second source can handle peak demand for three days, while the backup source can manage only 9 hours (t_{vital}). If the PSA-storage has been depleted and the second source fails, t_{vital} is the maximum refill time of the PSA-storage. This requires a production rate of 0.40 mol/s and two packages of storage cylinders (1.6 m³) which store the oxygen at 200 bar. This setup necessitates two 336L columns (3.5m height, 0.35m diameter, 0.36 m/s inlet velocity) and an air inlet flow of 126 m³/hr, supported by a vacuum pump and a compressor. The cycle steps for the adsorption, depressurization and vacuum (t_{AD} = 79 s, t_{DP} = 67 s, t_{VC} = 112.1 s) total 258.7 s, allowing two columns to run in parallel. A 3 m³ air pressure vessel at 10 bar maintains PSA operation for three minutes during compressor disturbances. This setup achieves 93.61% oxygen purity with 41% recovery for 93% oxygen concentration, increasing to 58% recovery for 90% oxygen concentration. Each column requires 127 kg of zeolite, producing 5.75 mol O_2 $kg^{-1}h^{-1}$ (0.66 m³ O_2 $kg^{-1}h^{-1}$ at adsorption pressure), with an energy consumption of 29.38 kJ per mole of oxygen, totalling 255 kWh/tO_2.

The total investment for a PSA plant is estimated at 215,190 EUR, with fixed equipment costs of 176,800 EUR. Using straight-line depreciation over 20 years results in annual depreciation of 9,890 EUR. Annual costs also include energy and maintenance. For an oxygen demand of 234 tons in 2023, the annual cost would be 25,590 EUR using PSA, significantly less than the current 60,840 EUR with the Liquefied Oxygen (LOX) installation. The levelized cost of oxygen over a period of 20 years for PSA is 128.61 EUR/ton, which is 2.1 times lower than the LCOO of LOX which is 270.52 EUR/ton.

The implementation of PSA plants for localized oxygen production in the Netherlands is both technically and economically feasible. A case study at Reinier de Graaf hospital shows significant cost savings compared to current liquid oxygen setups, with potential annual savings of 35,250 EUR. Required equipment is available and the setup size allows it to be installed inside or next to the hospital. Regulatory frameworks are already present and define clear requirements for using a PSA system as primary source. When implementing the right flow and pressure mechanisms the PSA plant can be connected to the current second and backup source, minimizing system adjustments for a smooth integration.

Future research should focus on several key areas to enhance the feasibility of using PSA in Dutch hospitals. Regulatory frameworks need approval or revision by experts in medical oxygen production. Analysing zeolite degradation and validating its performance are crucial for simulating the PSA unit's lifecycle. Improved modelling techniques, considering temperature variations, research on the validity of current assumptions and preventing backflow in the experimental setup will yield more accurate results. Additionally, industry practices should be reviewed to refine the proposed setup and obtaining precise cost estimates from quotes or hospital bills will improve the economic analysis.

Acknowledgements

Contents

Nomenclature

q	Component loading	[mol kg^{-1}]
$\bar{q}$	Average component loading	[mol kg^{-1}]
P	Total pressure	[Pa]
T	Temperature	[K]
c	Concentration	[mol m^{-3}] or [kg m^{-3}]
b	Coefficient of adsorption	[Pa^{-1}]
v	Heterogeneity parameter	[-]
H	Henry coefficient	[mol kg^{-1} Pa^{-1}]
H	Enthalpy	[J]
R	Recovery	[-]
R	Universal gas constant	[J mol^{-1} K^{-1}]
y	Molar gas fraction	[-]
Q	Volumetric flow rate	[mol s^{-1}] or [m^3 s^{-1}]
z	Upwards direction	[m]
μ	Dynamic viscosity	[Pa s]
ϵ	Void fraction	[-]
u	Average gas velocity	[m s^{-1}]
d	Diameter	[m]
D	Diffusivity	[m^2 s^{-1}]
r	Radial distance	[m]
k	Mass transfer coefficient	[s^{-1}]
ρ	Density	[kg m^{-3}]
C_p	Heat capacity at constant pressure	[J kg^{-1} K^{-1}]
w	Adsorbent mass fraction	[-]
ΔH	Heat of adsorption	[J mol^{-1}]
$\dot{q}$	Heat transfer	[J m^{-3} s^{-1}]
h	Heat transfer coefficient	[W m^{-2} K^{-1}]
x	Mole fraction in the adsorbed phase	[-]
N_C	Number of mixture components	[#]
p^*	Sorption pressure	[Pa]
ψ	Reduced grand potential	[mol kg^{-1}]
p	Partial pressure	[Pa]
α	Empirical parameter Sips equation	[-]
χ	Empirical parameter Sips equation	[-]
n	Number of moles in the gas phase	[mol]
t	Time	[s]
A	Surface area	[m^2]
V	Volume	[m^3]
v	Velocity	[m s^{-1}]
$\dot{N}$	Molar flow rate	[mol m^{-3} s^{-1}]
K_v	Coefficient of flow	[m^3 h^{-1} Pa$^{-1/2}$]
SG	Specific gravity	[-]
M	Molar weight	[g mol^{-1}]

List of abbreviations

LMICS	Low- and middle – income countries
MOC	Medical oxygen concentrator
CAS	Cryogenic air separation
ASU	Air separation unit
PSA	Pressure swing adsorption
GSE	Gibbs surface excess
VSA	Vacuum swing adsorption
TSA	Temperature swing adsorption
VPSA	Vacuum pressure swing adsorption
FP	Feed pressurization
AD	Adsorption
PE	Pressure equalization
DP	Depressurization
DPE	Depressurizing pressure equalization
PG	Purge
PPE	Pressurizing pressure equalization
BP	Backfill
VP	Purge under vacuum
E	Equalization
VA	Evacuation
VC	Vacuum
PN	Pressure normalization
LDF	Linear driving force
LOX	Liquefied oxygen
IAST	Ideal adsorption solution theory
CSTR	Continuously stirred tank reactor
LCOO	Levelized costs of oxygen
NPV	Net present value

Subscripts & superscripts

i	Component indicator
g	Gas
p	Particle
e	Effective
eq	Equilibrium
sat	Saturation
s	Solid
$surf$	Surface
a	Adsorbent
T	Total
C	Column
atm	Atmospheric
0	At reference point
w	Working
in	Inlet
out	Outlet
B	Bed
c	Compressor
$accu$	Accumulated
ads	Adsorbed
adv	Advected
$disp$	Dispersed
z	Zeolite

List of tables

List of figures

<div style="text-align: right;">

1. Introduction
</div>

The COVID-19 pandemic has highlighted the critical need for medical oxygen in hospitals. Numerous countries stated exponential increases in required oxygen demand and India even declared an 'Oxygen crisis'. In that country pre-COVID need for medical oxygen was about 700 metric tons (MT) per day. The demand surged to 3100 MT during the first wave and even up to 8900 MT per day during the second wave [1]. Even though oxygen is an essential medicine and vital for the effective treatment of patients, access is limited in many countries due to cost, infrastructure and logistical barriers. Even before COVID-19 nine in ten hospitals in low- and middle-income countries (LMICs) were unable to provide oxygen therapy, resulting in as many as 800,000 preventable deaths per year [2]. During the pandemic, the longstanding gap in availability in supplementary medical oxygen became even more pressing. An assessment of more than 530 hospitals across 26 countries by the United States Agency for International Development in 2022 revealed a gap in capacity to provide medical oxygen [3]. This gap can be understood by looking at **Figure 1**, which shows that monthly oxygen demands sometimes doubled in a period of only 2/3 months.
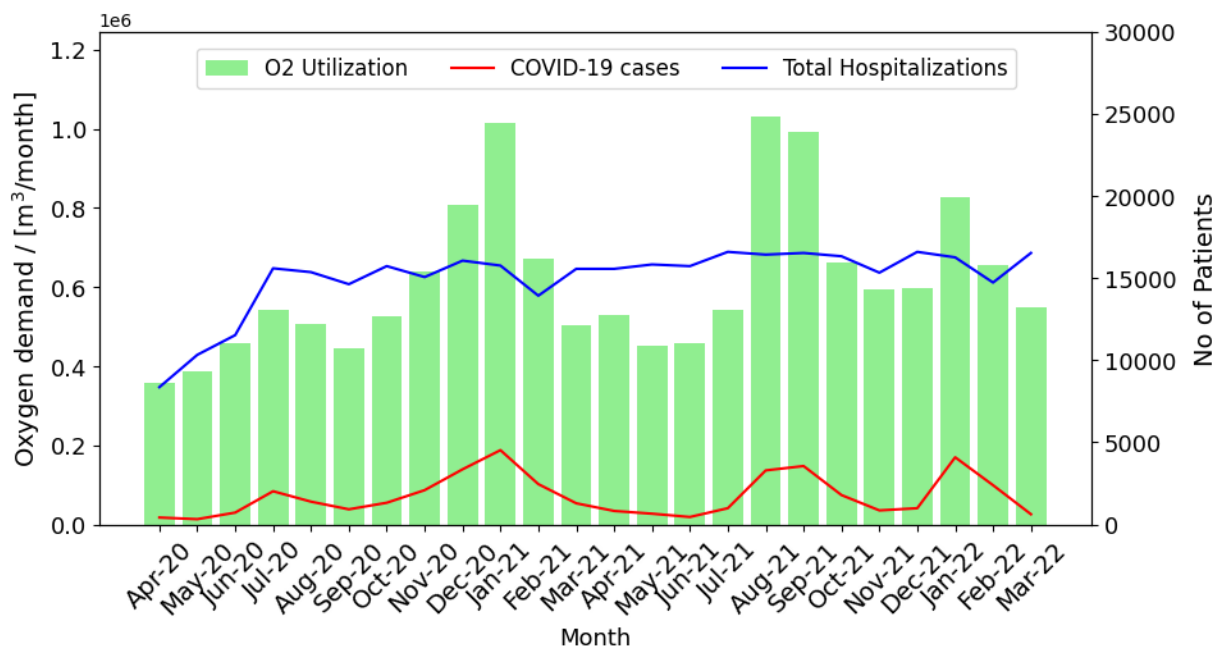
Figure 1: *Oxygen demand and hospitalization volumes during the COVID-19 pandemic within an integrated health system of 26 adult acute care hosptials in the Southern region of the USA. [4]*

The COVID-19 pandemic has shown that public health is becoming a key concern for many scientific professions and is no longer solely a medical issue. Consequently, multidisciplinary specialists from over the world are conducting research to prevent or manage such pandemics. A big part of this research is based on Medical Oxygen Concentrators (MOCs). These MOCs are mostly focused on air seperation techniques that can produce enriched oxygen for hospital usage. One can speak of enriched oxygen ones the oxygen concentration of a gas mixture, like air, is higher than the normal atmospheric level ($21\%_{oxygen}$). This enriched oxygen is used for a variety of reasons, a few examples are: oxygenation while providing anaesthesia, during treatment of lung illnesses that affect oxygen exchange and exposure to carbon monoxide. During these situations flow rates can range from 1 to 30 litres per minute with an oxygen concentration from 30% up to 70%.

There are several techniques to produce (enriched) oxygen, which can be categorized as natural, electrical, or industrial. In order to have oxygen in the air, there needs to be a natural production. This production comes in the form of photosynthesis where plants turn carbon dioxide and water into glucose and oxygen [5]. An upcoming technology in the face of the energy transition is the electrolysis of water. The most commonly used water electrolysis systems at the moment are alkaline water electrolyzers (AWE), proton exchange membrane (PEM) and solid oxide electrolysis cells (SOEC) [6]. Although these processes are mainly used for hydrogen production, as the potential fuel of the future, also oxygen can be captured. Most of today's medical oxygen is produced within industrial processes. The most common technologies ranging from lowest to biggest capacity in tons per day are: Membrane Technology, Pressure Swing Adsorption and Cryogenic Air Seperation [7].

Membrane Technology with polymeric materials uses the difference in diffusion rate between oxygen and nitrogen as a driving force for seperation. Based on the membrane material these systems can produce oxygen enriched air with a purity of 25-50% oxygen. Two of the main benefits for these systems are its simplicity and continuous operation at ambient conditions. The downside of such systems is the low capacity of only 20 tons/day and the end product being contaminated with water and carbon dioxide. [8]

Currently, the most productive and economically feasible method for creating significant amounts of gaseous or liquid oxygen is Cryogenic Air Separation (CAS). This relatively old technique makes use of the difference in boiling point between oxygen and nitrogen with an Air Separation Unit (ASU). This technique enables high oxygen concentrations of up to 99% when being able to remove argon (Ar) from the oxygen product [9]. **Figure 2** shows a schematic representation of a conventional CAS.
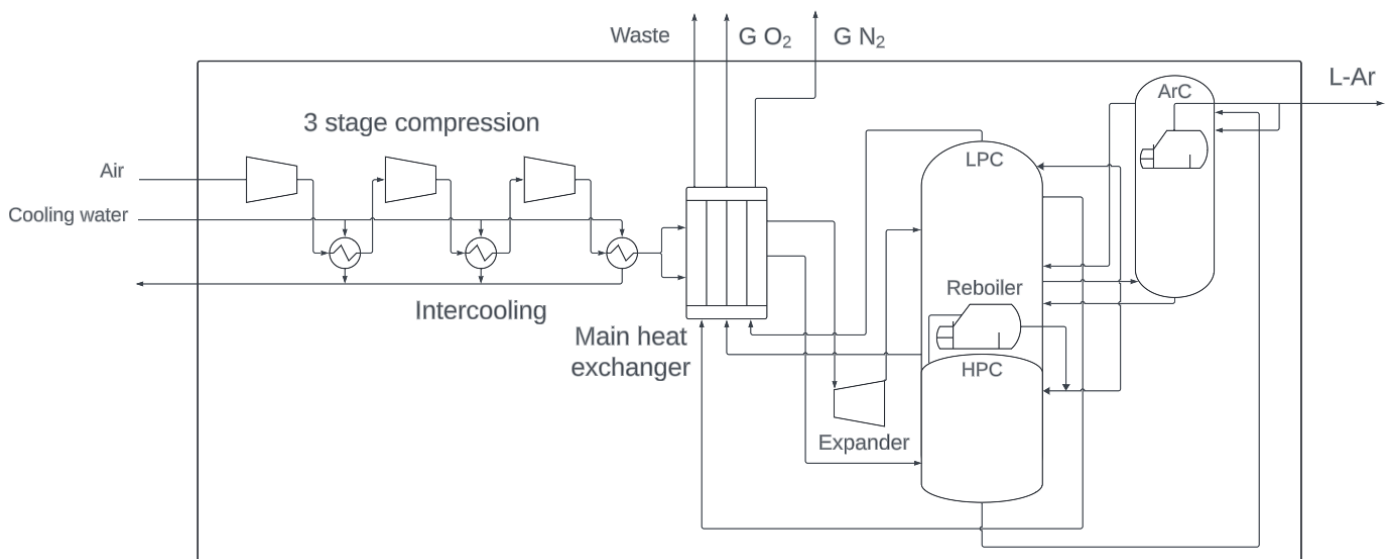
Figure 2: *Schematic represenation of a conventional Cryogenic Air Seperation Unit. Producing gaseous oxygen/nitrogen and liquid argon from air by using cryogenic distillation. [10]*

Large-scale cryogenic distillation facilities capitalize on the inherent economy of scale due to the requirement of large equipment and energy-intensive processes, enabling this method to produce up to 4000 tons of oxygen per day [11]. Liquified oxygen transported from the ASU-facility to hospitals via tanker trucks and gets stored in cryogenic storage tanks. When needed the liquid oxygen can be vaporized back into the gaseous state and stored in oxygen cylinders.

The problem with using CAS as main oxygen production method is its centralized character. Data shows that the 4.4 billion USD market for medical oxygen cylinders in 2023 has only seven prominent players [12]. In low-resource settings, like in LMICs, purchasing oxygen is not always an option due to a lack of suppliers or medical infrastructure. This forces hospitals into local oxygen production. Also for developed countries, which do have these facilities, it can be extremely beneficial to implement local oxygen production. During the COVID-19 pandemic the shortage in medical oxygen created a huge surge in prices. In India desperate citizens turned to the black market for oxygen where prices had risen by 1000% [13]. With the forecast of increased dependence on medical oxygen supplementation having an alternative production method becomes even more important.

A potential alternative to using medical oxygen by CAS is Pressure Swing Adsorption (PSA). Pressure Swing Adsorption (PSA) is a gas separation process that utilizes adsorbents to selectively capture and release gases under alternating pressure conditions. In a cyclic operation, high-pressure ambient air can be introduced and the adsorbent selectively adsorbs specific components like nitrogen, resulting in a purified oxygen stream. The pressure is then reduced, causing the adsorbent to release the captured gases, allowing for the separation and purification of air [14]. PSA plants are able to deliver oxygen flows with a concentration of up to 90-95% [15] and a have a capacity of up to 300 tons per day [10]. As these are local systems hospitals can gain more independence in managing their oxygen supply. Oxygen production can be adjusted based on the hospital's specific needs and potential supply chain disruptions do not affect the hospital. Also cost savings could come into play as they eliminate purchasing big amounts of oxygen. The initial investment in the PSA plant can potentially be offset by the long-term operation cost benefits.

These PSA plants are now mostly used in LMICs due to their resource-constrained settings and lack of alternatives. A social enterprise approach in Kenya, Rwanda and Ethiopia led to the establishment of 4 PSA plants which have delivered over 200,000 cylinders of oxygen since 2014 to a network of health care facilities [16]. A 2022 World Health Organization (WHO) initiative handed over a duplex PSA plant to Somalia in order to use within the De Martino Hospital which was specialized in COVID-19 treatment [17]. One of the greatest weaknesses and key risks of a PSA plant is breakdowns. A map from the Every Breath Counts Coalition, a public-private partnership supporting national governments to reduce pneumonia deaths in low- and middle-income countries, shows at least 165 PSA plants (as of October 2022) needing repair globally; 151 of these are located in sub-Saharan Africa [18].

Within this study the spotlight will be turned towards the application of PSA plants in developed nations. Unlike resource-constrained settings where PSA plants have been implemented to enhance local oxygen production, developed countries with robust medical infrastructure present a unique set of challenges and opportunities. In such contexts, strict regulations govern oxygen supply to hospitals, and alternative methods, like cryogenic distillation, have been the norm.

In close collaboration with 'het Reinier de Graaf' hospital in Delft, this study will use real-world oxygen consumption data provided by the hospital to inform the development of a customized Pressure Swing Adsorption plant system. The primary objective is to investigate the possibilities of designing a system that not only meets the specific oxygen demands of the hospital but also complies with the Dutch legal frameworks and forms an economically feasible case.

To achieve this objective a clear and answerable research question has been formulated along with sub questions.

Research question:

"How feasible is the implementation of Pressure Swing Adsorption (PSA) plants for sufficient localized oxygen production in the Netherlands, considering regulatory compliance, economic viability, and integration with existing healthcare infrastructure?"

This research question contains four important aspects with respect to PSA plants in the Netherlands: legal compliance[1], technical considerations[2], seamless integration[3] and economic viability[4]. All of these aspects will be addressed by separate sub questions.

Sub questions:

[1] *"What are the specific regulatory frameworks governing medical oxygen supply in the Netherlands and how do they impact the feasibility of implementing PSA plants?"*

[2] *"How can the technical design of a PSA plant be optimized to meet the specific oxygen demands of healthcare facilities in the Netherlands, ensuring efficient and reliable oxygen production?"*

[3] *"How adaptable are PSA plants to the existing healthcare infrastructure in the Netherlands and what modifications or considerations are necessary for seamless integration?"*

[4] *"What economic factors need to be considered when assessing the feasibility of PSA plants in the Netherlands, and how do they compare to alternative oxygen production methods?"*

2. Theoretical Background

The goal of this chapter is to provide the theoretical background of PSA plants. Starting off with more information on the alternative forms of oxygen production methods to gain more overall knowledge on the subject. As this study is focused on eventual PSA usage, a complete paragraph is dedicated to its exact usage and potential designs followed by a paragraph on the modelling & simulation of it. After this here is some insight provided on the economics of oxygen production. At last the chapter will dive into the current handling of oxygen by hospitals, addressing current practices, safety measurements and regulatory frameworks.

2.1 Oxygen Production Techniques

As mentioned in the introduction there can be made an extinction between different categories of oxygen production techniques: natural, electrical and industrial. This paragraph will go through these categories and address the different methods within them.

2.1.1 Natural Oxygen Production – Photosynthesis

During photosynthesis plants take in carbon dioxide (CO_2) and water (H_2O) from the air and soil. These are then transformed into oxygen carbon dioxide and glucose. The amount of oxygen produced by plants through photosynthesis is significant in the context of atmospheric oxygen levels. While the exact quantity varies, it is estimated that a single leaf can produce approximately 5-10 micromoles of oxygen per hour [19]. Although these numbers may seem modest, the collective impact of photosynthesis on oxygen levels is substantial with trees and rainforests producing around 28% of Earth's oxygen [20].

2.1.2 Electrical Oxygen Production - Electrolysis

Creating renewable energy sources to replace fossil fuels has become a crucial worldwide problem due to rising energy consumption and greenhouse gas emissions. A key strategy to lower greenhouse gas and particle emissions is the large-scale production of hydrogen by water electrolysis powered by renewable energy systems. Water, mostly freshwater, is used extensively in electrolysers to create hydrogen and oxygen at the cathode and anode, respectively. However, seawater is preferred because it is the most abundant water resource.

Current water electrolysis methods are battling with Steam Methane Reforming (SMR) as biggest producer of hydrogen and an efficiency of 63-85% [21]. Alkaline water electrolyzers, PEM electrolyzers and SOECs currently have energy efficiencies of respectively 50-65 %, 65-75% and 75-81% [22]. When relating this to oxygen production, a 71% electrolysis efficiency requires 500 kWh of electricity to produce 500 Nm^3 of oxygen along with 1000 Nm^3 of hydrogen. Cryogenic Air Seperation would require around 250 kWh of electricity for the same amount of oxygen production [23]. Immediately indicating that oxygen is only considered as by-product during electrolysis production instead of potential main product.

2.1.3 Industrial Oxygen Production – Membrane Technology

One of the membrane technologies which can be used to separate oxygen from air relies on exploiting the difference in rate of diffusion through a polymeric membrane. Polymeric membranes are often preferred to ceramic and metallic membranes since they have a low environmental impact, are easy to incorporate into large-scale modules, and have the lowest capital costs among the different membranes [24]. The downside of such polymeric membranes are their low capacity, short lifespan, thermal degradation [25] and susceptibility to fouling [26]. Performance of certain polymers for oxygen seperation from air can be described within selectivity and permeability trade-off plots like in **Figure 3.**
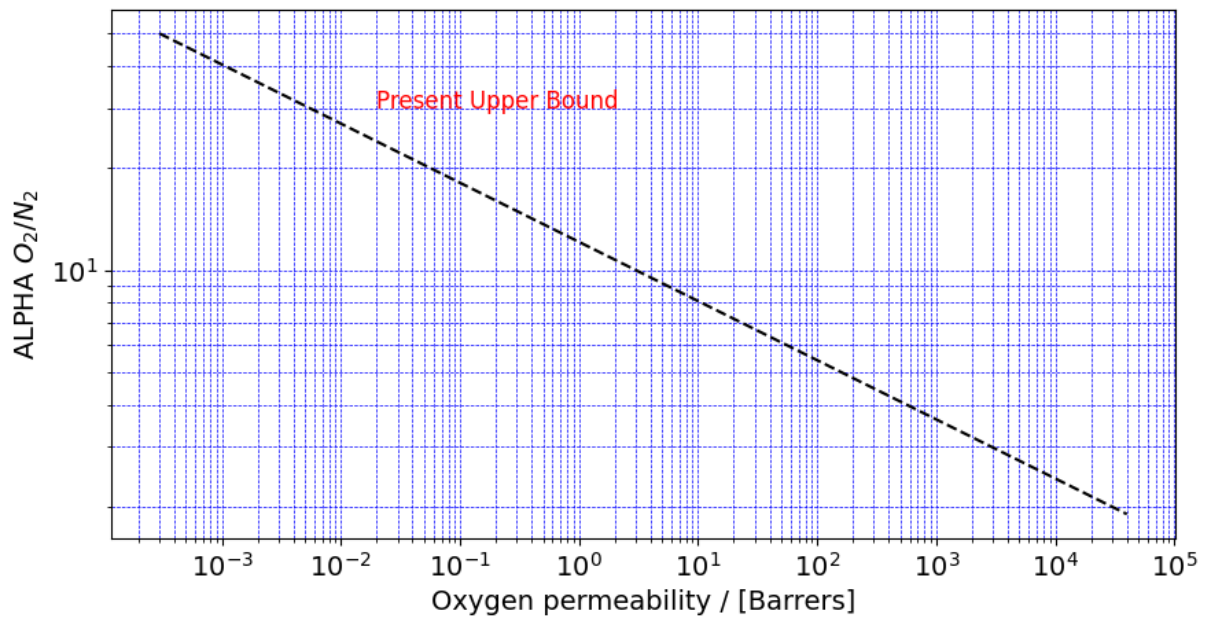
Figure 3: *Upper bound correlation for O_2/N_2 in membrane seperation technology [27].*

Within **Figure 3** the O_2/N_2 selectivity (ALPHA) is plotted again the logarithm of the permeability of O_2 (the higher permeable gas). The trend of measurements clearly shows a decrease in selectivity as oxygen permeability increases. This can easily be understood when imagining bigger pore sizes allowing more of both gases to pass the membrane when trying to increase oxygen permeability. This trade-off relationship was shown to be related to an upper bound relationship where the log of the separation factor versus the log of the higher permeability gas yielded a limit for achieving the desired result of a high separation factor combined with a high permeability.

A new promising type of membranes are called Ion Transport Membranes (ITM) due to their ability to conduct oxygen ions and separate oxygen from air with high purity ($99.9\%_{oxygen}$). These solid inorganic oxide ceramic materials operate at high temperatures, generally over 1100 °F. The implementation of these membranes within gas seperation is currently only conducted on laboratory scale. The high purity and relatively low energy demand (400 kWh/ton O_2 [11]) make this a really interesting alternative in the future.

2.1.4 Industrial Oxygen Production – Cryogenic Air Seperation

Cryogenic air separation is a process that separates air into its primary components, typically nitrogen, oxygen, and argon, by exploiting the differences in their boiling points. The technique involves compressing and cooling the incoming air to remove impurities, then feeding the cooled air into a distillation column, where the air is separated based on the differences in boiling points of its components. The process is characterized by very good quality of the products ($99\%_{oxygen}$), big capacities and high reliabilities. Single train Air Seperation Units are currently able to produce up to 4000 tons per day with an energy demand of around 200 kWh/ton O_2 [11]. Trough the past decades this technology has made a rapid increase in efficiency as can be seen in **Figure 4**. The latest big increase in efficiency was accomplished by accepting 95% purity instead of 99% leading to a 10% decrease in energy consumption. The figure also indicates the thermodynamic minimum work to separate oxygen from air which lies at 53.1 kWh/ton O_2.
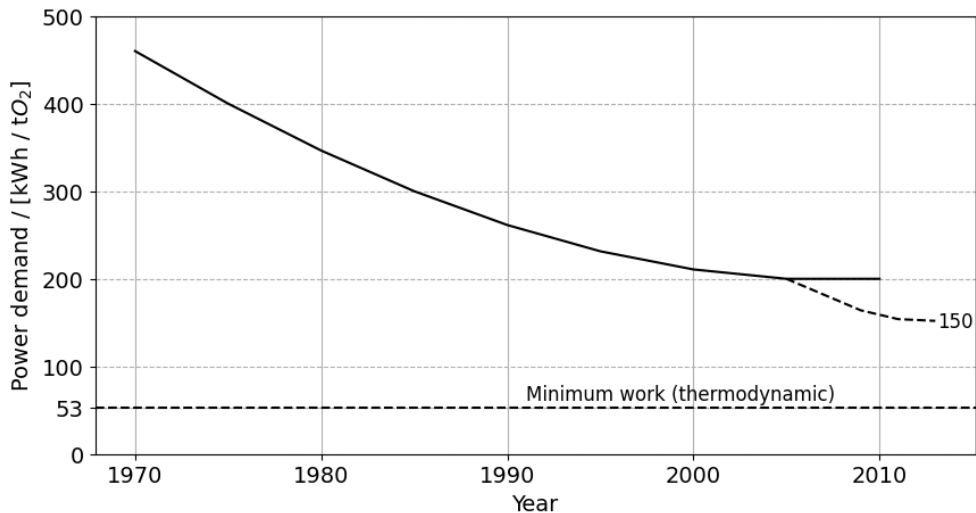
Figure 4: *Decrease in energy demand for oxygen seperation using cryogenic air seperation [11].*

Further decrease of energy consumption is considered unrealistic as the capacities of ASU single trains cannot be increased much because of transport and assembly problems. Due to the capital and energy intensive nature of this process, only a small number of companies is responsible for most of the oxygen production. In a developed country like the Netherlands, only one company is responsible for delivery of medical oxygen to hospitals. These type of monopoly situations can create dangerous situations in times of high demand.

2.2 PSA Principles

With examining the feasibility of a PSA plant being the main goal of research this chapter will be an extensive exploration on the principles of PSA. Having a close look at its fundamentals, adsorption materials, performance in oxygen seperation and the effects of different operation modes.

2.2.1 Adsorption Fundamentals

As a separation process, adsorption is widely applied in our manufacturing economy and in our daily life. Adsorption operations exploit certain solids' ability to preferentially concentrate specific substances from solutions (gaseous or liquid) onto their surfaces. The extent of adsorption of a given situation is reached once equilibrium is established between the adsorbent and its contacting solution. In practice, adsorption performance is also strongly influenced by the mass transfer of the species between the solution and the adsorbent surfaces and the adsorption reaction rate. Technically, adsorption is, therefore, an equilibrium-diffusion-reaction process. **Figure 5** shows a simplified schematic overview of the process along with some often used terms like desorption, adsorbate and adsorbent. [28]
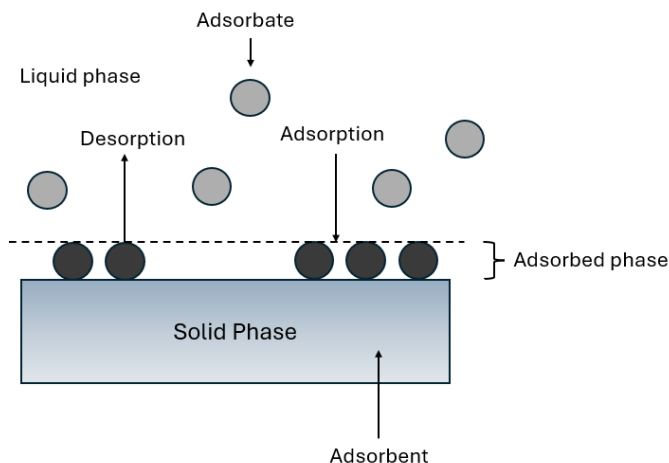
Figure 5: *Schematic overview on the fundamentals of adsorption.*

2.2.2   Introduction to Pressure Swing Adsorption – PSA

Pressure Swing Adsorption is a technology used in a wide range of applications for the seperation and purification of gases. Some applications are: solvent vapor recovery, production of hydrogen from steam methane reformers (SMR), seperation of carbon dioxide and methane from landfill gases and fractionation of air (oxygen purification). PSA belongs to a bigger group of seperation technologies, called adsorption-based seperation processes. The growth in the R&D on PSA technology has been huge since the first U.S patent, originating from 1960 authored by C.W. Skarstrom [29]. Surveys show hundreds of patents on PSA being issued already between 1980-2000 and a large amount of published papers with PSA as keyword [30]. The basic idea of the technology can be described by the Skarstrom-cycle illustrated in **Figure 6**.

Step	I	II	III	IV
Bed 1	Feed Pressurization	Adsorption	Blowdown	Purge
Bed 2	Blowdown	Purge	Feed Pressurization	Adsorption
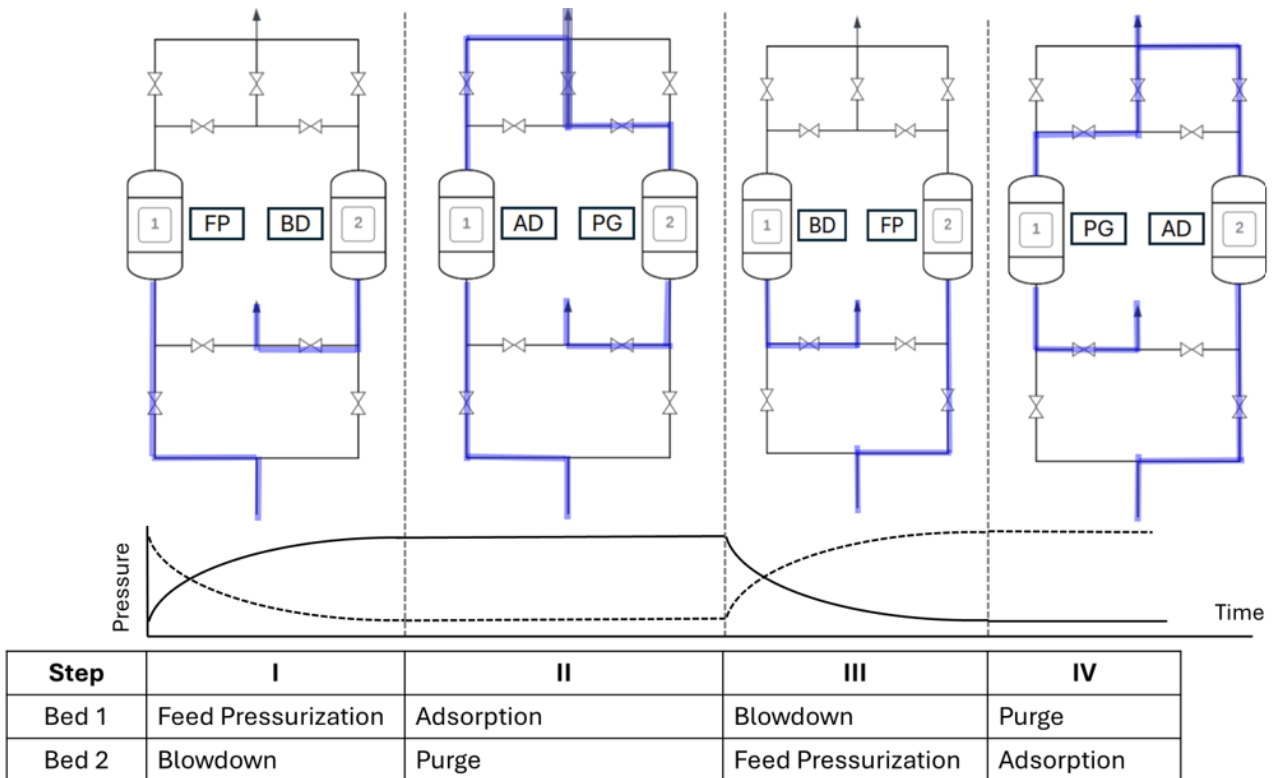
Figure 6: S*chematic overview of the traditional Skarstrom cycle [31]. Alternating pressure in a two-column system with four different cycle steps allows for a continuous production of concentrated oxygen. Solid line refers to column 1, dashed line refers to column 2.*

Often PSA setups consist of two packed columns which contain a solid adsorbent. Certain components of a gas mixture are selectively adsorbed on the microporous-mesoporous solid adsorbent at a relatively high pressure. Let's for now take the example of oxygen separation from air, assuming air only consists of nitrogen and oxygen. Step 1 fills bed 1 with ambient air while closing the top valve to increase pressure. Both beds contain an adsorbent material which absorbs nitrogen stronger than oxygen, making the exit stream richer in oxygen. When the adsorbent in bed 1 is saturated, the top valve is opened. Part of the oxygen rich stream is led through bed 2 to remove nitrogen which is still present in the bed, this is called purge. After closing the top valves on bed 1 and 2, the feed stream is led to bed 2 while bed 1 is being depressurized (blowdown). Now the exact same process happens vice versa creating a continuous flow of enriched oxygen. Different column sizes, pressure levels, adsorbent materials, cycle times, temperature and the number of beds provide a large amount of parameters to optimize the process on the specific needs.

2.2.3 Adsorbent Materials

Based on the working principles of PSA one can imagine the importance of implementing the right adsorbent material to end up with the desired product. Various types of adsorbents are used in PSA processes, depending on the specific gas separation requirements. Activated carbons are often used in removing impurities from gases like methane, described in a study by Zheng et al. (2019) [32]. Dehydration processes for removing water vapor from gases make use of silica gel or molecular sieves. For processes like oxygen purification, zeolites are of often use. Zeolites are crystalline aluminosilicate minerals with a porous three-dimensional framework structure. These microporous structures allow zeolites to selectively adsorb and desorb molecules based on their size and shape. **Figure 7** shows the molecular structure of a zeolite.
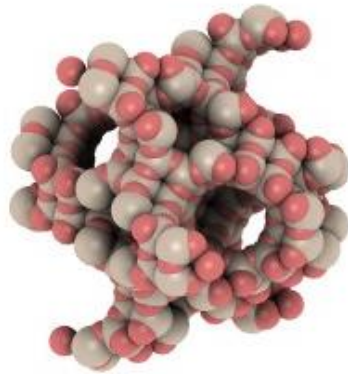
Figure 7: *Molecular structure of the BEA zeolite using iRaspa Visualizer [33].*

In PSA MOCs; synthetic Zeolite 13X and 5A are most commonly used zeolites to produce medical oxygen. The number indicating the nominal pore size in angstroms, zeolite 13X has nominal pore sizes of around 10 angstroms. The letter indicates the zeolite structure. Type X zeolites have Si/Al ratio between 1 and 1.5 which affects the cation exchange capacity. The choice of cation influences the selectivity and affinity of the zeolite for specific gases. Adsorption performance of zeolites for specific gases can be described by adsorption curves.

Figure 8 shows the adsorption isotherms for pure oxygen and nitrogen on two different heterogeneous LiX zeolite using a Langmuir model. Clearly indicating an increased amount of adsorbed gas when temperature is decreased and pressure is increased until it reaches a plateau. Indicating saturation as the adsorption sites become occupied.
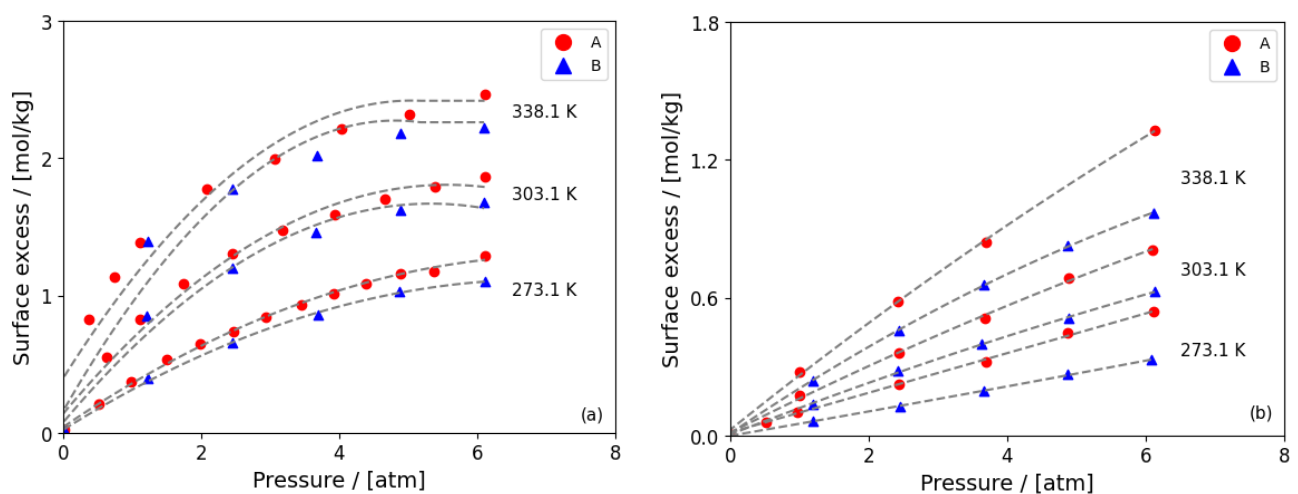
Figure 8: *Pure gas equilibrium adsorption isotherms on LiLSX zeolite materials A (circles) and B (triangles) at different temperatures: (a) N2; (b)O2. [34]*

Both gases can also be observed in a binary mixture to see the adsorption isotherms and selectivity of the zeolites. **Figure 9** indicates the Gibbs Surface Excess (GSE) as a function of N_2 in the gas-phase (y_1) for the two different zeolites. This thermodynamic quantity describes the excess amount of gas at the surface of the zeolite compared to its bulk concentration in the gas mixture. The figure shows that the GSEs of N_2 on both zeolites are comparable for any y_1. The GSEs of O_2 are lower for material B than those of A. So in conclusion, coadsorption of oxygen is lower for material B, indicating a higher selectivity of adsorption of nitrogen over oxygen.
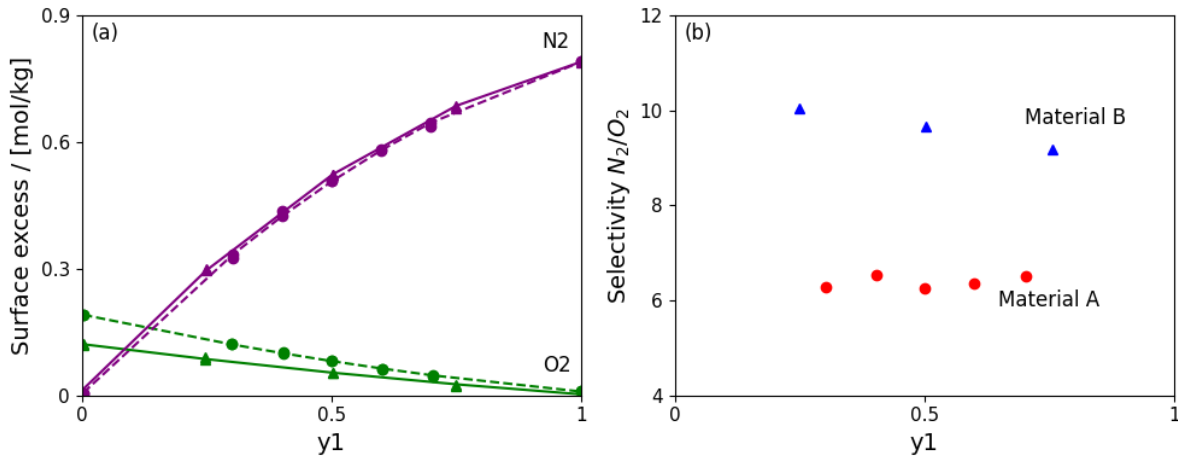
Figure 9: *(a) Binary gas (N2+O2) adsorption isotherms: circles (material A); triangles (material B). (b) Binary selectivity versus y1 at 1 atm and 303.1 K. [34]*

Figure 9b compares the selectivity values of the different materials as a function of y_1. Indicating that the selectivity of material B is larger than material A over the entire composition range. For air seperation the selectivity should be evaluated around $y_1 = 0.21$, considering *normal* air conditions. Making material B a better suited zeolite for PSA than material A. The example above shows the importance of choosing the best-suited zeolite for the application. Important to notice is the fact that also parameters like temperature can play an important role. **Figure 10** shows the selectivity of two different zeolites for N_2 as a function of temperature. From the Li-LSX zeolite it becomes clear that selectivity can differ a lot with temperature.
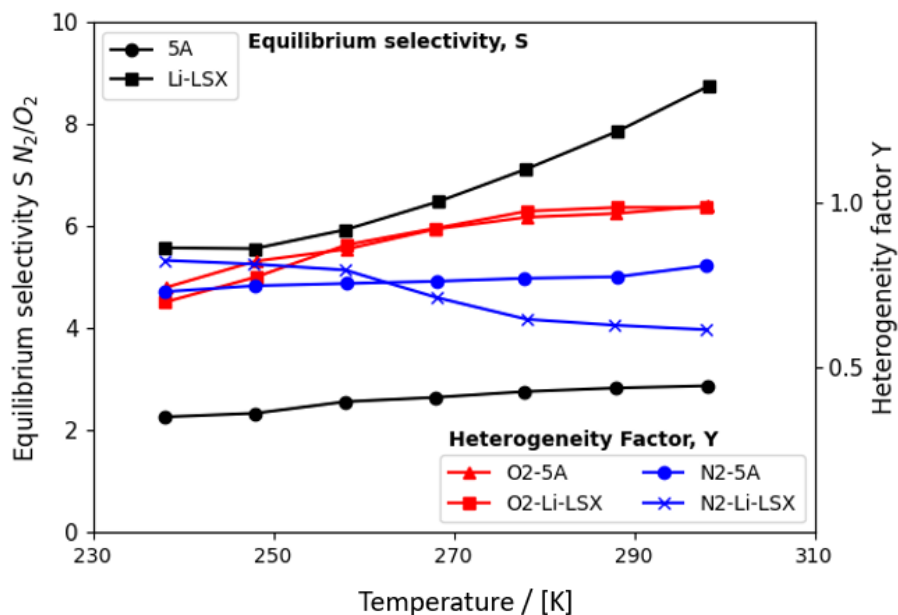
Figure 10: *Variations of N2/O2 selectivity with temperature for 5A and Li-LSX [35].*

Besides the pressure, temperature and zeolite type also contamination can have a big influence on the performance of a zeolite in adsorbing certain components. When using PSA for oxygen generation potential contaminants are water and carbon dioxide, which both can be found in ambient air. **Figure 11** shows the percentage of activation of an adsorbent for two columns along its axial coordinate z. The percentage of activation is expressed as the ratio between the nitrogen concentration in the adsorbed phase and the maximum concentration of nitrogen in the same phase at 20 ˚C. The dashed line is the activation of the adsorbent after being contaminated with water, the solid line is the activation of the adsorbent after being contaminated with carbon dioxide. Water contamination at the bottom of the column clearly has a huge effect on the ability to adsorb nitrogen. Therefore dehumidification is crucial in PSA to maintain oxygen purity.
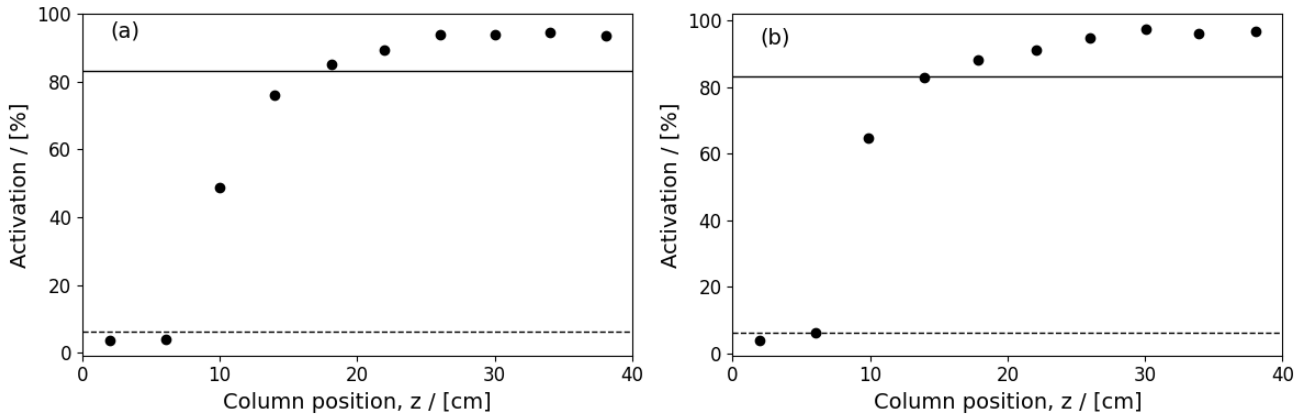
Figure 11: *Percentage of the activation of the adsorbent at 20 ˚C along the column height. (a) left column, (b) right column. dashed line: activation after water contamination, solid line: activation after carbon dioxide contamination. [36]*

2.2.4 Performance Metrics for Oxygen Adsorption-based Seperation Processes

Oxygen adsorption-based seperation systems are always evaluated with oxygen purity, recovery, productivity and energy consumption. Oxygen recovery (R) is calculated as

$$R = \frac{y_{O_2,P} Q_P}{y_{O_2,F} Q_F} \qquad 2.1$$

with $y_{O_2,P}$ being the average oxygen purity in the product, Q_P the flow rate of the product, $y_{O_2,F}$ the oxygen purity in the feed/air, Q_F the flow rate of the feed. In words this can be described as the section of the feed oxygen which is obtained in the end product. Oxygen purity indicates the volumetric percentage of the oxygen within a gaseous mixture, e.g. the oxygen purity in air is around 21%. The productivity evaluates the utilization of the absorbent and is constructed as

$$Productivity = \frac{Oxygen\ production\ (L/h)}{Amount\ of\ absorbent\ (kg)} \qquad 2.2$$

At last there is the energy consumption. This metric indicates the efficiency of the process and is determined as

$$Energy\ consumption = \frac{Total\ Energy\ Input\ (kW)}{Oxygen\ produced\ (Nm^3)} \qquad 2.3$$

2.2.5 Adsorption-based Separation Process Cycle Designs

The PSA process described in Introduction to Pressure Swing Adsorption – PSA is the most basic version of a PSA cycle. Research and development in the field have led to different cycle designs. Enhancing the versatility of gas seperation processes and improve efficiency. Nowadays adsorption-based seperation processes are characterised by the number of columns/bed, the number of cycle steps and the adsorption swing type. The adsorption swing type up to now has been PSA. However this is not the only adsorption swing type available at the moment. Two others are Temperature Swing Adsorption (TSA) and Vacuum Swing adsorption (VSA). Combinations of different types are also possible like in Vacuum Pressure Swing Adsorption (VPSA). E.g. the Skarstrom-cycle is a: 2-bed 4-step PSA, cycle type. This paragraph will dive into the different available cycle designs and their operation.

Pressure equalization (PE):

Inclusion of PE steps into PSA cycles can enhance the recovery of components as well as decrease required mechanical energy. In general, PE is done by connecting two beds, one which just has been purged and the other that has just completed the high-pressure feed step. **Figure 12** schematically shows what such steps looks like in a 2-bed 6-step PSA system.

Bed 1	AD	DPE	DP	PG	PPE	FP
Bed 2	PG	PPE	FP	AD	DPE	DP
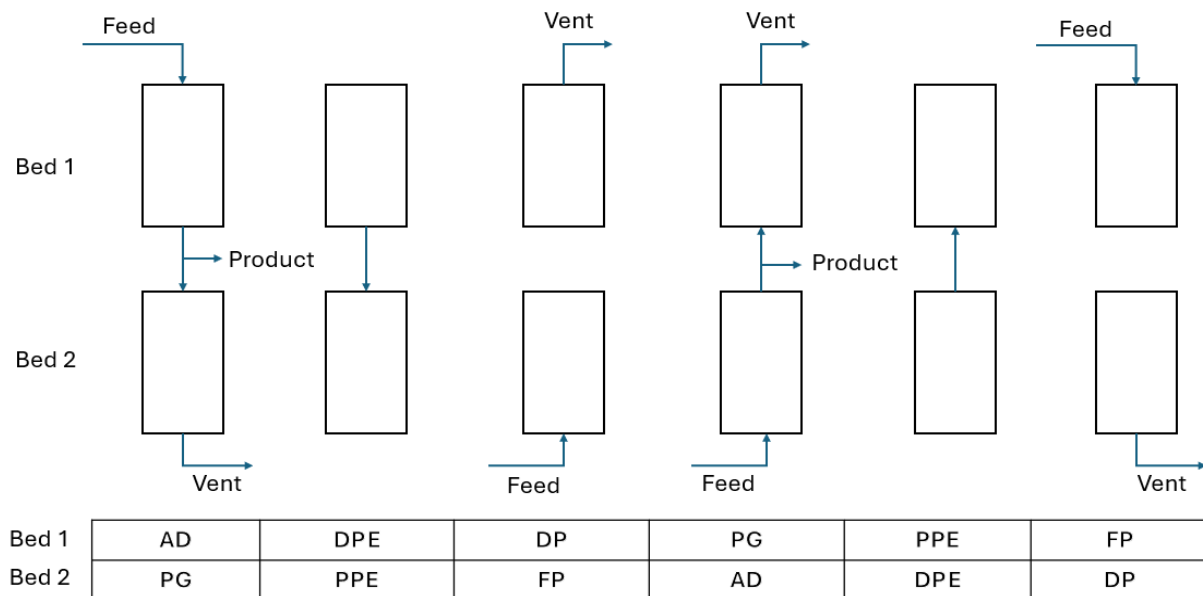
Figure 12: *Pressure equalization step in a 2-bed 6-step PSA system [37]. AD, adsorption ; DPE, depressurizing pressure equalization ; DP, depressurization ; PG, purge ; PPE, pressurizing pressure equalization ; FP, feed pressurization.*

When comparing this to the Skarstrom-cycle, step 2 and 4 are new. Step 2 is called the depressurizing pressure equalization. The high pressure in bed 1, which just has adsorbed most of the nitrogen, causes a gas flow enriched in oxygen to flow into bed 2 until the pressure in both beds is equal. Step 4 is called the pressurizing pressure equalization. There bed 2 has a higher pressure, causing gas to flow from bed 2 to bed 1 before pressure is equalized.
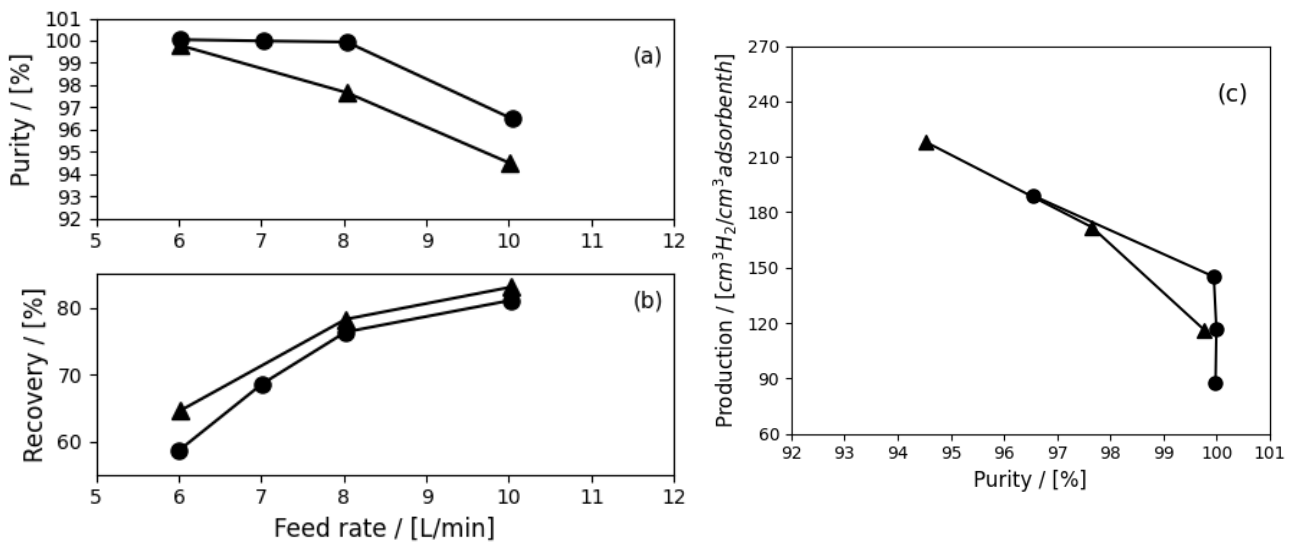
The effect of the backfill step in a layered bed can be examined by looking at **Figure 14**. There we see the effect of feed rate on the purity and recovery of the process. It clearly shows the seven-step process was better than the six-step process with respect to purity. The six-step process scores better on recovery for most feed rates as some of the product is consumed during the backfill. Productivity for the six-step process were better up to the 99% purity point for equal feed rates. These effects can be understood better by looking at the concentration profiles at the end of every step in **Figure *15***. Please note that the goal of this PSA system is to obtain enriched hydrogen instead of oxygen.
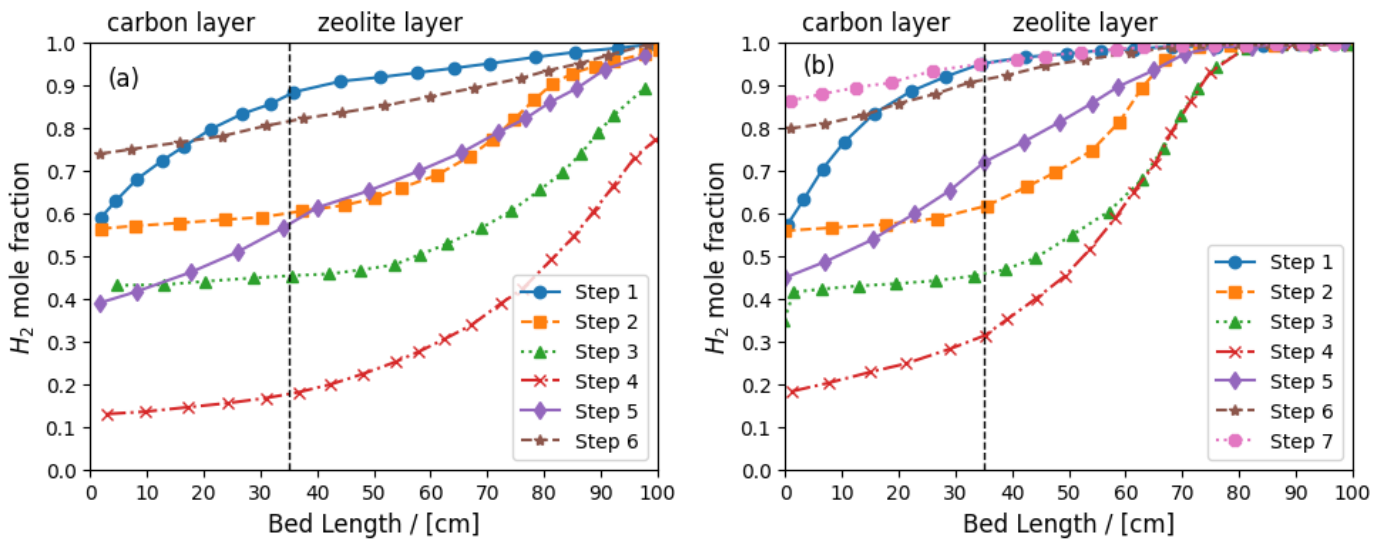
Figure 15: *H₂ concentration profiles along the column length at the end of each cycle step.*
(a) six-step process, (b) seven-step process. [37]

The figure clearly indicates a widespread wavefront of hydrogen during the pressurization step (VI). This causes the purity of the product at the bed end to be lower. For the seven-step-process the hydrogen concentration at the end of the bed ensures higher purity. This is caused by the big hydrogen concentration increase between the pressurizing pressure equalization (V) and the backfill (VI).

Multi-bed designs:

Up to now only 2-bed systems have been discussed. It is however also possible to have adsorption-based seperation systems with more than 2 beds. Some systems require this for continuous operation as bed cycle times are too short for only using 2 beds. Other reasons are scalability of the capacity, adaptability in variable feed conditions and cascading of adsorption beds to reach high purities. Schematic tables and figures of multi-column systems become increasingly complex as columns are added. One way of dealing with this is by using a graphical unit block approach like in **Figure 16** for a 5-bed 11-step process.

Figure 16: *PSA cycle schedule for a 5-bed 11-step system [38].*

Time is placed along the horizontal axis where the fifteen columns i.e. A through O represent time steps of equal length. The different beds are put along the vertical axis. A row represents the sequential order in steps for a single bed with bed 3 indicating the cycle sequence. A column represents what cycle step each bed is in at a certain time step within the process. All beds within a process operate indentically so the same cycle steps are run by consecutive beds after a fixed time interval. Meaning the same operation in one bed is repeated in another after this time interval. This is encapsulated in a unit block, indicated by the thick blue line. Within a unit block all steps in the schedule are run by one of the beds. The number of unit blocks should equal the number of beds.

Temperature Swing Adsorption – TSA:

This method of physical adsorption is the first method that was applied in industry. It relies on the fact that absorption capacity can be temperature dependent. The process can be explained by looking at **Figure 17**. The zeolite's adsorption capacity of N_2 is way higher than that of O_2 and Ar. After the adsorption step the zeolite will be saturated with mostly nitrogen. For the zeolite to be regenerated the temperature can be increased to bring down the adsorption capacity, releasing most of the adsorbed nitrogen. For the next adsorption step the bed has to be cooled again. Due to the need of heating and cooling, TSA is often conducted in systems with multi-bed designs. The major drawbacks of TSA over PSA are longer desorption times, higher energy requirements and rapid adsorbent deactivation due to coking at high temperatures [39].
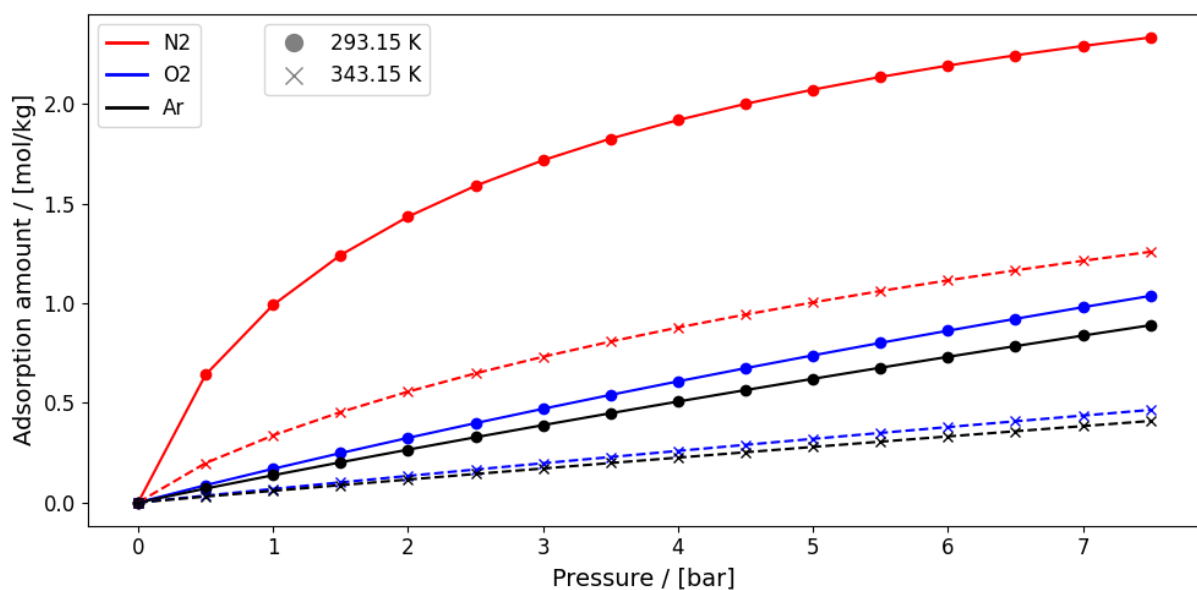
Figure 17: *Adsorption isotherms for zeolite Oxysiv MDX showing temperature effects [36].*

Vacuum Pressure Swing Adsorption (VPSA):

A different way to regenerate the bed is by using a vacuum during the desorption phase. The vacuum is created by a vacuum pump at the bottom of the beds which is schematically depicted in **Figure 18**. The figure also shows the pressures during a cycle to show the sub atmospheric pressure levels.
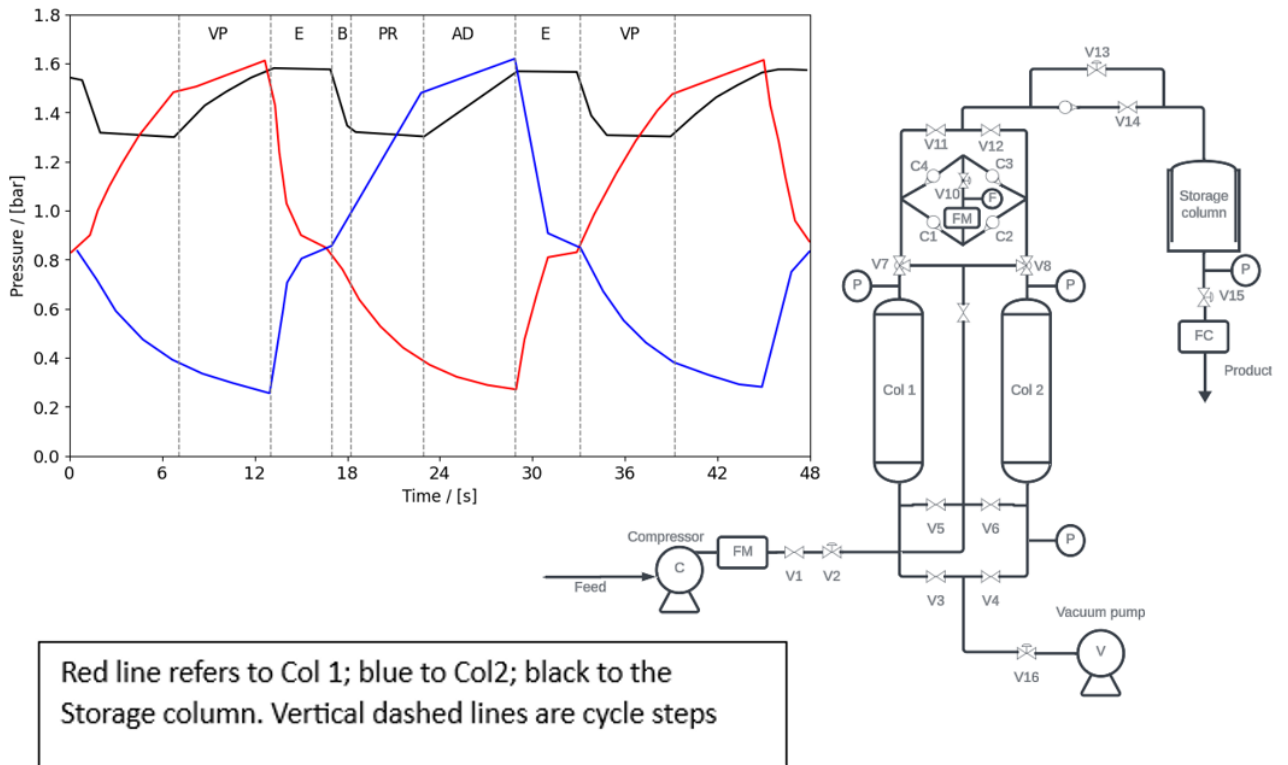
Figure 18: *Schematic representation of a VPSA unit and its pressure history inside the columns VP, purge under vacuum ; E, equalization ; B, backfill ; PR, pressurization ; AD, adsorption ; VA, evacuation. [40]*

Figure 19 shows a comparison between a PSA and VPSA system under the same process conditions. The plot shows the effect of different adsorption times on the process performance. What becomes evident is that the VPSA system has better product recovery for each adsorption time. High recoveries are reached faster in PSA systems but both systems have a maximum recovery of ~93%.
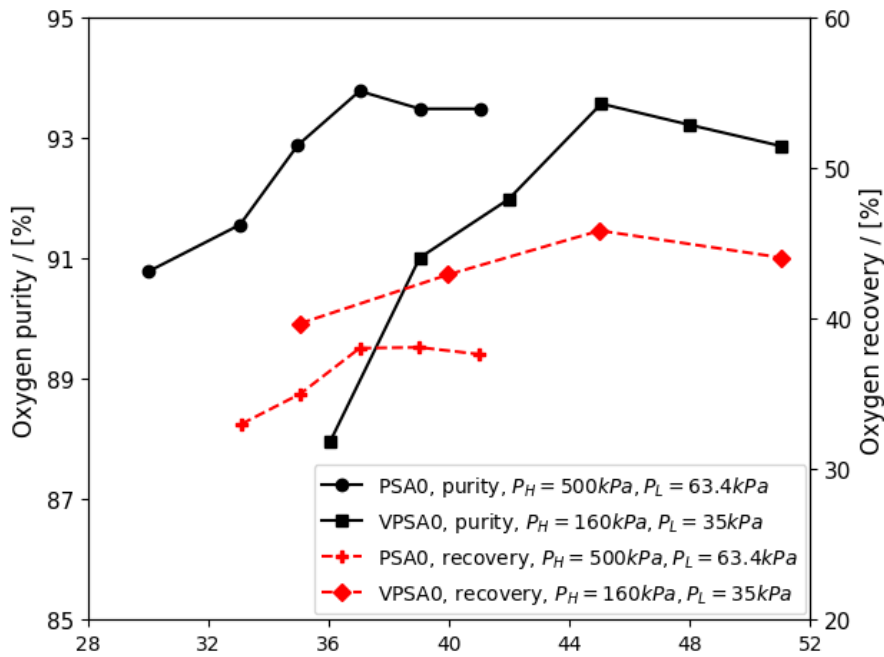
Figure 19: Performance comparison between a PSA and VPSA process when varying the adsorption time while keeping all other process conditions the same. [41]

2.3 Modelling & Simulation

Experimental methods for PSA technology are time-consuming and it is difficult to obtain the changes in process parameters. For that reason numeric modelling is a potential way of optimizing and controlling a PSA cycle process. This paragraph will dive into the numerical methods which can be used to model a periodic, cyclic and dynamic process. **Figure *20*** shows the typical mathematical model for an adsorption bed.
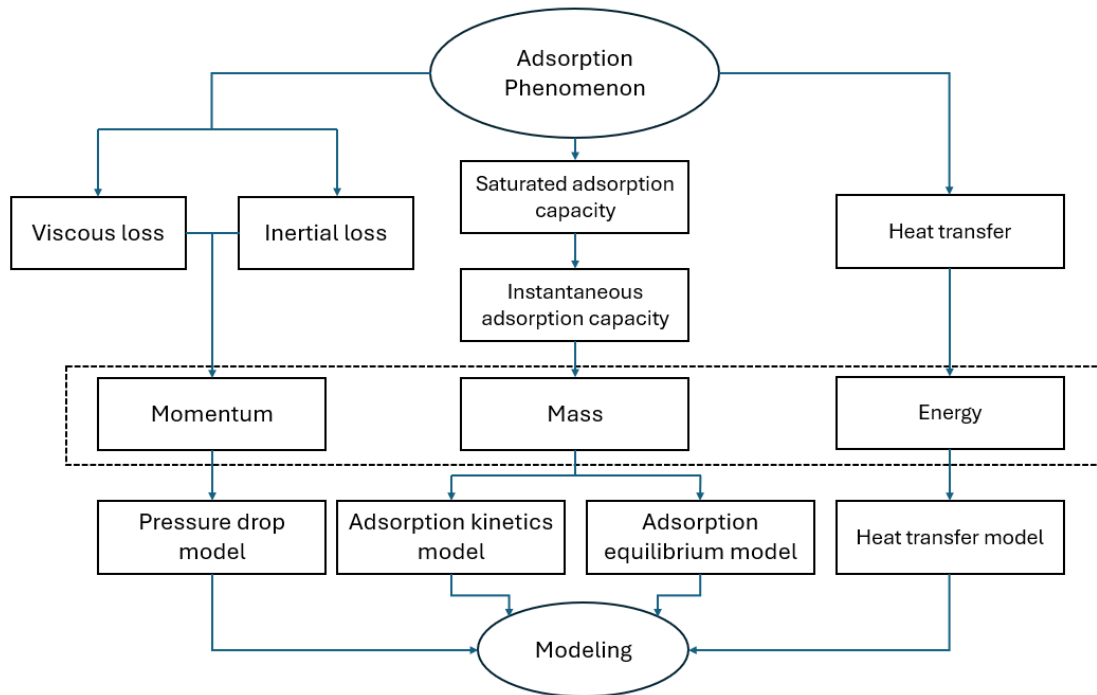
Figure 20: *Mathematical Modelling Pathway for a PSA Process [42].*

The fundamentals for simulating an adsorption bed are momentum-transfer models, mass-transfer models and energy-transfer models. For the mass-transfer model there is an extinction to be made between the adsorption kinetics model and the adsorption equilibrium model. With the adsorption kinetics describing the external diffusion, internal diffusion and surface-adsorption behaviour. **Figure *21*** indicates what these terms mean for a porous adsorbent.
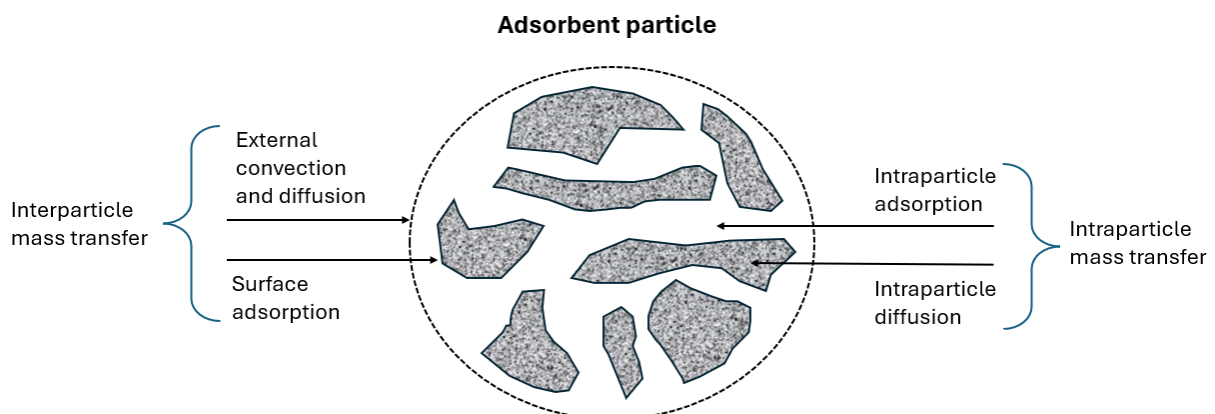
Figure 21: *Schematic overview of adsorption process in porous adsorbent [43].*

The adsorption equilibrium model describes the equilibrium state between gas and absorbent after external and internal diffusion. For accurate model behaviour it is important to select suitable adsorption-equilibrium-isotherms. The rest of the paragraph will address the bottom row elements of **Figure *20***.

2.3.1   Pressure-Drop Model

The name PSA already indicates the importance of pressure within the system. When the gas is led through the packed column a pressure drop occurs. This pressure drop directly affect the recovery and purity of the product and should therefore be considered. One way to do this is by using the Ergun equation [44]. This equation is characterized by containing both a laminar and a turbulent part. Especially the contribution of the turbulent part is important to consider within a packed column.

$$-\frac{\partial P}{\partial z} = \frac{150\mu_g(1-\epsilon)^2 u}{\epsilon^3 d_p^2} + \frac{1.75\rho_g(1-\epsilon)u^2}{\epsilon^3 d_p^2} \qquad\qquad 2.4$$

The pressure drop is evaluated along the z-axis which is the upwards direction for a standing column. μ_g as the gas viscosity, ϵ being the void fraction , u the average gas velocity and d_p the average adsorbent particle diameter.

2.3.2   Adsorption Equilibrium Model

The fundamental concept in adsorption science is the adsorption isotherm. This isotherm represents the equilibrium relationship between the adsorbed material and the pressure or sometimes the concentration in the bulk phase, all at constant temperature. For a single adsorbate this can be expressed as:

$$q_{eq} = f(P) \; at \; constant \; T \qquad\qquad 2.5$$

When dealing with more adsorbates the adsorption of component i not only depends on the pressure or its concentration in the bulk phase but also on the equilibrium concentrations of all other adsorbates:

$$q_{eq,i} = f\left(c_1, c_2, \dots, c_{N_C}\right) \; at \; constant \; T \qquad\qquad 2.6$$

q_i expresses the loading of component i onto the adsorbent in mol / (kg framework).

This relationship also holds when using partial pressures of all components instead of equilibrium concentrations:

$$q_{eq,i} = f\left(p_1, p_2, \dots, p_{N_C}\right) \; at \; constant \; T \qquad\qquad 2.7$$

Literature shows lots of different isotherm models based on different model assumptions. Some of the considerations are:

(1) Monolayer / multilayer adsorption: monolayer adsorption assumes that only one molecule of adsorbent can adsorb on one adsorption site, whereas multilayer adsorptions allows for multiple adsorbent molecules to adsorb on one adsorption site.
(2) Homogeneous / heterogenous surface: homogeneous surfaces assume equal adsorption sites along the entire surface. Heterogenous surfaces indicate differences in adsorption sites along the material.
(3) (No) Lateral interactions between adsorbed molecules: lateral interactions between already adsorbed molecules can influence the behaviour of adsorbed molecules and therefore influence the adsorption isotherms.

Some of the isotherm models which will be used to model the PSA process will be described here. Starting off with the Langmuir model; this model assumes a homogeneous surface with monolayer adsorption and no lateral interactions.

$$q_{eq}(p) = q^{sat} \frac{bp}{1 + bp} \quad \text{with } q^{sat} \geq 0 \text{ and } b > 0 \qquad 2.8$$

q^{sat} being the saturation capacity and *b* the coefficient of adsorption.

Sips model:

$$q(p) = q^{sat} \frac{(bp)^{1/v}}{1 + (bp)^{1/v}} \qquad 2.9$$

v being the parameter characterising the heterogeneity of the system allowing for deviations from Langmuir model's assumptions. It both accounts for surface heterogeneity and non-ideal adsorption behaviour such as multilayer adsorption or lateral interactions. Values of unity indicate a material with homogeneous binding sites and the isotherm model becomes the Langmuir model. This model is a semi-imperical equation.

Langmuir-Freundlich model:

$$q(p) = q^{sat} \frac{bp^v}{1 + bp^v} \qquad 2.10$$

Just like the Sips model the Langmuir-Freundlich model does not have correct limiting behaviour at low pressure. At low pressure there should occur a Henry's regime, characterised by the Henry coefficient which is the slope of the isotherm at very low pressure:

$$H_k = \lim_{p \to 0} \frac{q(p)}{P} = \lim_{p \to 0} \frac{dq}{dp} \qquad 2.11$$

In this infinite dilution regime there is no adsorbate-adsorbate interaction and adsorption is linearly related to the affinity of the adsorbate. The Henry regime only occurs when $v = 1$.

2.3.3 Adsorption-kinetics model

For the modelling of the kinetics one has to make an assumption on the absorbent characteristics i.e. homogeneous/heterogeneous, porous/non-porous. One of the diffusion models is called the homogeneous-solid diffusion model (HSDM). This model assumes adsorption to occur on the solid surface followed by diffusion of the adsorbate into the adsorbent particle. The model is often used for microporous-mesoporous materials such as zeolites [43]. The intraparticle diffusion is calculated according to the following equation

$$\frac{\partial q_i}{\partial t} = \frac{D_e}{r^2} \frac{\partial}{\partial r} \left(r^2 \frac{\partial q_i}{\partial r} \right) \qquad 2.12$$

q_i being the concentration of species i inside the adsorbent, D_e the effective diffusivity, *r* is the radial distance from the centre of the adsorbent particle. For the uptake rate of a gas into the adsorbent a first-order linear-driving-force (LDF) can be applied.

Assuming the uptake rate is proportional to the linear difference between the concentration of the gas at the outer surface of the adsorbent (the equilibrium adsorption capacity) and in the bulk.

$$\frac{\partial q_i}{\partial t} = k(q_{eq,i} - q_i) \qquad 2.13$$

k is the rate constant which is approximated by : $\quad k = \frac{15D_e}{r_p^2} \quad , \quad \frac{D_e}{r_p^2}$ expressing the diffusion-time constant.

This simple LDF model is known to underestimate the adsorption rate according to Ma et al. [45]. An improved LDF is derived from the parabolic concentration profile of the interparticle adsorbate expressed in equation [46].

$$\frac{\partial q_i}{\partial t} = \frac{15D_e}{r_p^2}(q_{eq,i} + 0.2789q_{eq,i}e^{\frac{-q_i}{2q_{eq,i}}} - q_i) \qquad 2.14$$

2.3.4 Heat Transfer Model

The heat transfer model of a PSA cycle is part of the bigger fluid flow model. Current PSA modelling practices often use 1D adsorption models. Meaning temperature, pressure and concentration only differ in the longitudinal direction and not in the radial direction. If these variables do differ in the radial direction one can speak of radial dispersion. Important to consider is that heat transfer models differ when making different assumptions based on the transfer of energy in the form of heat. Equations below come from three different heat transfer models by Ali et al. (2021) [47]. A big variable in the heat transfer model is the enthalpy of the adsorbed phase H_i

$$H_i = \rho_s C_p w_i \frac{\partial T_{sur}}{\partial t} \qquad 2.15$$

ρ_s and C_p are the solid density and heat capacity, w_i is the adsorbent mass fraction and T_{sur} the adsorbent's surface temperature. During adsorption heat is released which is expressed by the equation below where ΔH_i is the heat of adsorption (assumed constant).

$$HT_i = \frac{\partial w_i}{\partial t}\Delta H_i \qquad 2.16$$

To get the total heat of adsorption these HT components have to be summed, $\rho_s \sum_i(-HT_i)$

When considering a non-isothermal situation where the gas temperature and adsorbent temperature differ, another equation has to be added. In thermal equilibrium: $T_g = T_a$

$$\dot{q}_s = C_{p,a}a_g(T_g - T_a) \qquad 2.17$$
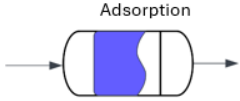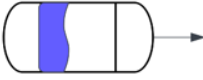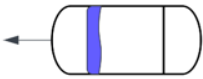
q_a describing the amount of heat being transferred per unit volume of the adsorbent, $C_{p,a}$ as the heat transfer coefficient of the adsorbent and a_g being the change in concentration of the gas. The last term takes into account that there is also heat transfer to the wall of the column.

$$\frac{4h_T}{D_C}(T_g - T_{wall}) \qquad 2.18$$

h_T being the total heat transfer resistance of the wall and D_C the diameter of the column.

When working with these kind of differential equations boundary conditions are of big importance. One way of implying them is by using the build-in conditions which are prescribed by Aspen and are shown in **Table 1**. There we see the boundary conditions for the different steps within the PSA process.

Table 1: *Aspen nummerical boundary conditions for each PSA cycle step [48]. Z being in the direction of the column going from left to right.*

Step	Z = 0	Z = L
Adsorption	$u_{0,inlet}C_{inlet,i}\big|_{z=0} = u_0 C_i - \varepsilon_b D_{ax} C \frac{\partial y_t}{\partial z}$ $u_{0,inlet}C_{inlet,i}\big|_{z=0} = u_0 C$	$P\big|_{z=L} = P_{outlet}$ $\frac{\partial T_g}{\partial t}\big|_{z=L} = 0$ $\frac{\partial C_t}{\partial t}\big|_{z=L} = 0$
Equalization and co-current depressurization	$u_0\big|_{z=0} = 0$ $\frac{\partial T_g}{\partial t}\big|_{z=0} = 0$ $\frac{\partial C_t}{\partial t}\big|_{z=0} = 0$	$P\big|_{z=L} = P_{outlet}$ $\frac{\partial T_g}{\partial t}\big|_{z=L} = 0$ $\frac{\partial C_t}{\partial t}\big|_{z=L} = 0$
Blowdown	$P\big|_{z=0} = P_{outlet}$ $\frac{\partial T_g}{\partial t}\big|_{z=0} = 0$ $\frac{\partial C_t}{\partial t}\big|_{z=0} = 0$	$u_0\big|_{z=L} = 0$ $\frac{\partial T_g}{\partial t}\big|_{z=0} = 0$ $\frac{\partial C_t}{\partial t}\big|_{z=L} = 0$
Purge	$P\big|_{z=0} = P_{outlet}$ $\frac{\partial C_t}{\partial t}\big|_{z=0} = 0$ $\frac{\partial T_g}{\partial t}\big|_{z=0} = 0$	$u_{0,inlet}C_{inlet,i}\big|_{z=L} = u_0 C_i - \varepsilon_b D_{ax} C \frac{\partial y_t}{\partial z}$ $u_{0,inlet}C_{inlet,i}\big|_{z=L} = u_0 C$
Equalization pressurization and Pressurization	$u_0\big|_{z=0} = 0$ $\frac{\partial T_g}{\partial t}\big|_{z=0} = 0$ $\frac{\partial C_t}{\partial t}\big|_{z=0} = 0$	$u_{0,inlet}C_{inlet,i}\big|_{z=L} = u_0 C_i - \varepsilon_b D_{ax} C \frac{\partial y_t}{\partial z}$ $u_{0,inlet}C_{inlet,i}\big|_{z=L} = u_0 C$

2.4 Economics

When examining the feasibility of a technology money plays a big role. A project being economically viable often determines whether it will be implemented or not. The economic landscape of oxygen production can be a complex terrain when considering aspects like capital investments, operational costs, local electricity prices and emission factors. Considering hospitals in developed countries mostly use liquified oxygen (LOX) from CAS, it is important to compare both technologies on a cost basis. **Table 2** below gives an insight on the fixed capital investment that comes with implementation either PSA or LOX in Germany. Note that this table is from a consumers perspective, so capital investments of CSA units are not in it, storage capacity for LOX are. All prices are in EUR.

Table 2: *Total fixed capital investment comparison between PSA and CSA, both systems producing 101 Nm³/h of oxygen at 99.5% purity [49].*

Item	Description	PSA	LOX	
ISBL	Equipment	243,600*1	68,500*2	
ISBL	Equipment – accesories	0	2,400	
ISBL	Piping, electrical lining	25,800	6,850	
ISBL	Measurement & regulation	3,700	2,600	
ISBL	Total ISBL plant costs	18,300	3,425	+
OSBL	Offsite costs	291,400	83,775	
EC	Engineering costs	14,570	4,189	
CoC	Contingency charges	15,299	4,399	+
FIC	Total fixed investment cost (CAPEX)	336,568	96,762	

*1 PSA: compressor unit = 74,500 EUR, air treatment line = 20,000 EUR, PSA unit = 149,100 EUR.
*2 LOX: storage tank = 56,600 EUR, two evaporators = 4,000 EUR, automatic switcher between evaporators = 7,900 EUR

A big part of the initial investment for a PSA unit comes is the form of equipment like compressors, air treaters and the unit itself i.e. the packed column beds, valves etc. These costs are much lower for the LOX technology as you only need a storage tank, two evaporators and a switch between the evaporators. PSA units require more piping and electrical lining to control the dynamic process. Making the inside battery limits (ISBL) plant costs for a PSA unit a factor 3.5 times bigger than that of the LOX technology. The outside battery limits (OSBL) costs like engineering and offsite costs, for a PSA plant are also 3.5 times bigger. One of the driving forces behind a PSA plant is that, if well-designed, production costs for oxygen can be kept lower than that of the oxygen bought from a LOX-producer. Especially in times of big demand and increased LOX-prices this would be beneficial. **Table 3** shows what production costs should be considered when evaluating both techniques.

Table 3: *Production cost comparison between PSA and CSA, both systems producing 101 Nm^3/h of oxygen at 99.5% purity during 8,160 operating hours per year [49].*

Item	Description		PSA	LOX	
VOC	Electric energy		69,654*[1]	570	
VOC	Raw material + transporation			104,410*[2]	
VOC	Operating labour, Supervision, Maintenance, Consumables, Reserve		20,350*[1]	9,970*[2]	+
	Variable operating costs		90,004	117,258	
FOC	Deprecitation		33,657	9,677	
FOC	Taxes, interest & insurance		306	88	+
	Fixed operating costs		33,963	9,765	+
	Operating cost (OPEX)		123,967	127,023	
	General expenses		3,757	3,757	+
	Total product costs	[Eur y^{-1}]	127,724	130,780	
	Total product costs	[Eur Nm^{-3}]	0.155	0.167	
	Total product costs	[Eur kg^{-1} O$_2$]	0.115	0.118	

*[1] PSA: electricity = EUR 77.6 MWh^{-1}, labour cost = 13.6 h^{-1}. (2019)
*[2] LOX: electricity = EUR 77.6 MWh^{-1}, labour cost = 13.6 h^{-1}, LOX transportation (150 km) = EUR 47. (2019)

Looking at the production costs of oxygen for both technologies we see the following. Electrical energy accounts for approximately 60% of the operating costs for PSA. Maintenance and depreciation of the equipment are the second largest costs at 30%. High initial capital investments are responsible for it. Looking at the LOX technology it shows that 81% of production costs come from buying liquified oxygen. Economic comparisons between PSA and LOX technology are extremely country dependent. This is caused by different electricity pricing and regulations along with labour costs. A good way of seeing this is by looking at **Table 4**. Electricity prices differ for local oxygen production and LOX technology. As this difference in prices in Germany is lower than in the Czech Republic, PSA turns out to be the cheapest solution in Czech Republic but not in Germany.

Table 4: *Production cost comparison between Germany and the Czech Republic, all systems producing 101 Nm^3/h of oxygen at 99.5% purity during 8,160 operating hours per year. [49]*

Item	Unit	Czech Republic		Germany	
		PSA	LOX	PSA	LOX
Electricity	EUR	77.6	139.6	156.9	180.9
Labour cost	MWh^{-1}	13.6	13.6	41.2	41.2
LOX	EUR h^{-1}	-	93	-	105
Transport (150 km)	EUR t^{-1}	-	47	-	50
Total product cost	EUR h^{-1}	15.66	16.03	26.75	20.09
Total product cost	EUR kg$^{-1}_{O2}$	0.115	0.118	0.196	0.147

2.5 Oxygen Delivery in Hospitals: Current Practices, Safety Measurements & Regulatory Frameworks

The feasibility of PSA plants in the Netherlands strongly depends on how well it fits within regulatory frameworks and current practices. Ideally only the liquified oxygen storage tank is replaced by a PSA unit, maintaining most of the current piping and other equipment. As there is no room for failure safety measurement are of huge importance. Often these safety measurements come from regulatory frameworks and are implemented within current practices. This paragraph will have a closer look at these aspects.

2.5.1   Current Practices

As mentioned before most developed country hospitals nowadays make use of liquefied oxygen originating from a CAS process. This liquefied oxygen is then stored in one or more storage tanks nearby the hospital. The oxygen can then be delivered to patients through a pipeline system after evaporation. For a better understanding of the system, **Figure 22** shows a schematic representation of a 2-storage bulk oxygen delivery system for a hospital. This paragraph will only focus on the operation of the process. Safety measurements will be discussed in the next paragraph.
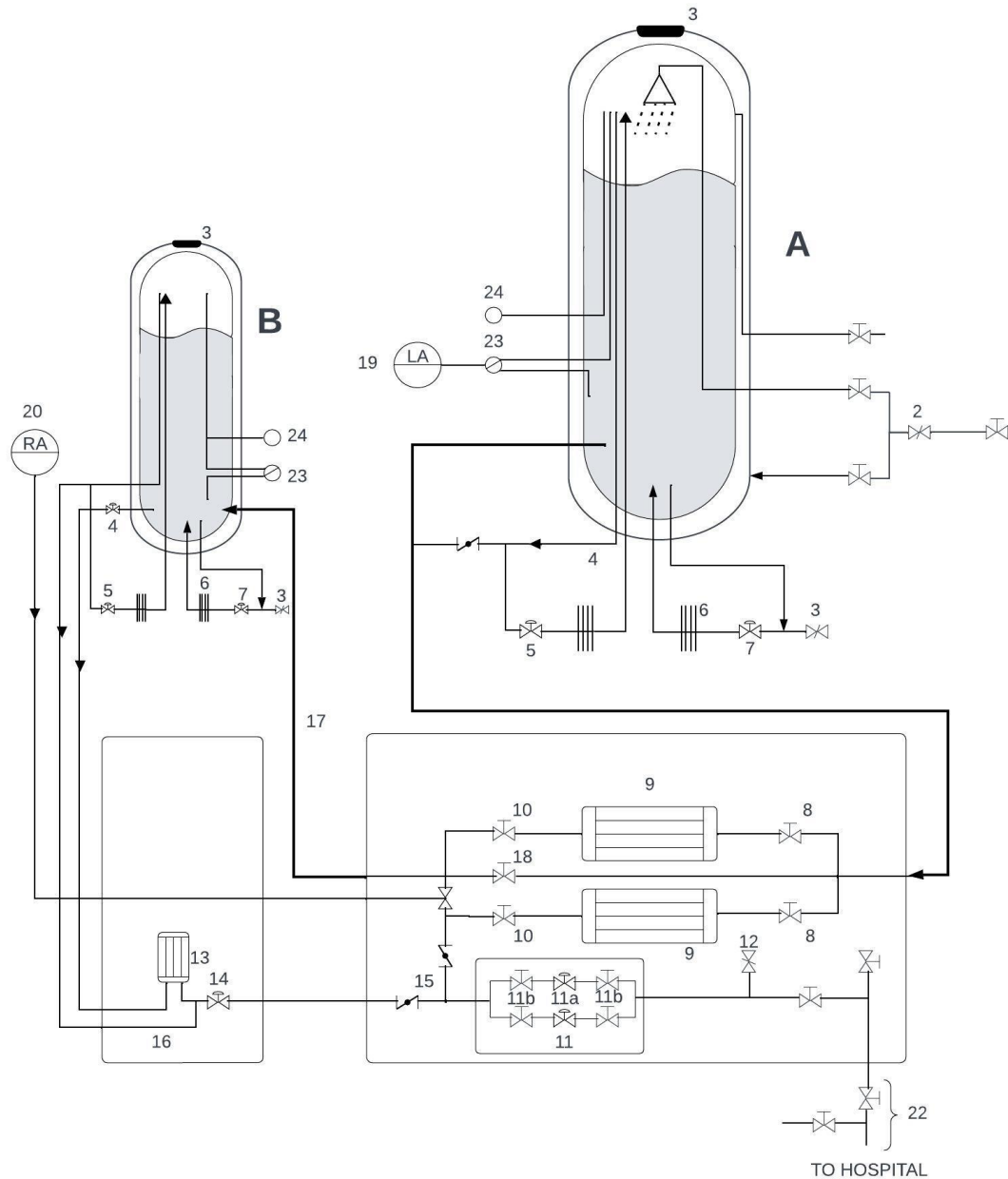
Figure 22*: Schematic overview of a general hospital's bulk liquid oxygen delivery system [50].*

(A) and (B) indicate the two reservoirs, both reservoirs stand in the same enclosure. The vessels are often made of stainless steel and have a double shell-structure, separated by a gap with a vacuum in it. Liquefied oxygen is delivered to the system through line (2) which separates into a bottom and top fill line. Oxygen at the top is sprayed into the vessel to lower the temperature and therefore decrease gas pressure. Vaporization of some of the oxygen maintains the gas pressure inside the system. The vaporized oxygen is introduced into the economizer circuit i.e. number (4). Where the gas pressure regulator (5) regulates the amount of gas in the economizer circuit. To regulate the supply pressure at a constant level, gas or liquid is channelled through a small vaporizer beneath each vessel, indicated with number 6. Along with number 3 (reservoir pressure relief valve), 7 (liquid regulator) and the economizer circuit this is called the pressure-building circuit. Liquid oxygen leaves the vessel through the bold lines near the bottom left and is then led to the main vaporizers (9) via a cryogenic liquid-control valve (8). These aluminium alloy vaporizers have fins to increase heat adsorption from the atmosphere. While passing through the vaporizers the liquid oxygen will turn into a gas.

The gaseous oxygen then passes to the main supply regulators which are inside the box at the bottom of the figure. (11) indicating the primary line pressure regulator, (11a) the secondary line regulator and valves to isolate regulators for repair (11b). (12) indicates a pressure relief valve for the main pipe-line. If necessary the reserve (B) can be used, which is a smaller version of (A). Vaporized oxygen from the reserve is added to the main piping system (16), requiring the reserve to be refilled even when not in use. This is done via line (17) which transports liquid oxygen from the main vessel. The reserve has its own vaporizer followed by a reserve line pressure regulator (14).

Often hospitals even make use of three oxygen sources, leading to a 3-source system and therefore providing even more security of delivery. Often the third source is a cylinder manifold consisting of several cylinders containing pressurized (gasesous) oxygen. The manifold is divided into two equal banks of oxygen cylinders with a centrally located control panel. This control panel contains a bank-switch and pressure regulator. Only one bank should operate at any one time so that the other can be on stand-by or can be replaced. The cylinders within a bank are open and connected through non-return valves to a central pipe.

2.5.2   Safety Measurements

Considering the importance of sufficient, continuous, high quality oxygen production safety measures are of huge importance. Some were already shortly discussed in the previous paragraph like the 3-source system. This paragraph will highlight additional measures. Making a distinction between process safety measures and product safety measures. Process safety measures focus mainly on sufficient and continuous delivery of oxygen. Product safety measures ensure meeting quality requirements.

Process safety measures:

- o   Pressure relief valves are fitted on the vessels to prevent pressures exceeding the safety point.
- o   If the vapor pressure inside one of the vessels drops below a set point, a regulator will open and allow some oxygen into the vaporizer. Pressure levels are measured by vapor pressure gauges (24).
- o   Elongated valve stems for valves with liquid oxygen going through them ensure the valve-stem packing is protected from the cryogenic liquid.
- o   Valves (10) behind the main vaporizers allow for maintenance on the vaporizers during production. This might be needed frequently as ice forms on the vaporizers, blocking heat transfer which could potentially cause the oxygen to still be a liquid after the vaporizers. This will damage the pressure regulators and pipelines.
- o   Pressure relieve valve behind the main-line regulator to bring down the pressure if the line pressure exceeds a certain amount above normal levels.
- o   A low-liquid-level alarm (19) goes off as soon as the liquid level drops below a certain threshold.
- o   A reverse-in-use alarm (20) goes off as soon as the supply pressure in the main supply line drops below a certain pressure.
- o   The main line pressure alarm (21) senses upwards or downwards variations in the main line pressure.
- o   The main shut-off valve allows for complete shut-off of the oxygen supply and is located inside the hospital.
- o   A valve with T fitting (22) allows for emergency oxygen supply when main supply where to be damaged. This could for instance be the cylinder manifold.
- o   The total storage capacity of the cylinder manifold should be a one week's supply, with a 3-day supply of spare cylinders kept in the manifold room.

Product safety measures [51], [52], [53]:

- o LOX provided to the vessels should be tested before supplying to the system.
- o Oxygen gas cylinders should be stored at standard room temperature.
- o Pure water has to be used to hydrate oxygen.
- o Allow for rotation of cylinders, so that the oldest are used first.
- o If using an oxygen concentrator, a clean well-ventilated space should be chosen for placement.
- o Avoid rotation equipment which can generate particles by shearing surfaces against each other.
- o Avoid crevices as they can be a place where particles accumulate. For instance prefer butt-welded joints instead of fillet welder or socket welded joints.
- o Use filters and clean them frequently. For instance according to a predefined cleaning plan.
- o Avoid component and system vibration. Propper supporting and sizing is important to avoid vibrations which could shake loos particles into the system.

2.5.3 Regulatory Frameworks

This paragraph will focus on the regulatory frameworks concerning medical oxygen supply. As the focus will be on 'het Reinier de Graaf' hospital, only Dutch regulations will be discussed.

Medicines, which oxygen is one of, need to meet high purity requirements. Medical gasses are only allowed to be provided under the supervision of a hospital's pharmacist. In construction of new gas systems, renovations, maintenance and management, various standards are applicable, which gas systems must comply with. These standards contain the minimum requirements for installation, functions, implementation, documentation, testing, certification and validation of the medical gases installation. All this is to ensure the reliable supply and required quality of the systems and gases for which they are intended. Medical gas systems and distribution systems must be designed, assembled, tested and validated according to these standards.

As a result. these gas distribution pipelines should contain only these specific gases and that they are correctly connected with gas-specific couplings. Also, the quality of the gas offered to the take-off points must have been tested and demonstrated.

In the Netherlands the standards are according to: NEN-EN-ISO; it indicates that a particular standard has been adopted and endorsed by the Dutch Standards Institute (NEN), conforms to European standards (EN), and is also in line with international standards set by the International Organization for Standardization (ISO). Another standard which is used is the NVN-ENV, it generally indicates a Dutch preliminary standard that is also aligned with the European pre-standardization process. The most importance Dutch regulations and their applications are listed below together with some of their key take-aways,

- o NEN-EN-ISO 9170-1:2008 en: take-off points for medical gases. This standard is specifically designed to ensure that gas-specific components are used and that there can be no mix-ups with other gases.

    - ▪ The hospital pharmacist, in joint consultation with the purchasing department, directs the selection of the manufacturer and the assessment for reliability and quality requirements of the supplier.

- - The supply system shall be composed of a minimum of three supply sources so that if one circumstances one source fails, a continuous supply of gas is still guaranteed.
    - The sources must each be able to function completely independently and supply the entire gas demand.

  - NEN-EN-ISO 7396-1:2007 en: pipeline systems for compressed medical gases and vacuum. This section specifies requirements for design, installation, operation, documentation, testing and commissioning of pipeline systems for compressed medical gases, compressed air and vacuum in health centers to ensure a continuous supply of appropriate gas.

    - The piping systems are of seamless, round copper tubes, grease-free and capped (according to standard NEN-EN 13348:2008 en).
    - In medically used rooms of class 3, according to NEN 1010:2007+C1:2008/A1:2011+C1:2011 nl, the metal pipes for gas gases must be fitted with isolation couplings at those places where these pipes enter or leave these spaces.
    - For maintenance and safety purposes, so-called zone block service and purge valves are mounted in medical gas piping systems.
    - For signalling alarms and malfunctions of the medical gases and to ensure the supply of medical gases in case of a calamity for zones like operating rooms, individual quick shut-off valves are always fitted.

  - NVN-ENV 737-6:2003 en: piping systems for medical gases. In this section, the dimensions and assignment of the fittings for the sampling points for the medical gases and vacuum are listed.

  - Medicines Act. This law refers to the regulations in the European Pharmacopoeia. Regulating the quality of drugs like oxygen. Providing a monograph for medical gasses with requirements for their identity and purity.

  - GMP quality guidelines. This method of production, called Good Manufacturing Practice (GMP), is required for the production of medical gases.

  - Substance guidelines from the hazardous substances publication series (PGS). In addition to general information on the hazard properties of a substance, the substance-specific guidelines contain detailed regulations on technical and organizational measures. For example, bulk oxygen tanks must comply with the guideline PGS 9 (liquid oxygen storage). Storage of packaged hazardous substances (including gases) must comply with guideline PGS 1.

3. Nummerical Modelling

The aim of this chapter is to show how each step of the process has numerically been modelled and linked with its subsequent step. For the modelling Python and Ruptura [54] have been used. Ruptura is a simulation code for breakthrough, ideal adsorption solution theory computations and fitting of isotherm models. With certain adjustments it can be used to model a PSA cycle.

3.1 Determining the mixture isotherms

One of the aspects that will come back in each cycle step are the multi-component adsorption equilibria. Direct measurements of mixture adsorption equilibria is complicated and time consuming. Using theoretical models is currently still the default tool. One thermodynamic framework for computing the mixture adsorption which is thermodynamically consistent and which only uses pure component data is the Ideal Adsorption Solution Theory (IAST). This theory produces a set of powerful equations which enable you to do the following:

- If the total pressure and the mole fractions in the gas phase of the N_c components are known, then the following unknowns can be computed:
    - N_c mole fractions in the adsorbed phase (x_i)
    - N_c sorption pressures (p_i^*)
    - the total amount adsorbed and the component amount adsorbed
- If the adsorbed mole fractions x_i and the total adsorbed amount q_T are known, then the following can be calculated:
    - N_c mole fractions in the gas phase (y_i)
    - N_c sorption pressures (p_i^*)
    - the total pressure (P_T)
- If the adsorbed mole fractions x_i and the total pressure are given, then the following unknowns can be calculated:
    - N_c mole fractions in the gas phase (y_i)
    - N_c sorption pressures (p_i^*)
    - the total adsorbed amount q_T

The pure components isotherm equation form is arbitrary for usage in IAST. However, especially the low pressure data needs to be accurately represented and errors at low pressures lead to large errors in multi-component calculations. The IAST makes use of the so called reduced grand potential, indicated with ψ, which provides a measure of the stability of the adsorbed phase relative to the gas phase. In practical terms, the reduced grand potential is often used in theoretical modelling and simulations to predict adsorption behaviour, such as determining adsorption isotherms, understanding surface coverage, and studying the thermodynamics of adsorbate-surface interactions.

Below shows some insight in determining the adsorption isotherm of a gas mixture based on single component Langmuir-Freundlich isotherms with known parameters.

Component 1: $\quad q_1(P) = q_1^{sat} \dfrac{b_1 P^{v_1}}{1 + b_1 P^{v_1}} \qquad$ Component 2: $\quad q_{22}(P) = q_2^{sat} \dfrac{b_2 P^{v_2}}{1 + b_2 P^{v_2}}$

$$p_i^*(\psi) = \frac{1}{b_i^{1/v_i}} \left[exp\left(\frac{v_i \psi}{q_i^{sat}}\right) - 1 \right]^{1/v_i}$$

3.1

This reduced grand potential can be found by using a root finding algorithm considering that is has to be consistent with the adsorbed phase mole fractions adding up to 1.

$$\sum_{i=1}^{N_c} x_i - 1 = \sum_{i=1}^{N_c} \frac{y_i P}{p_i^*(\psi)} - 1 = 0 \qquad \qquad 3.2$$

Solving the IAST has several numerical methods. Some of them are: the nested loop algorithm, FastIAS, Modified fast IAS (IAST) and Segregated IAST (SIAST). The downside of the nested loop algorithm is its slower convergence and dependency on a first guess. The FastIAS is already an improvement on the nested loop algorithm but is inferior to the Modified fast IAS, which is one of the options in Ruptura alongside with the SIAST. The modified fast IAS, abbreviated just as IAST, is fast, robust and will converge unless physically unrealistic sorption pressures are obtained. The SIAST approach does not consider the available adsorption volume as a continuous space but divides it into distinct adsorption sites. The different sites are considered uniform, making it possible to apply IAST to every individual site. For these reasons SIAST works better when there are distinct adsorption sites and the components inside the gas prefer a certain adsorption site over the other.

The goal of each method is to find the reduced grand potential. From this potential and the known parameters the sorption pressures can be derived. Applying these sorption pressures in to **Equation 3.3** :

$$x_i = \frac{y_i P}{p_i^*} \qquad \qquad 3.3$$

The adsorbed phase mole fractions are known as well. With the reduced grand potential and the adsorbed phase mole fractions, the total adsorbed amount q_T can be calculated as well as the loadings of the individual components.

$$q_T = \frac{1}{\sum_{i=1}^{N_c} \dfrac{x_i}{\dfrac{q_i^{sat} \cdot b_i \cdot p_i{}^{v_i}}{1 + b_i \cdot p_i{}^{v_i}}}} \qquad \qquad 3.4$$

$$q_i = x_i \cdot q_T \qquad \qquad 3.5$$

Doing this for a range of pressures leads to mixture isotherms, depicted in **Figure 23**.
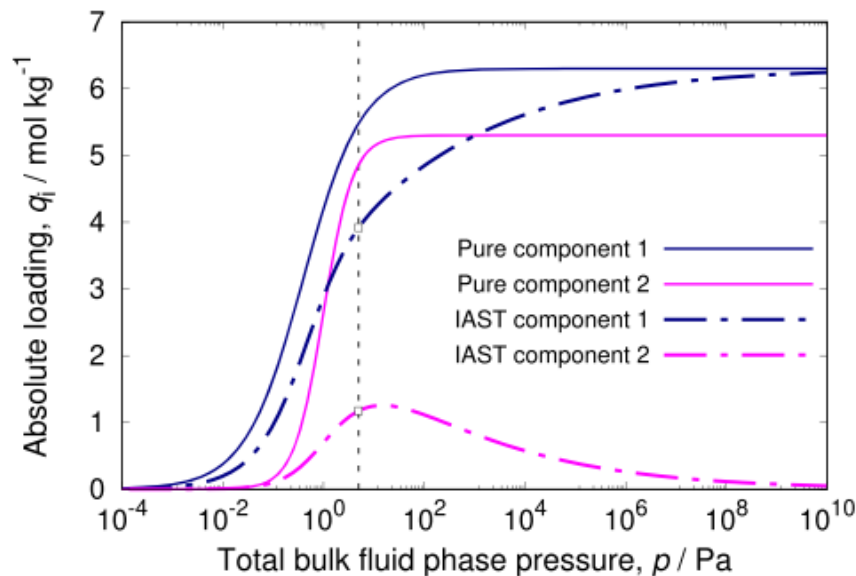
Figure 23: IAST prediction example for a binary mixture described by Langmuir-Freundlich isotherms [54].

To be able to determine $q_{eq,i}$ it is important to have the right Langmuir-Freundlich parameters for the gases inside air. **Table 5** shows the parameters for Oxygen, Nitrogen and Argon when using the Sips model, see **Equation 2.9.**

Table 5*: Parameters of the Monocomponent Sips equation for Oxysiv MDX at T_0 = 20 ˚C [36].*

	N$_2$	O$_2$	Ar
q_0^{sat} (mol/kg)	3.425	6.056	7.946
$b_0 \cdot 10^5$ (Pa^{-1})	3.356 x 10-1	2.665 x 10-2	1.610 x 10-2
$1/v_0$	0.8227	0.9797	0.9787
$\Delta H/R$ (K)	3160.37	1820.15	1673.81
α	0.0556		
χ	0.0213		

With,

$$q^{sat} = q_0^{sat} \ exp\left[\chi(1 - \frac{T}{T_0}\right]$$

$$b = b_0 \ exp\left[\frac{\Delta H}{RT_0}(\frac{T_0}{T} - 1)\right]$$

$$\frac{1}{v} = \frac{1}{v_0} + \alpha(1 - \frac{T_0}{T})$$

Which leads to the following Sips-parameters:

Table 6*: Ruptura-format parameters of the Monocomponent Sips equation for Oxysiv MDX at T = 20 ˚C.*

	N$_2$	O$_2$	Ar
q^{sat} (mol/kg)	3.245	6.056	7.946
b (bar^{-1})	3.36 x 10^{-6}	2.67 x 10^{-7}	1.61 x 10^{-7}
v	1.21551	1.02072	1.02176
$1/v$	0.8227	0.9797	0.9787

Note however that IAST makes use of the Langmuir-Freundlich adsorption model instead of the Sips model. Therefore parameter fitting of the original Sips data has been performed to retrieve the Langmuir-Freundlich parameters

Table 7*: Parameters of the Langmuir-Freundlich equation for Oxysiv MDX at T = 20 ˚C.*

	N$_2$	O$_2$	Ar
q^{sat} (mol/kg)	3.245	1.519	1.390
b (bar^{-1})	3.15 x 10^{-5}	1.75 x 10^{-8}	1.81 x 10^{-8}
v	0.8224	1.3581	1.3442

Equation numbers: 3.6, 3.7, 3.8

A Python code has been written which creates an image like **Figure 23**. Both the single component isotherms and the mixture isotherms have been plotted.
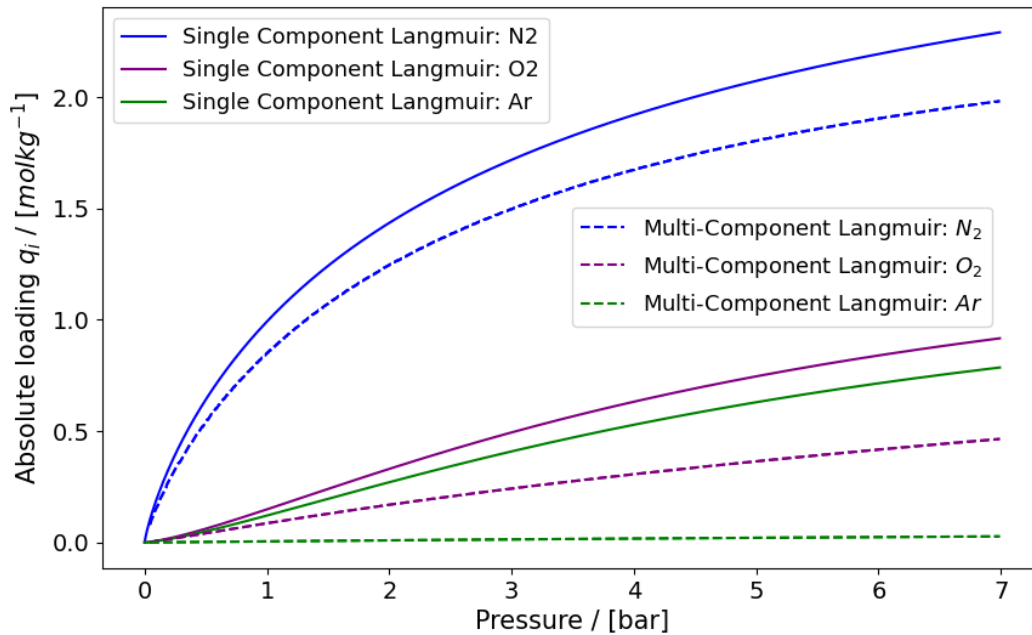
Figure 24: Single and multi-component isotherms of air components on Oxysiv MDX using IAST at 20 ˚C.

3.2 Feed Pressurization

The first step within the PSA-cycle is pressurizing air within a storage tank which can be fed into the adsorption columns. This pressurized air can then be released on the working pressure, Pw, for adsorption. Modelling this step gives valuable insights into what amount of time it takes for the storage tank to fill up with enough air to provide sufficient flow for the adsorption process. During this part of the modelling the storage tank is modelled as a continuously stirred tank reactor (CSTR) with the following assumptions:

- The gas is assumed to behave as an ideal gas both after the compressor and inside the storage tank.

$$c_i = \frac{y_i P}{RT} = \frac{p_i}{RT} \qquad\qquad 3.9$$

- No leaking takes place during pressurization or storage.

Considering the above assumptions, one can generate the following equation based on the conservation of mass for the change in amount of moles in the gas phase:

$$\frac{\partial n}{\partial t} = \frac{Q_{in}(P_c) \cdot P_c}{R \cdot T_c} \qquad\qquad 3.10$$

n	:	number of moles in the gas phase inside the tank	mol
Q_{in}	:	inlet flow	m^3/s
P_c	:	compressor pressure	Pa
R	:	gas constant	m^{3}Pa/Kmol
T_c	:	temperature after compression	K

This inlet flow is also time dependent as it will vary along the performance curve of the compressor. When the storage tank pressure is low, the inlet flow will be high but at a lower pressure. As the storage tank pressure starts to rise, the volumetric flowrate of the compressor decreases but the pressure increases. This dynamic can be better understood by looking at **Figure 30** which shows the performance curve of the compressor. For time integration the Forward Euler Method has been used due to the simplicity of the equation and the already accurate results of this method, as later will be shown during the model validation. The increased amount of moles in the gas phase can be related to a pressure increase through the ideal gas law. Leading to the following discretization with j indicating the time index.

$$n(j) = n(j-1) + \Delta t \cdot \frac{Q_{in}(P_c(j-1) \cdot P_c(j-1)}{R \cdot T_c} \qquad 3.11$$

$$\Delta n(j) = n(j) - n(j-1) \qquad 3.12$$

$$P(j) = P(j-1) + \Delta P(j) = P(j-1) + \frac{\Delta n(j) \cdot R \cdot T_c}{V} \qquad 3.13$$

V :   total volume of the storage tank m^3

3.3 Adsorption

The next step during the PSA process is the actual adsorption phase. For this phase Ruptura will be used with some slight corrections to the original code. The adsorption process is not modelled as CSTR but discretized into grid points along the adsorption column. Just like during the feed pressurization, there are some important assumptions that have been made during the modelling.

- The fixed bed is tubular and the zeolite particles are spherical and packed uniformly.
- No chemical reactions occur in the column.
- Axial dispersion is not considered.
- The pressure gradient does not vary with time and column position and is independent of the adsorption process.
- The fluid velocity will vary along the column because of pressure variations and adsorption.
- At the end of the vacuum step the loadings of all components equal their equilibrium loadings.

The amount of adsorbate that is adsorbed inside a control volume $dV = Adz$ can be calculated by a mass balance equation:

$$\dot{N_{accu}} + \dot{N_{ads}} = \dot{N_{adv}} + \dot{N_{disp}} \qquad 3.14$$

In words this formula states the following: the amount of particles that are adsorbed or accumulated inside the control volume equals the difference in the input and output of particles going through the control volume. Models that do consider the axial dispersion are called dispersed flow models, models which do not account for axial dispersion are plug-flow models. For this numerical simulation the latter model is assumed, leading to a reduced mass balance equation:

$$\dot{N_{accu}} + \dot{N_{ads}} = \dot{N_{adv}} \qquad 3.15$$

$$\dot{N_{accu}} = \epsilon_B dV \frac{\partial c_i(t,z)}{\partial t} \qquad 3.16$$

c_i being the adsorbate concentration of component i in the fluid phase, *z* the position along the length of the column, ε_B the bed void fraction and V the volume of the column.

$$\dot{N}_{ads} = (1 - \epsilon_B)\rho_p \frac{\partial \bar{q}_i(t,z)}{\partial t} \qquad 3.17$$

$\bar{q}_i$	:	loading of component i onto the zeolite	mol/kg
ρ_p	:	density of the zeolite particle	kg/m^3

$$\dot{N}_{adv} = -\epsilon_B dV \frac{\partial\big(v(t,z)c_i(t,z)\big)}{\partial z} \qquad 3.18$$

v being the interstitial velocity of the gas phase, related to the superficial gas velocity by u with: $v = \frac{u}{\epsilon_B}$

Applying the different terms for each component leads to the following main governing equation for the fixed-bed model:

$$\frac{\partial c_i(t,z)}{\partial t} = -\frac{\partial\big(v(t,z)c_i(t,z)\big)}{\partial z} - \frac{1-\epsilon_B}{\epsilon_B}\rho_p \frac{\partial \bar{q}_i(t,z)}{\partial t} \qquad 3.19$$

As the gas mixture is assumed to be an ideal gas, the equation can also be written in terms of the partial pressures of each component:

$$\frac{1}{RT}\frac{\partial p_i(t,z)}{\partial t} = -\frac{1}{RT}\frac{\partial\big(v(t,z)p_i(t,z)\big)}{\partial z} - \frac{1-\epsilon_B}{\epsilon_B}\rho_p \frac{\partial \bar{q}_i(t,z)}{\partial t} \qquad 3.20$$

With, $\frac{\partial \bar{q}_i(t,z)}{\partial t} = \frac{15D_i}{r_p^2}\big(q_{eq,i} - \bar{q}_i\big) = k_i\big(q_{eq,i} - \bar{q}_i\big)$ as the LDF model is used.

the Fickian diffusivity of component i (D_i)

D_i	:	the Fickian diffusivity of component i	m^2/s
r_p	:	the zeolite particle radius	m
k_i	:	mass transfer coefficient of component i onto the zeolite	1/s
$q_{eq,i}$	:	the equilibrium loading of component i	mol/kg

As mentioned in the assumptions the interstitial velocity is not constant along the column. To derive this velocity profile, the material balance for the overall mixture is considered by summing **Equation 3.20** for all components:

$$\frac{\partial P}{\partial t} = -\frac{\partial(vP)}{\partial z} - \sum_{i=1}^{N_c}\Big(RT\frac{1-\epsilon_B}{\epsilon_B}\rho_p k_i\big(q_{eq,i} - \bar{q}_i\big)\Big) \qquad 3.21$$

One of the other assumptions was the total pressure along the column being independent of time $\frac{\partial P}{\partial t} = 0$ and having a constant gradient along the column ,$\frac{\partial P}{\partial z} = constant$. Modifying **Equation 3.21** into the following equation:

$$P\frac{\partial v}{\partial z} = \sum_{i=1}^{N_c}\Big(RT\frac{1-\epsilon_B}{\epsilon_B}\rho_p k_i\big(q_{eq,i} - \bar{q}_i\big)\Big) - v\frac{\partial P}{\partial z} \qquad 3.22$$

This constant pressure gradient along the column is calculated by the Ergun equation:

$$\frac{\Delta P}{L} = \frac{150\mu L}{d_p^2} \frac{(1-\epsilon_B)^2}{(\epsilon_B)^2} v + \frac{1.75L\rho_f}{d_p} \frac{(1-\epsilon_B)}{(\epsilon_B)^3} v|v| \qquad 3.23$$

μ is the dynamic viscosity, d_p is the particle diameter, ρ_f the fluid density and $\frac{\Delta P}{L}$ the pressure ratio over the column with length L.

The equations for the rate of adsorption and velocity form a system of differential algebraic equations involving partial differential equations and non-linear algebraic equations. Within this research these equations will be solved by using the Finite Difference Method (FDM). Other methods are the Finite Element Method (FEM) and Finite Volume Method (FVM). The first-order spatial discretization of the equations for the mass transport, LDF and velocity are done as follows:

$$\frac{\partial p_i}{\partial t} = \frac{-v(j)p_i(j) - v(j-1)p_i(j-1)}{\Delta z} - RT(\frac{1-\epsilon_B}{\epsilon_B})\rho_p k_i(q_{eq,i}(j) - \bar{q}_i(j)) \qquad 3.24$$

$$\frac{\partial \bar{q}_i}{\partial t} = = k_i(q_{eq,i}(j) - \bar{q}_i(j)) \qquad 3.25$$

$$(\frac{\partial v}{\partial z})_j = \frac{v(j) - v(j-1)}{\Delta z} \qquad 3.26$$

Enabling us to write the function for the velocity at a certain grid point:

$$v(j) = v(j-1) - \Delta z \frac{1}{P} \sum_{i=1}^{N_c} (RT \left(\frac{1-\epsilon_B}{\epsilon_B}\right) \rho_p k_i \left(q_{eq,i}(j) - \bar{q}_i(j)\right) - \Delta z \frac{1}{P}(v(j-1)\frac{\partial P}{\partial z}) \qquad 3.27$$

Initial conditions

At the beginning of the adsorption step Ruptura assumes the column to be completely filled with a non-adsorbing carrier gas which has index i = 0:

$$P_{carrier\ gas}(t = 0, z) = P_W(t = 0, z)$$

Obviously when concentrating oxygen from air this is not the case since there is no carrier gas. Removing this carrier gas from the Ruptura code gives a lot of complications. For that reason a different initial condition was introduced for the partial pressures in **Equation 3.30** which is physically correct and does not require deleting the carrier gas and its initial condition. At the start of the adsorption step the entire column is at P_w with the loadings and partial pressures from the last timestep during the vacuum step. This timestep is indicated with j_{vc}.

$$v(t = 0, z) = v(0,0) \frac{P(0,0)}{P(0,0) + \frac{\partial P}{\partial z}j \cdot \Delta z} \qquad 3.28$$

$$P(t = 0, z) = P_W(t = 0, z) + \frac{\partial P}{\partial z}j \cdot \Delta z \qquad 3.29$$

$$p_i(t = 0, z > 0) = p_i(j_{vc}) \ and \ \ \overline{q}_i(t = 0, z > 0) = \overline{q}_i(j_{vc}) \ for \ i = 1, \dots, N_c$$

$$p_0(t = 0, z > 0) = P_w - \sum_{i=1}^{N_c} p_i(t = 0, z > 0) = P_w - \sum_{i=1}^{N_c} p_i(j_{vc}) \ and \ \overline{q_0}(t = 0, z > 0) = 0$$

3.30

At t = 0 also $\overline{q}_i(t = 0, z > 0) = q_{eq,i}(j_{vc})$, reducing **Equation 3.21** to:

$$\frac{\partial v}{\partial z} = -\frac{1}{P(z)}\left[v\frac{\partial P}{\partial z}\right]$$

3.31

Splitting the equation into variables and integrating both sides, gives:

$$P(t, z) = P^{in} + \frac{\partial P}{\partial z}z$$

3.32

$$v = v^{in}\frac{P^{in}}{P^{in}+\frac{\partial P}{\partial z}z}$$

3.33

<u>Boundary conditions</u>

At the column inlet the interstitial velocity of the gas phase is fixed as well als the partial pressure for each component.

$$v(t, z = 0) = \frac{u_{in}}{\epsilon_B} \ and \ p_i(t, z = 0) = y_i^{in} \cdot P_W$$

3.34

<u>Temporal discretization</u>

Time integration can be performed in many different ways. Either explicit or implicit in order to integrate the temporal derivatives. Within this process step one on the methods from the Runge-Kutta family will be used, namely the SSP-RK(3,3) which is a third order method with three stages. This method is popular due to its high accuracy and fewer number of steps than its higher order counter parts.

3.4 Depressurization

During this step the column is brought back towards atmospheric pressure by venting it to the ambient air through a valve. This way the pressure is already brought back from the working pressure P_W to P_{DP} without having to use the vacuum pump. P_{DP} being the pressure at which the vacuum pump is switched on. To estimate the gas flow through the valve the following empirical relation will be used:

$$Q_g = 21.76 \cdot K_v \sqrt{\frac{(P^2 - P_{atm}^2)}{SG \cdot T}}$$

3.35

With:

K_v	:	coefficient of flow	$\frac{Nl\sqrt{K}}{min\cdot bar}$
P	:	pressure inside the column	bar
SG	:	specific gravity of the gas inside the column	-
T	:	temperature	K

Due to the fact that the pressure decreases, desorption could start taking place. This would have a positive effect on the pressure since adsorbed gas molecules enter the gas phase again. The column will be modelled as a CSTR-tank during this step of the process with the following governing equations:

$$\frac{\partial n_i}{\partial t} = \frac{-Q_g \cdot y_i \cdot P_{atm}}{R \cdot T} - k_i \cdot \left(q_{eq,i} - \bar{q}_\iota\right) \cdot \rho_z \cdot V \cdot (1 - \varepsilon_B) \qquad 3.36$$

$$\frac{\partial n_i}{\partial t} = \frac{-21.76 \cdot K_v \sqrt{\frac{(P^2 - P_{atm}^2)}{SG \cdot T}} \cdot y_i \cdot P_{atm}}{R \cdot T} - k_i \cdot \left(q_{eq,i} - \bar{q}_\iota\right) \cdot \rho_z \cdot V \cdot (1 - \varepsilon_B) \qquad 3.37$$

$$n_i(j) = n_i(j-1) + \Delta t \cdot \left(\frac{-21.67 \cdot K_v \sqrt{\frac{P^2(j-1) - P_{atm}^2}{SG \cdot T}} \cdot y_i \cdot P_{atm}}{R \cdot T} - k_i \cdot \left(q_{eq,i}(j-1) - \bar{q}_\iota(j-1) \cdot \rho_z \cdot V \cdot (1 - \varepsilon_B)\right.\right) \qquad 3.38$$

$$\Delta n_i(j) = n_i(j) - n_i(j-1) \qquad 3.39$$

$$P(j) = P(j-1) + \sum_{i=0}^{N_c} \frac{\Delta n_i(j) \cdot R \cdot T}{V_g} \qquad 3.40$$

$$\bar{q}_\iota(j) = \bar{q}_\iota(j-1) + \Delta t \cdot k_i \cdot (q_{eq,i}(j) - \bar{q}_\iota(j-1)) \qquad 3.41$$

<u>Initial conditions</u>

The last timestep during the adsorption step is called j_{AD}. At this timestep the partial pressures and component loadings can be used as initial condition during the depressurization:

$$P(t = 0) = P_w \qquad 3.42$$

$$p_i(t = 0) = p_i(j_{AD}) \qquad 3.43$$

$$q_{eq}(t = 0) = q_{eq}(j_{AD}) \qquad 3.44$$

$$\bar{q}_\iota(t = 0) = \bar{q}_\iota(j_{AD}) \qquad 3.45$$

3.5 Vacuum

As the column pressure starts reaching the atmospheric pressure the outflow of gas starts to decrease. Then it is time to turn on the vacuum pump in order to bring the pressure level inside the column to sub-atmospheric pressure. Resulting in the following governing equation when modelling as a CSTR:

$$\frac{\partial n_i}{\partial t} = \frac{-Q_{out}(P) \cdot P}{R \cdot T} - k_i \cdot \left(q_{eq,i} - \bar{q}_\iota\right) \cdot \rho_z \cdot V \cdot (1 - \varepsilon_B) \qquad 3.46$$

Instead of a positive source term from the compressor, its now have a negative sink term which represents the vacuum pump. The vacuum pump flow is dependent on the pressure inside the column. The discretization for the time dependent variables which are not worked out below are the same as for the previous steps.

$$n_i(j) = n_i(j-1) + \Delta t \cdot \left(\frac{-Q_{out}(P(j-1)) \cdot P(j-1)}{RT}\right) - k_i \cdot \left(q_{eq,i}(j-1) - \bar{q}_\iota(j-1) \cdot \rho_z \cdot V \cdot (1 - \varepsilon_B)\right) \qquad 3.47$$

Initial conditions

The last timestep during the depressurization step is called j_{DP}. Leading to the following initial conditions when the vacuum pump is switched on:

$$P(t = 0) = P(j_{DP})$$

$$3.48$$

$$p_i(t = 0) = p_i(j_{DP}) \ \ for \ i = 1, \dots, N_c$$

$$3.49$$

$$q_{eq}(t = 0) = q_{eq}(j_{DP}) = \bar{q}_i(t = 0) = \bar{q}_i(j_{DP}) \ for \ i = 1, \dots, N_c$$

$$3.50$$

4. Experiments

Two experimental setups of small-scale PSA-devices have been built in the Process & Energy Lab at TU Delft. The main goal of these setups is to validate model parameters by running the process on a smaller scale. Some of the variables which are mentioned in the previous chapter play an import role in the model outcome and thus have to be verified by experiments. **Figure 25** shows the experimental setups.
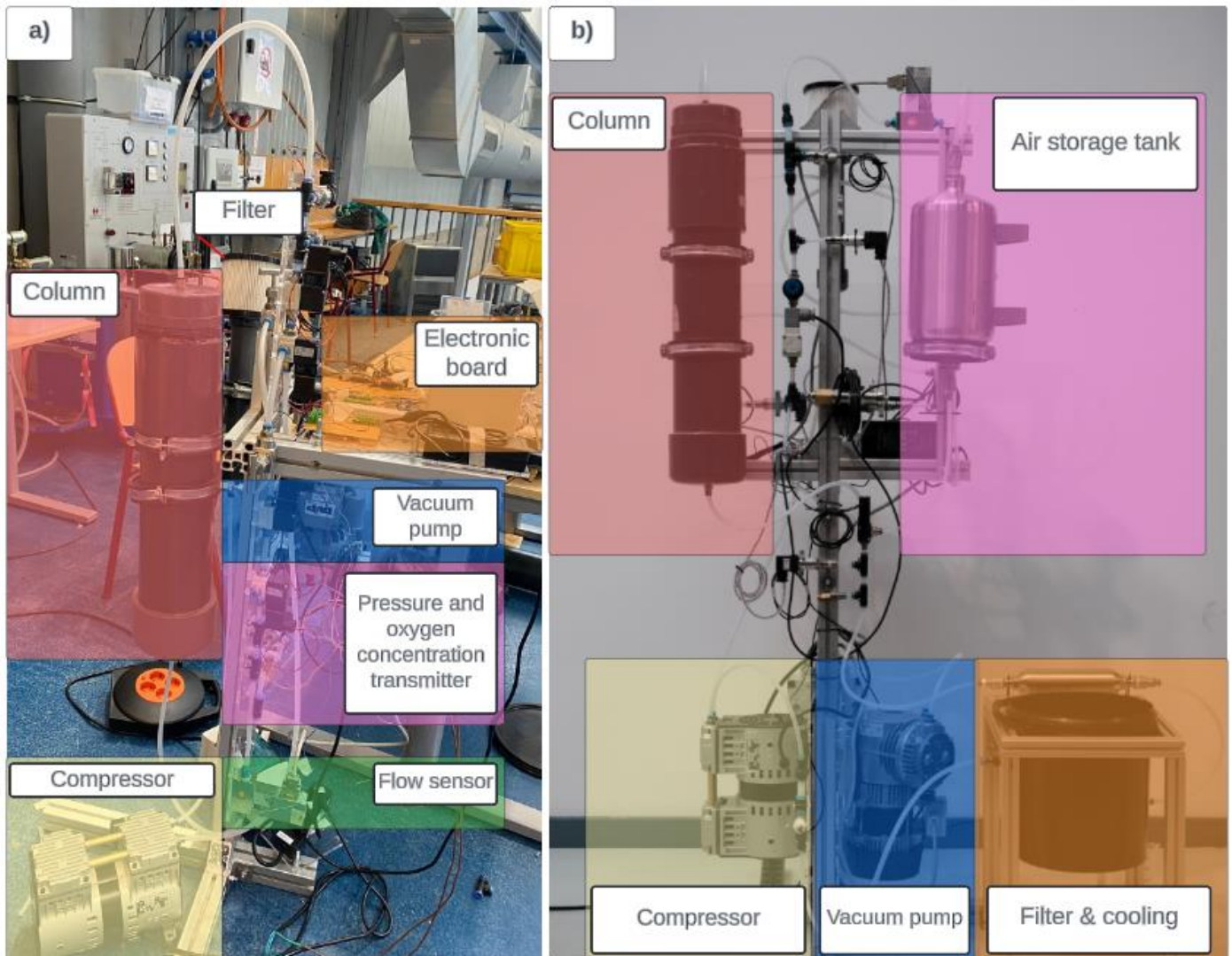
Figure 25: Picture of the experimental setups (a & b) in the P&E lab.

There were two primary reasons for using two distinct setups. First, some equipment had long delivery times. Second, during the course of this thesis, a group of bachelor students in mechanical engineering initiated a project aimed at enhancing the PSA setup. The outcome of their project is setup B, which included several improvements over setup A, thereby increasing the reliability of the model validation. For each validated model parameter, the corresponding experiment and the experimental setup used will be specified.

4.1 Experimental Setup

Table 8 shows the variables within a certain process step which can be validated with the experimental setup. As each process step requires different process configurations, **Figure 26** up to **Figure 29** represent the schematics of each process step in subsequent order. The figure also shows whether setup A or B has been used.

Table 8: Process variables in different cycle steps that will be validated by experiments.

Process Step	Process Variable
Feed Pressurization	Q_{in}
Adsorption	$u_{in}, \dfrac{\partial P}{\partial z}$
Depressurization	K_v
Vacuum	Q_{out}
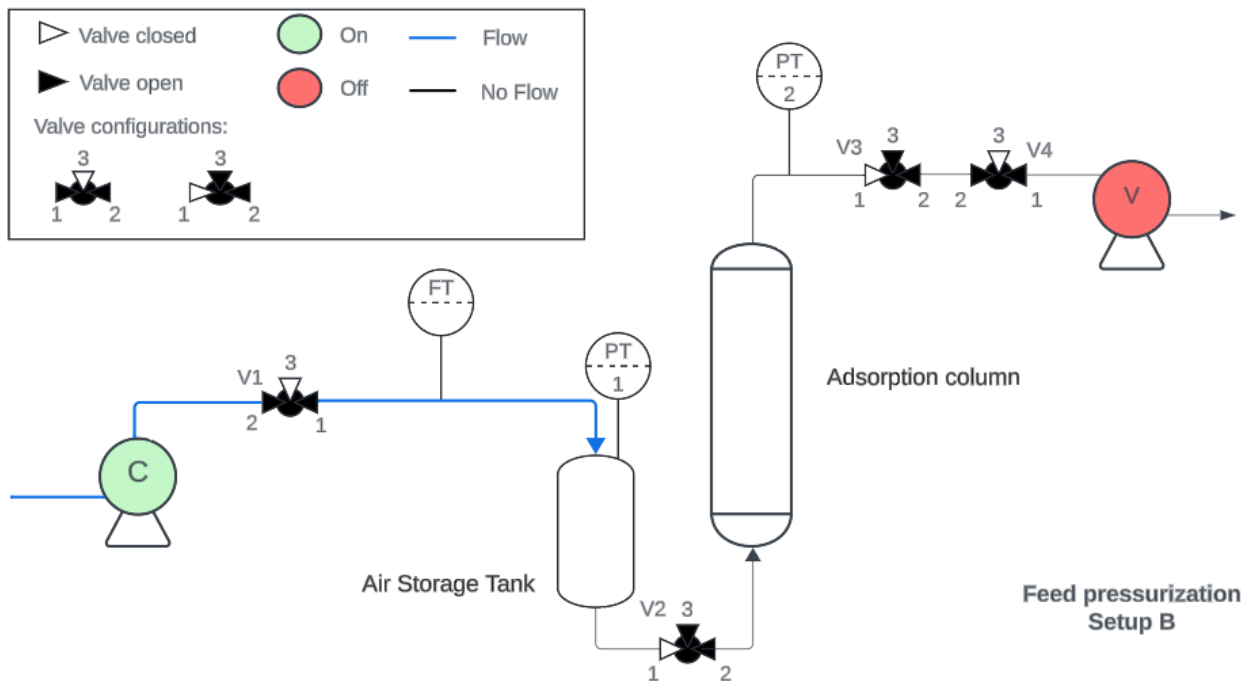
Figure 26: Schematic configuration feed pressurization, measuring compressor performance.

Within the configuration the storage tank is filled with air by the compressor (C). The digital flow transmitter (FT) in front of the tank measures the flow produced by the compressor, Q_{in}. At the same time the pressure at the top (PT1) of the tank is measured by a pressure transmitter. For the experiments three-way valves have been used. Valve opening 2 is always open and based on the electrical input either opening 1 or 3 gets opened. Resulting in two possible valve configurations 2-1 and 2-3 as shown in **Figure 26**.
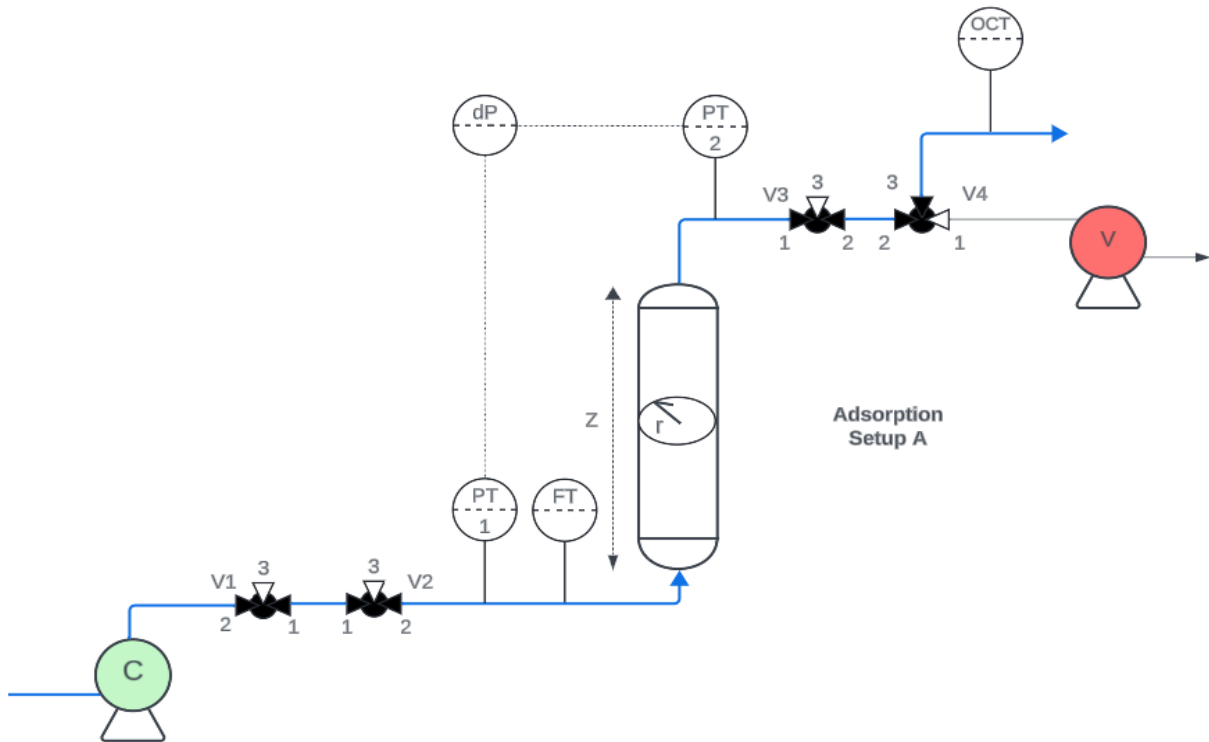
Figure 27*: Schematic configuration adsorption, measuring pressure drop and inlet velocity.*

During the adsorption step the enriched oxygen mixture should flow out of the column. In order to do this V3 is set to 2-1 and V4 to 2-3. This way the mixture passes through the oxygen concentration transmitter, OCT. The pressure measurements from PT1 and PT2 enable to calculate the pressure drop over the column, $\frac{\partial P}{\partial z}$. By knowing the flow through FT along with the column radius, r, an estimation can be made for $u_{in} = \frac{Q_{in}}{\pi r^2}$. During this step the column is at the working pressure P_w. Please note that in reality the feed air comes from the storage tank. The experiment was already done before setup B was finished. For the pressure drop it would make no difference if the flow comes from the compressor or air storage tank as long as the flow is kept equal. Keeping the flow equal would mean that the inlet velocity is equal as well. Managing the flow can be done by choosing the correct valve for V2.
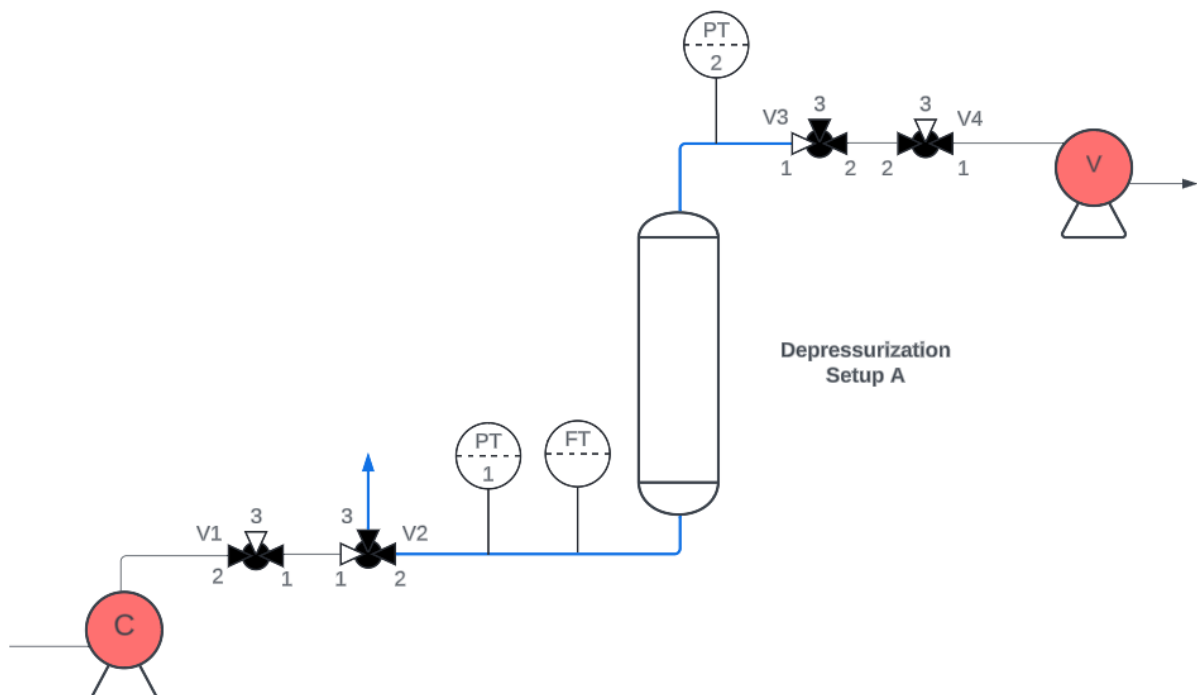
Figure 28*: Schematic configuration depressurization, measuring valve flow coefficient.*

After the adsorption step excess air at a pressure of P_W is vented to the surroundings through a valve, V2 within the experimental setup. By measuring the flow through the valve with FT while knowing the pressure drop over the valve based on PT1, the valve flow coefficient can be determined. In order to do this experiment the top of the column is closed while the bottom is opened.
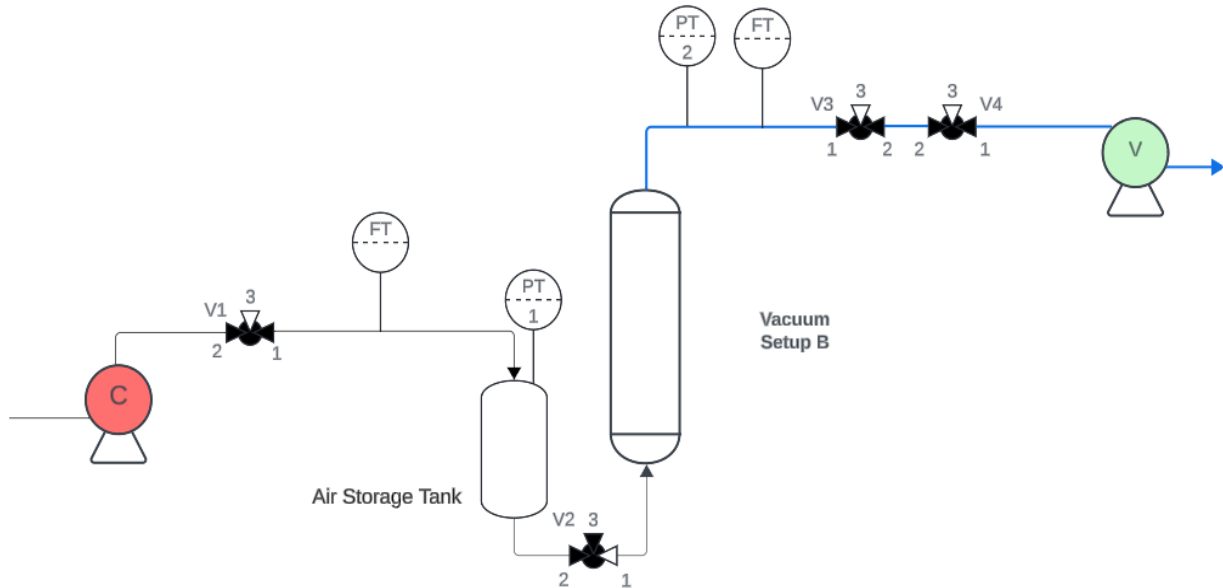
Figure 29: *Schematic configuration vacuum, measuring vacuum pump performance.*

To vacuumize the column V2 is set to the 2-3 configuration, closing the system on the compressor side while both V3 and V4 are set to 2-1. Note that the flow transmitter is now at the top of the column of V2 is switched in order to close the system to the side of the air storage tank. At the time of the experiments only one flow transmitter was available, requiring the system to be adjusted. With this configuration the pressure at the top of the column is measured along with the gas flow exiting through the top, Q_{out}.

4.2 Experimental Results

Having detailed the experimental methodology and the specific configurations, this paragraph will show the outcome of the different experiments. It shows how these results affect the model process variables, providing insights into the system's performance.

4.2.1 Compressor performance (Q_{in})

The result of this experiment is a curve which represents the relationship between the storage tank pressure and the normal flow in Nl/min of the compressor. When working with moles in the model, this flow obviously needs to be corrected for the pressure, resulting in l/min.
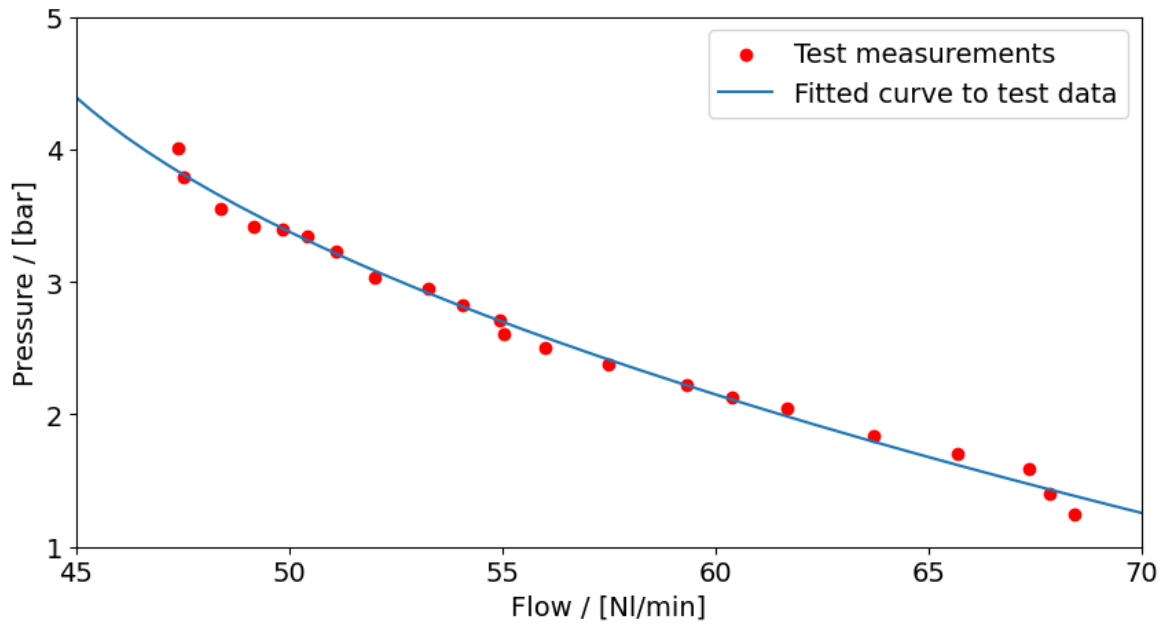
Figure 30: *Compressor performance based on experiments.*

4.2.2 Pressure drop $\left(\frac{\partial P}{\partial z}\right)$

By measuring the pressure in front of the column and after the column, along with the column length ($l = 0.5\,m$), $\frac{\partial P}{\partial z}$ can be derived. In order to do this, the average of the test results has been taken. Leading to an average pressure drop of 0.08 bar with a column length of 0.5 m, $\frac{\partial P}{\partial z} = -0.16\ bar\ m^{-1}$.
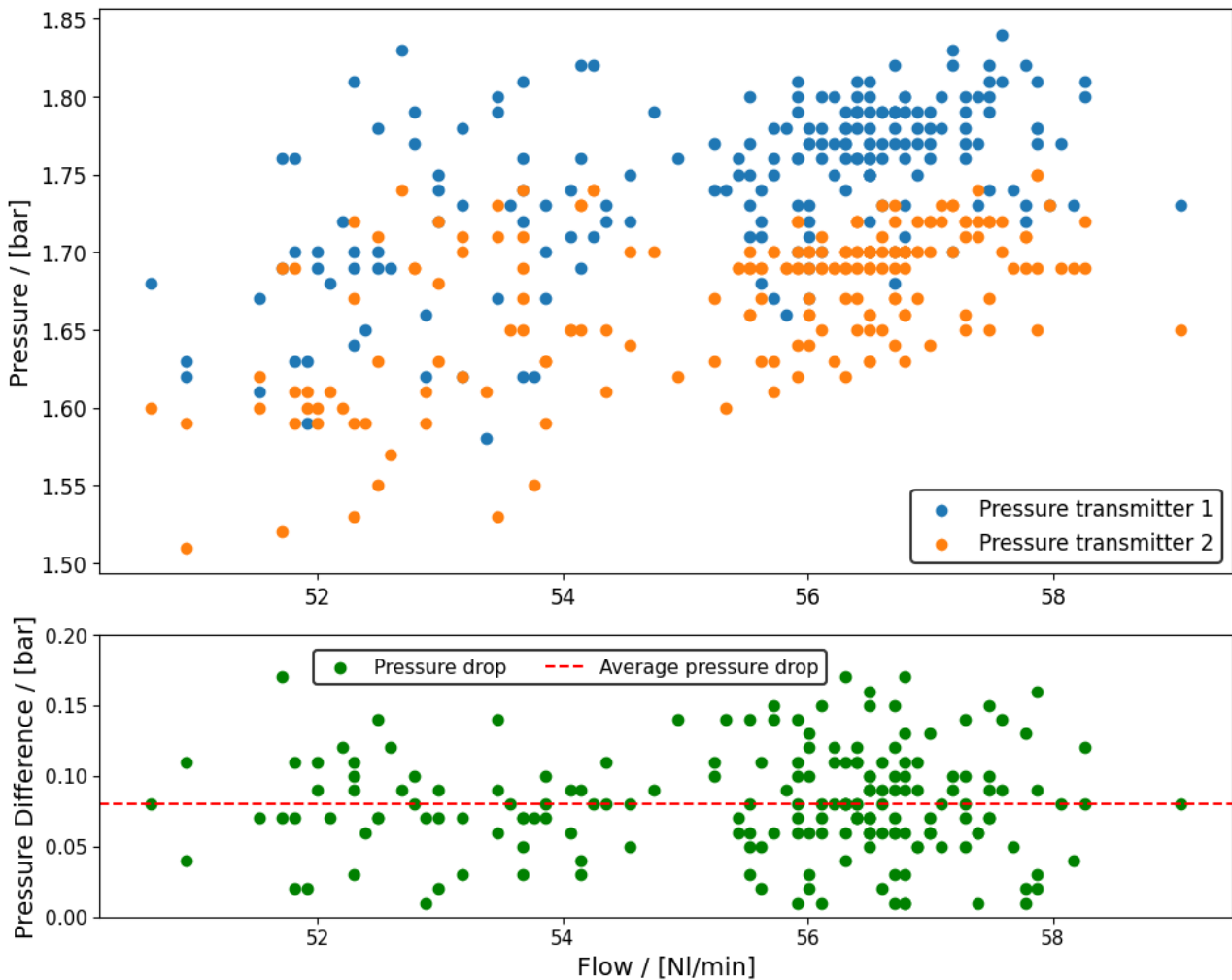
Figure 31: *Column pressure drop based on experiments during the adsorption step.*

4.2.3   Inlet velocity (*v*)

The histogram below shows the frequency of the flow measurements during the measuring period. This gives insight into the minimum and maximum inlet velocity. With the lowest velocity occurring at the lowest flow. The inner radius of the column is 6 cm. Resulting in a minimum inlet velocity of 0.09 m/s.
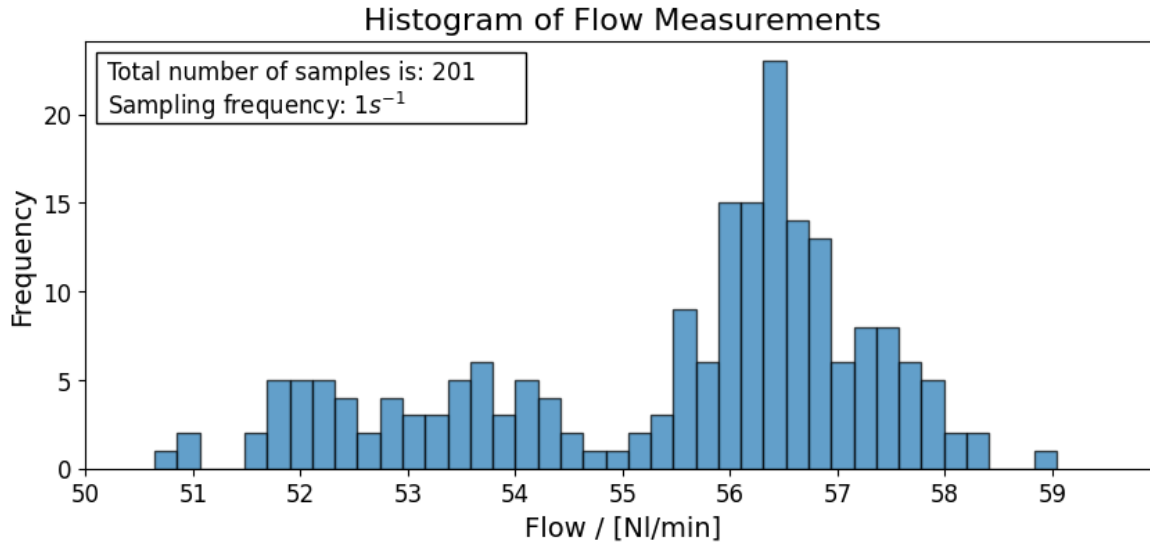
Figure 32: Histogram of the flow measurements during the adsorption step.

4.2.4   Valve flow characteristic (Kᵥ)

The different test runs immediately show the parabolic relationship between the pressure drop over the valve and the flow through it in **Figure 33**. This is expected when looking at **Equation**Error! Reference source not found. again. Non-linear least squares fitting is then applied to the different datasets in order to get the valve flow characteristic, K_v. Note that the value for K_v is now estimated on a pressure difference in bar and a flow in Nl/min. If one want to use the pressure difference in Pascals and flow in Nm³/s, Kᵥ needs to be multiplied by a factor of $6 \cdot 10^{-9}$.
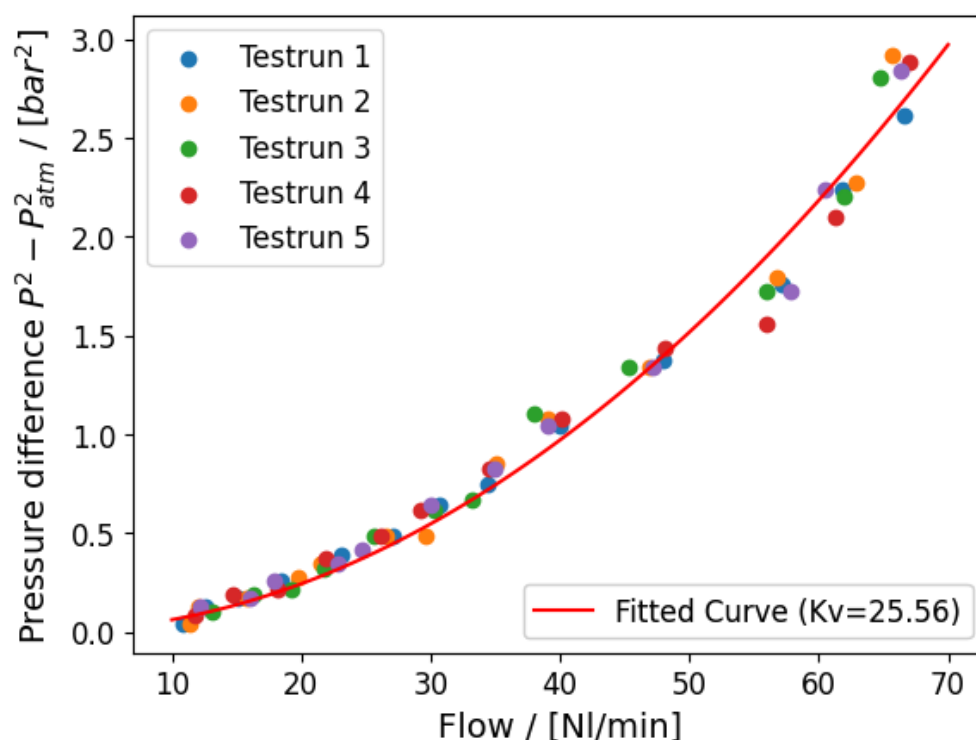
Figure 33: Valve flow characteristic estimation during the depressurization step.
T = 293.15 K and SG =1.

4.2.5   Vacuum pump performance (Q_{out})

The final experiment resulted in an estimation on the performance of the vacuum pump. **Figure 34** shows the measurements during the experiment along with the fitted curve to the test data. During this experiment an empty column was used to isolate the compressor performance and leave out adsorption effects.
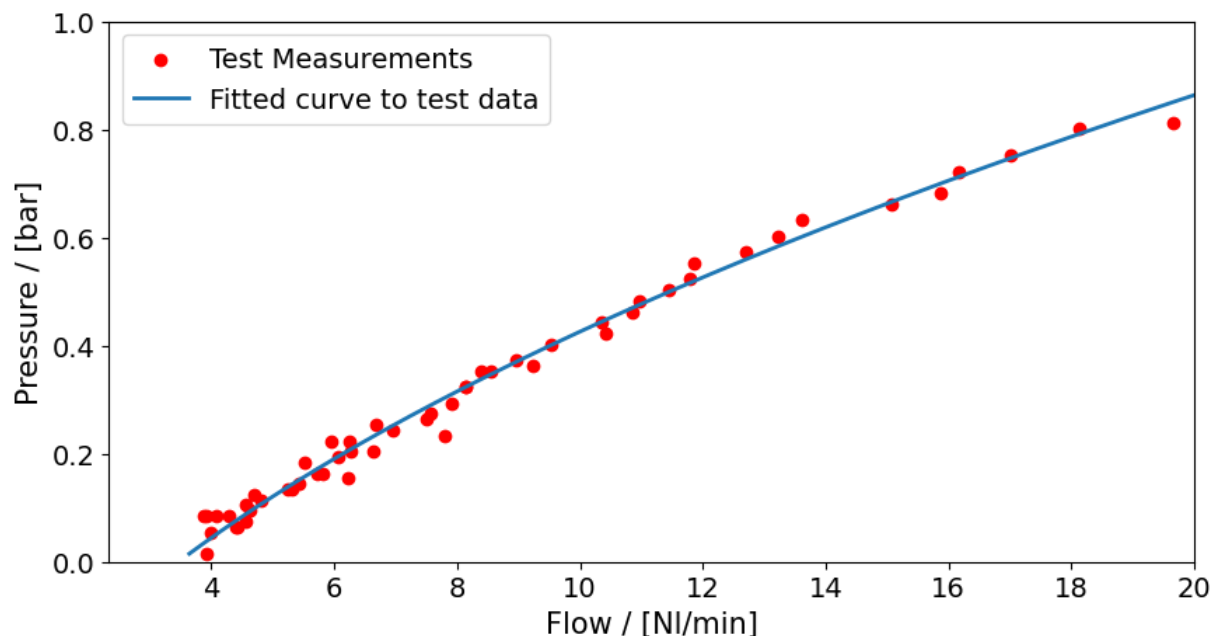
Figure 34: *Vacuum pump performance during vacuum step.*

5. Model validation

The model has been validated by running it with the same parameters as used in the experimental setup. The different parameters can be divided into different categories:

- Material properties: This category contains parameters related to the gases involved in the adsorption process, such as their molecular masses and fractions. Gas-adsorbent specific properties like mass transfer coefficients and adsorption isotherm parameters. Properties specific to the adsorbent material, such as its density and particle size
- System geometry and conditions: Parameters related to the physical setup and conditions of the system fall under this category. This includes dimensions (e.g., column diameter, length), volumes (total column volume, void fraction), and operational conditions (e.g., temperature and pressure).
- Equipment performance: Parameters related to the performance of equipment, such as the compressor, vacuum pump and control valves.
- Nummerical parameters: Parameters which are purely related to the numerical simulation like the number of grid points, timestep and number of timesteps.

It is also important to define the origin of the parameter values i.e. literature/specifications, experimental or user-defined. This distinction will show which parameters are fixed and which parameters can adjusted for process optimization. **Table 9** shows all parameters along with their value and origin within the different categories.

***Table 9**: Model parameters including their origin for model validation.*

Material properties

Parameter	Adsorbent (JLOX-103A)	Origin
$\rho_z\ (kg/m^3)$	630	Specs.
$r_p (mm)$	1.5	Specs.
$\epsilon\ (-)$	0.4	Literature

	N$_2$	O$_2$	Ar	
$q^{sat}\ (mol/kg)$	3.245	1.519	1.390	
$b\ (bar^{-1})$	3.15 x 10-5	1.75 x 10-8	1.81 x 10-8	Literature
$v\ (-)$	0.8224	1.3581	1.3442	Literature
$k\ (s^{-1})$	0.16	0.25	0.22	Literature
$M\ (g/mol)$	28.03	32	39.948	Literature
$y\ (-)$	0.78	0.21	0.01	Literature

	Air	
$v_{in}\ (m/s)$	0.09	Experimental

System geometry and conditions

Column diameter (m)	0.12	User-defined
Column length (m)	0.5	User-defined
$P_{AD}\ (bar)$	2	User-defined
$P_{DP}\ (bar)$	1.2	User-defined
$P_{VC}\ (bar)$	0.04	User-defined
$P_{atm}\ (bar)$	1	Experimental
$T\ (K)$	293.15	Experimental
$\partial P /_{\partial z}\ (bar/m)$	-0.16	Experimental

Equipment performance

Compressor Q (*Nl/min)* vs. P (bar*)*	$Q = 87.9 - 16.1P + 1.4P^2$	Experimental
Vacuum Q (*Nl/min)* vs. P (*bar)*	$Q = 3.5 + 11.6P + 8.7P^2$	Experimental
$K_{v,DP}\ (\frac{Nl\sqrt{K}}{min \cdot bar})$	25.56	Experimental

Numerical parameters		
Timestep (s)	0.01	User-defined
Number of grid points (#)	31	User-defined

5.1 Pressurization time validation

In order to have a sufficient and continuous flow of concentrated oxygen there should always be enough air fed into the system. Therefore it is important to validate the pressurization time of the numerical model with the experiments. Below in **Figure 35** one can see the results of the pressurization time validation. It takes the compressor about 9 seconds to increase the pressure of the air storage tank from 1 bar up to 3 bar. Considering the linear trend, this translates into around 0.33 bar/s within this low pressure range. It can be seen that both the pressure and flow in time are estimated accurately by the model when compared to the experiment.
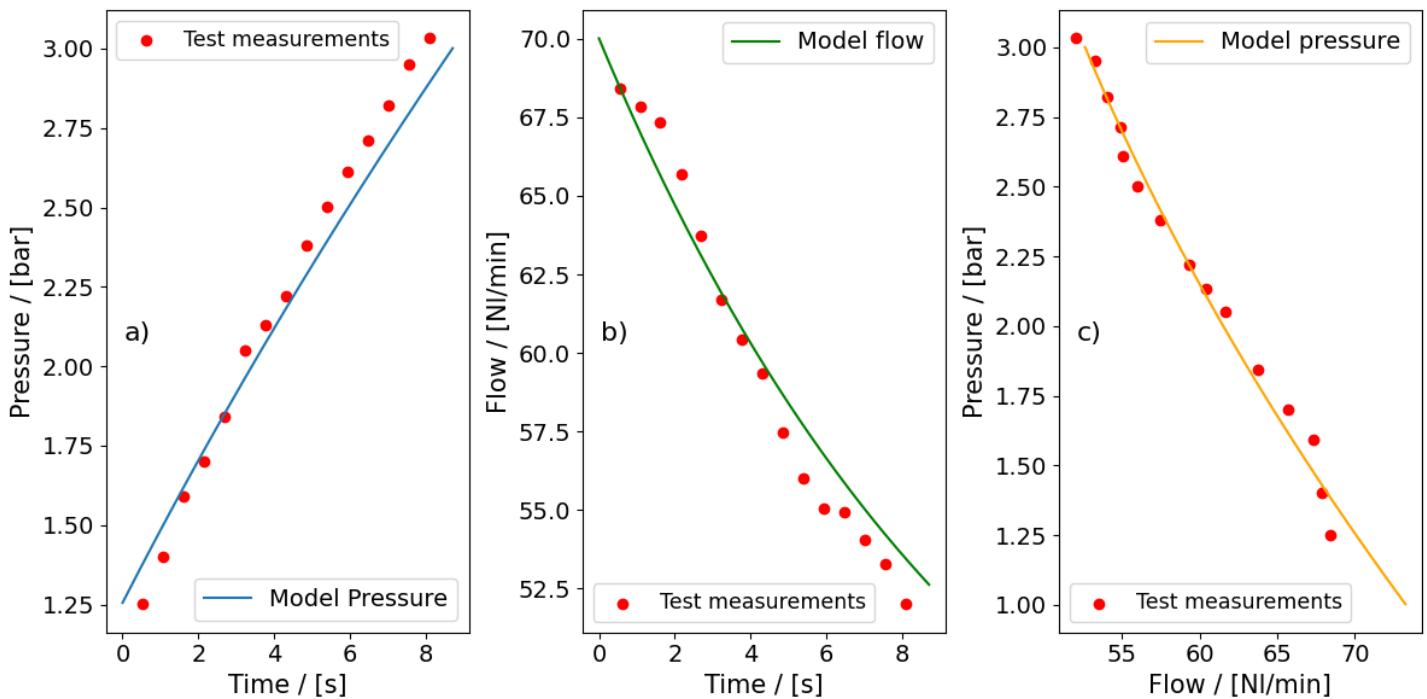
Figure 35: *Model validation results for the pressurization time of the air storage tank. V = 5 L.*

5.2 Vacuum time validation

The vacuum time consists of two phases, the first phase is the depressurization step and the second phase is when the vacuum pump is turned on. These steps combined form the total vacuum time.

5.2.1   Depressurization time

Figure 36 shows both the pressure and flow for the model and the experiments when the column is depressurized. During this measurement and within the model there is no help of the vacuum pump. The model validations below correspond to setup A where the column did contain zeolite. Note that within the actual setup the vacuum pump would be switched on at P_{DP} which is greater than 1 bar.
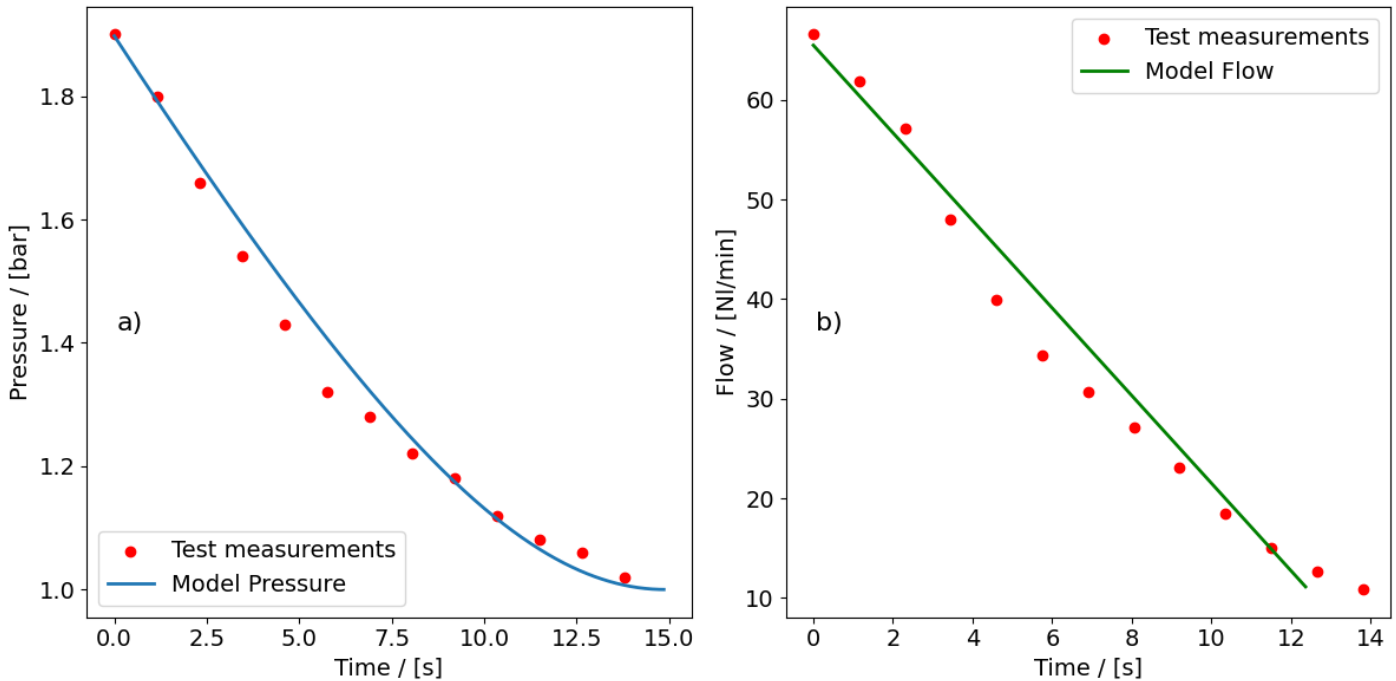
Figure 36: *Model validation results for the depressurization time of the column containing zeolite. V = 5 L.*

5.2.2   Vacuum pump time

The second phase of the vacuum time is when the vacuum pump is switched on. The measurements of this experiment and the model estimates are shown in **Figure 37**. The validation was done for an empty column, thereby isolating the compressor behaviour of the model and not including adsorption effects.
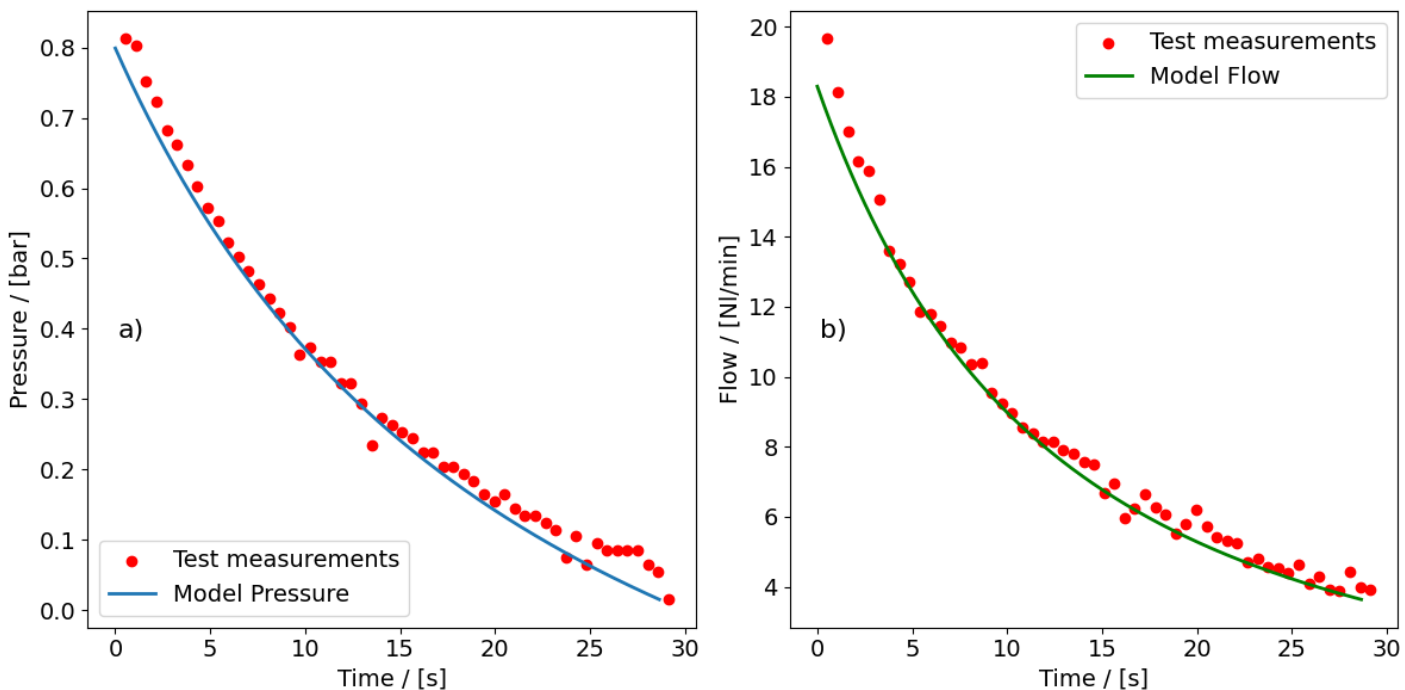
Figure 37: *Model validation results for vacuum pump time of column without zeolite. V = 5 L.*

Obviously also the adsorption or in this case desorption effects during the vacuum step have to be validated. The results of this validation can be seen in **Figure 38**. The model accurately includes the desorption behaviour leading to drastically increased vacuum pump times in order to reach the same vacuum level.
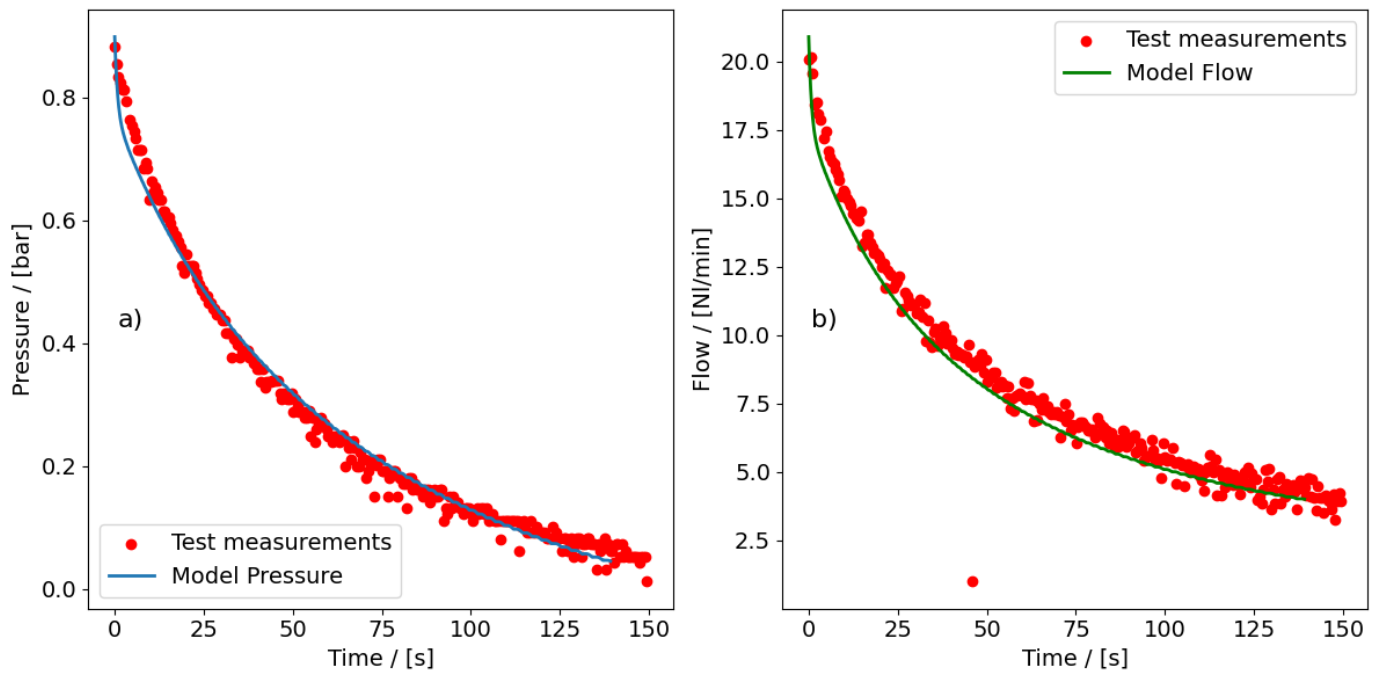
Figure 38: *Model validation results for the vacuum pump time of the column containing zeolite. V = 5 L.*

6. Regulatory frameworks regarding a PSA-unit

Requirements for design, installation, function, performance, testing, commissioning and documentation of pipeline systems used in healthcare facilities have been changed frequently. The first ISO norms dating back from 1987 have been revised 6 times up to now. Currently the norms from 2016 and 2019 are still active. The latter, NEN-EN-ISO 7396-1+A1:2019, nl will be primarily used within this chapter since it is the most recent and focusses on medical storage and delivery systems with oxygen concentrators. Due to the scope of this thesis, which is the production and storage of oxygen, only these aspects will be thoroughly examined within this chapter. For the rest of this chapter '*these systems*' or '*the system*' refer to medical delivery systems of oxygen, like a PSA-plant.

Compressors within the system need to be connected to an emergency power supply and are not allowed to be used for compressed air systems for medical air. As already mentioned in 2.5.3 Regulatory Frameworks the oxygen supply needs to consist of three sources. The oxygen concentrator i.e. PSA-plant should be able to provide the design flow if both the secondary and backup source fail.

If the oxygen concentrator serves as primary source it should contain the following elements:

a) At least one oxygen concentration unit;
b) An oxygen storage which contains oxygen at a purity of at least 93% (oxygen 93);
c) A sampling point directly downstream of the 93% oxygen storage tank;
d) Pressure relief valves;
e) Filters:
f) Facilities to check the status of filter elements if regular replacement is not planned;
g) Oxygen analysers

With the use of an oxygen concentrator as primary source and the secondary or backup source not being oxygen concentrators the following requirements apply:

a) One of both sources needs to consist of at least one battery of cylinders, cylinder package or high pressure storage tank of oxygen 93.
b) In case multiple of the in a) mentioned sources are delivered at the same time and one of them is depleted, there should be an automatic switch to the other source.
c) Secondary source: the source should be connected in parallel to the primary source. Backup source: the source should be connected downstream of the oxygen 93 storage tank.

Oxygen 93 is not just an easy concentration threshold but consists of several extra conditions:

a) Nominal oxygen concentration of 93% +/- 3% V/V;
b) A carbon monoxide concentration $\leq$ 5 ml/m^3;
c) A carbon dioxide concentration $\leq$ 300 ml/m^3;
d) An oil concentration $\leq$ 0.1 mg/m^3 measured at ambient temperatures and pressure corrected to 0℃;
e) Water vapor content $\leq$ 67 ml/m^3;
f) Concentration of nitrous gasses NO/NO$_2$ $\leq$ 2 ml/m^3;
g) Sulfur dioxide concentration $\leq$ 1 ml/m^3

On top of these composition requirements the oxygen 93 should be filtered before the source valve to minimize contamination by particles.

Each concentrator unit that is part of the delivery system should be able to deliver product gas of the required composition over the full range within the specified flow rates capable of delivering. A concentrator unit consists of the following elements:

a) A compressed air feed with at least one compressed air system which is allowed to be connected to a compressed air storage tank. This compressed air storage tank is allowed to be supplied by only one compressor but needs to contain the following elements;
   a. One or more valves, an automatic condensation drain, a manometer and a safety valve;
   b. A pressure regulator e.g. a pressure regulator or pressure transmitter,
b) At least one filter unit;
c) Switch vales;
d) At least one carbon monoxide alarm sensor downstream all of the treatment units e.g. adsorption columns, compressor.

As mentioned earlier in this chapter, each source needs to be equipped with at least one oxygen analyser. There should be facilities which allow to read and document the oxygen concentrations. Control mechanisms should be able to shut down the PSA-plant once the concentration drops below the above described concentration levels for oxygen 93. The oxygen analyser and isolation valve need to be installed upstream of the oxygen 93 storage tank. Low concentrations , < 93%, should trigger an urgent alarm whereas high concentrations, > 93 %, should trigger an informative alarm. A sampling point needs to be installed upstream of the final valve before the oxygen is delivered to the hospital.

Finally there are some regulations regarding local filling of the high pressure oxygen 93 storage tanks. The filling process should never have any negative consequences for the supply of the oxygen 93 to the hospital. Check valves need to prevent oxygen flowing from the high pressure storage, often 200 bar, back to the PSA-plant. Appropriate barriers need to be installed to protect employees. In case a booster compressor is used, each step needs to have a temperature sensor with built-in alarms for high temperature limits. These alarms need to be triggered in case of too high: housing temperature, outlet gas temperature, power consumption and pressure. In case any of these alarms are triggered the compressor needs to switch off. At last there needs to be a facility to flush the oxygen 93 storage tank.

7. Results

This chapter presents the results from the numerical model developed to address the first sub question of this thesis. The primary aim is to optimize the PSA plant to meet specific oxygen demands. Initially, the results will focus on the concentration and supply capabilities of the test setup. The goal for this test setup was to produce an oxygen flow of 30 Nl/min at 2 bar with a minimum oxygen concentration of 70%. Subsequently, the analysis will be scaled to a large-scale PSA setup designed to fulfill the oxygen requirements of a hospital, such as RdGG.

7.1 Test setup optimization and capability

The oxygen demand can be divided into two main components: the required oxygen concentration and the required amount of oxygen. These two components are connected, as a higher required concentration at the same flow rate results in a greater amount of oxygen. Looking back at **Table 9**, it is evident that one of the primary user-defined inputs are the different pressure levels. These pressure levels must be chosen carefully, as they significantly influence various parameters, such as the total cycle time and adsorption behaviour. Additionally, the dimensions of the column, specifically its length and diameter, and the gas inlet velocity play a crucial role.

The first key pressure level that has been investigated is the vacuum pressure P_{VC}. In the end this pressure level is responsible for cleaning the zeolite before it is brought into the adsorption step. Moreover, is also determines the amount of gas which will remain inside the column when a new adsorption step begins. If the vacuum pressure is too high, this will result in elevated nitrogen concentrations in the gas phase and insufficient adsorption capacity of the zeolite. Leading to a situation where the required oxygen concentration cannot be met.
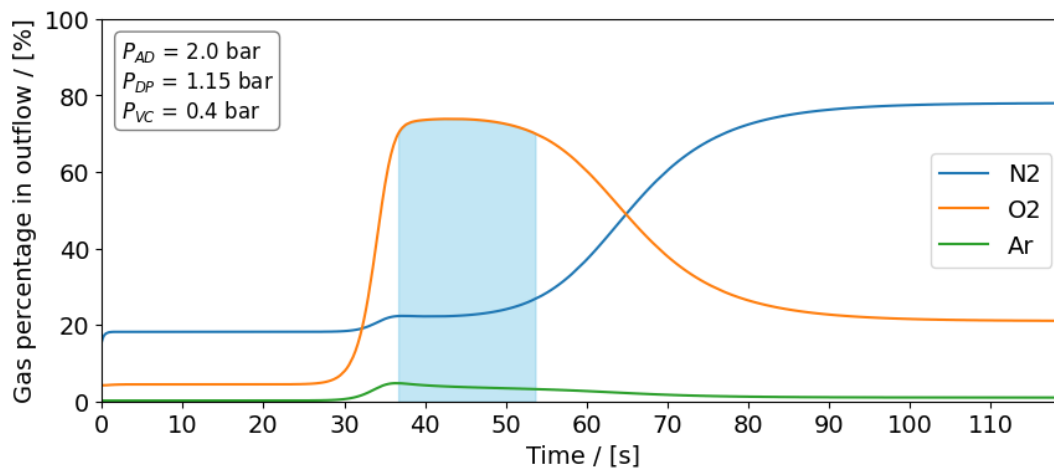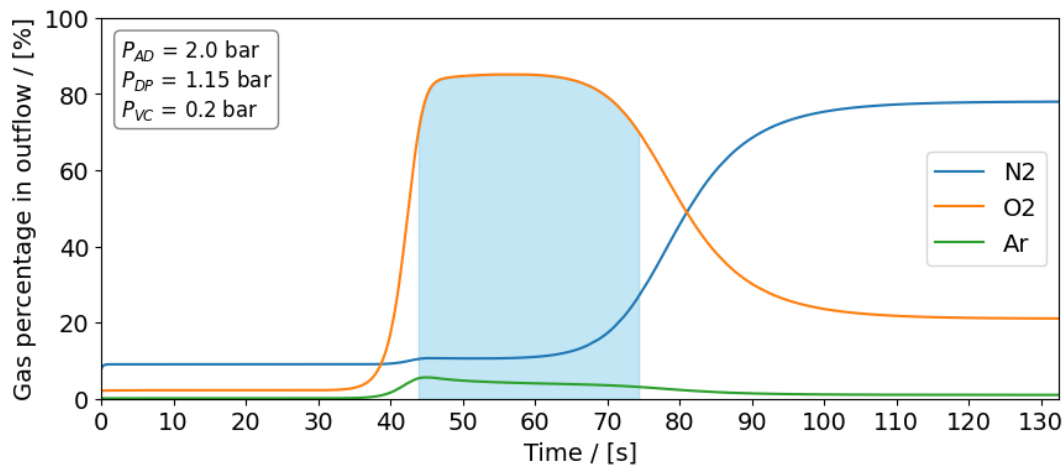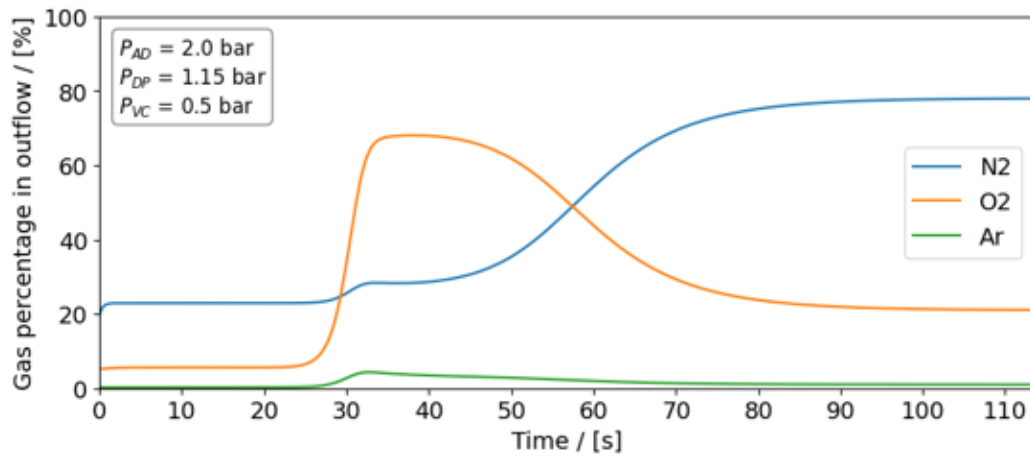
Figure 39*: Breakthrough curves for increasing vacuum pressures. Blue area indicating an oxygen concentration of 70% or higher.*

Figure 39 shows the outlet gas percentages as a function of time for different vacuum levels. The blue area indicates the timeframe for which the gas mixture coming from the adsorption column exceeds a 70% oxygen concentration. As the vacuum pressure is increased the initial gas concentrations increase at the beginning of the adsorption process. When the vacuum pressure is 0.5 bar or higher, the setup is never able to produce enriched oxygen of 70%. Besides the initial gas pressure of nitrogen being too high also the initial loadings on to the zeolite are too high, not allowing for sufficient adsorption.
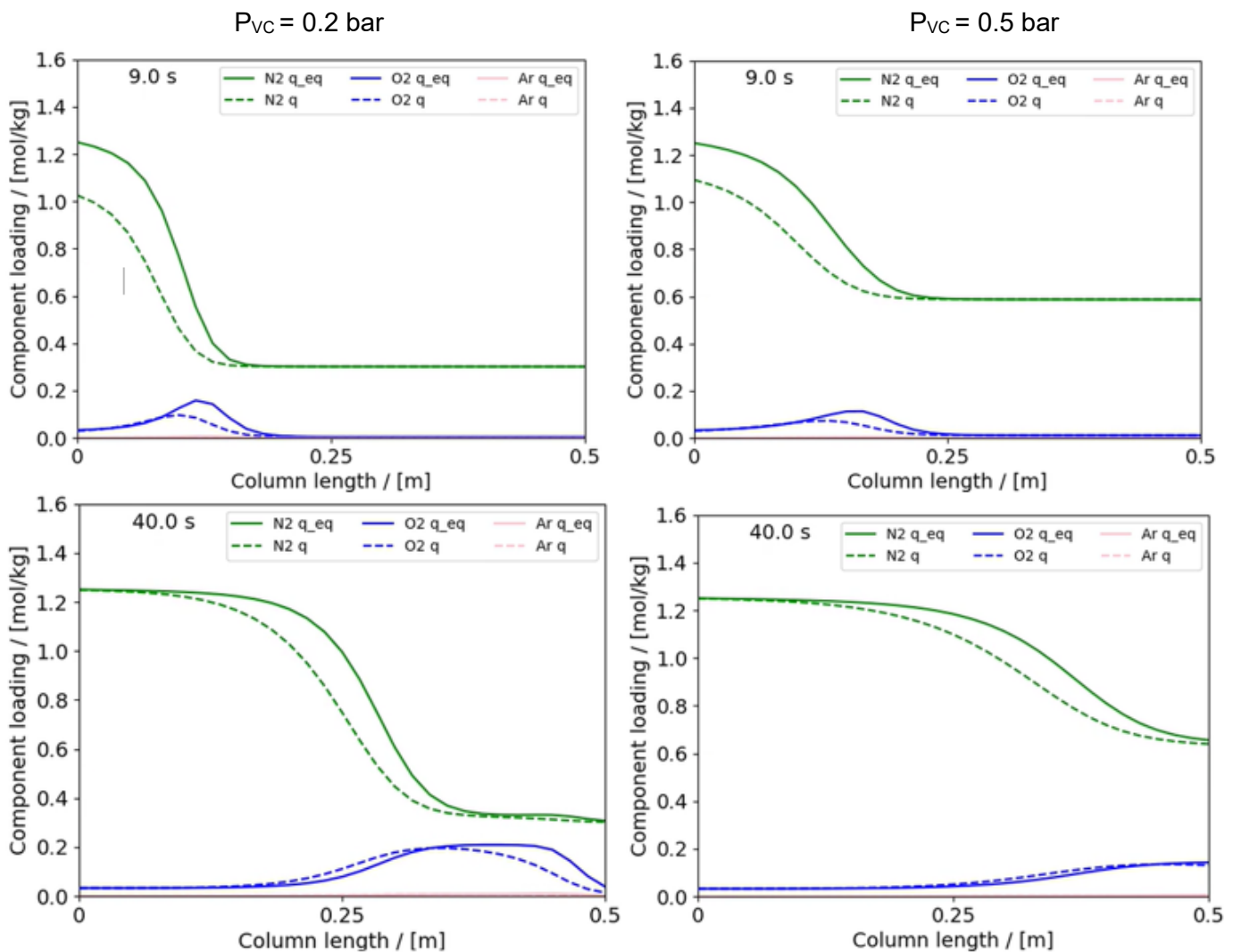
Figure 40*: Component (equilibrium) loadings for different vacuum pressures at 9 and 40 seconds into the adsorption step. P_{AD} = 2 bar.*

Figure 40 shows the component (equilibrium) loadings for P_{VC} = 0.2 bar and P_{VC} = 0.5 bar at 9 and 40 seconds into the adsorption step. Clearly showing that the difference between the equilibrium loading and the actual loading, which is the potential to adsorb, is significantly lower for P_{VC} = 0.5. The lower right image at 40 seconds into the adsorption step already shows large saturation of the zeolite. At 40 seconds into the adsorption step for P_{VC} = 0.2 bar there is still much more adsorption which can take place.

The depressurization pressure itself does not influence the potential purity levels of the enriched oxygen. This is predominantly determined by the adsorption and vacuum pressure. The depressurization pressure does however have an impact on energy efficiency and the total cycle time. When venting the column without the help of the vacuum pump, no electrical energy is required. Looking at **Equation 3.35** and **Figure 33** it does become evident that the pressure starts decreasing slowly as the column pressure and outside pressure start to get close to each other. This is the point where the vacuum pump should be switched on in order to clear more gas from the column.
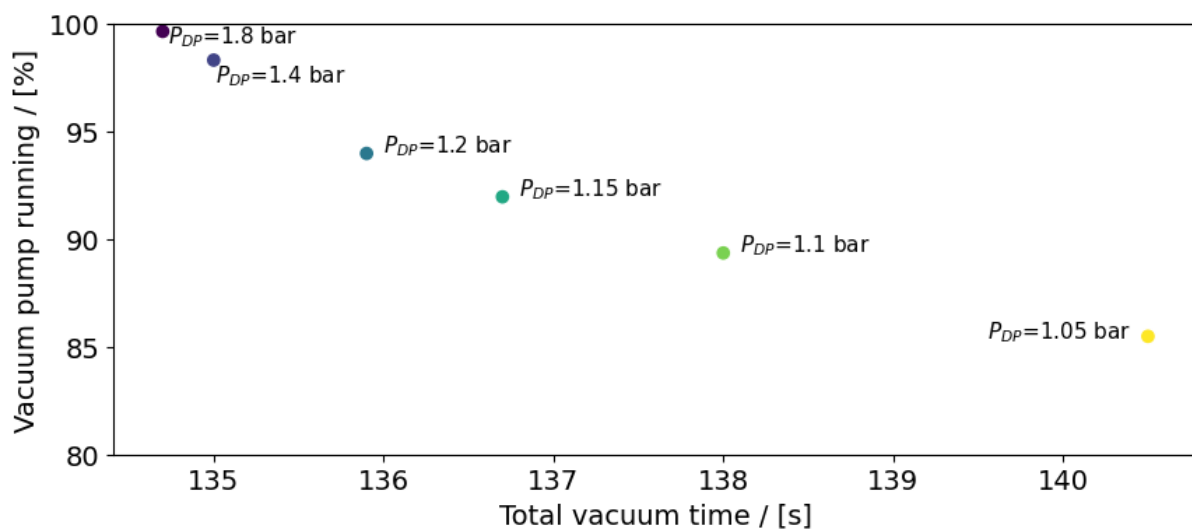
Figure 41: Effect of depressurization pressure on the total vacuum time.
P_{AD} = 2 bar and P_{VC} = 0.2 bar

Figure 41 shows the total vacuum time versus the percentage of time that the vacuum pump is running within that time. Six different depressurization pressures where tested in order to show the effect of decreasing this pressure. The figure shows that in general the total cycle time is shorter when the compressor is turned on at a higher P_{DP}, but that this effect is minimal. Having the compressor on for 99.6%, P_{DP} = 1.8 bar, of the vacuum time only reduces the vacuum time by 5.8 seconds when compared to the situation where P_{DP} = 1.05 bar. This can be explained by **Figure 42**, which shows that for high depressurization pressures the venting and vacuum pump produce almost equal flows. For lower depressurization pressures the vacuum pump shows slightly increased flow rates, therefore clearing the column a little faster when switched on early. The conclusion from this analysis would be to only turn on the vacuum pump early when it is absolutely necessary to gain around 6 seconds, which accounts for a 4.1% vacuum pump time reduction. This reduction in time does require the vacuum pump to be on for 14.1% longer. If this small time gain is not necessary, the compressor should therefore be switched on at low depressurization pressures in order to save energy.
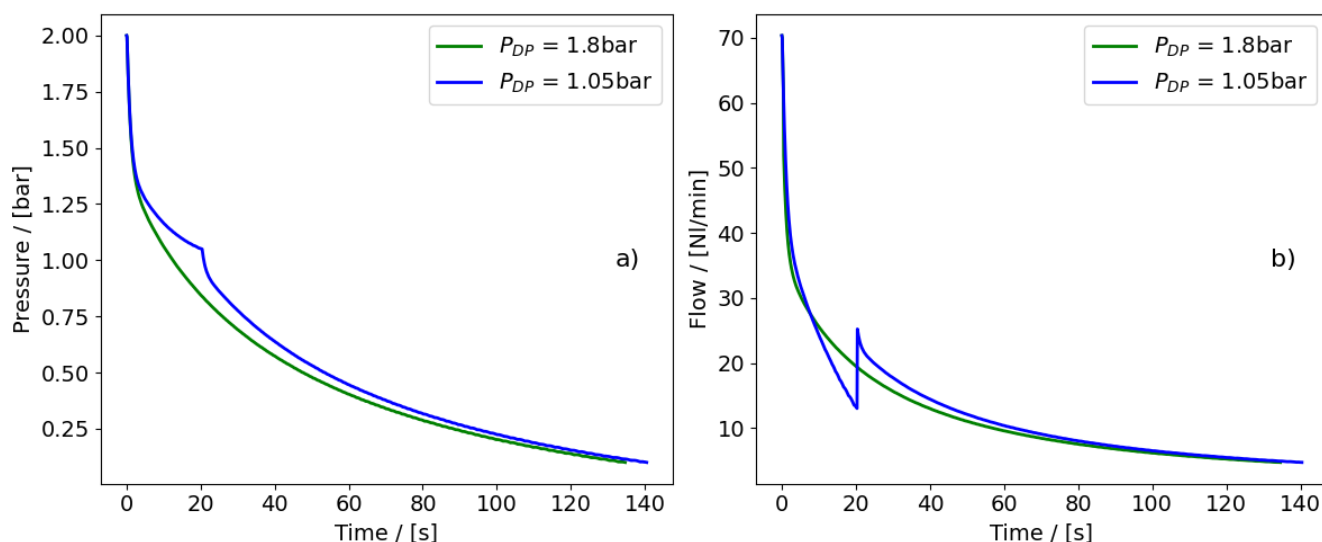
Figure 42: Pressure (a) and flow behaviour (b) for two different depressurization pressures.
P_{AD} *= 2 bar and* P_{VC} *= 0.1 bar.*

With the vacuum pressure being mainly responsible for reaching the desired concentration, the adsorption pressure, column size and inlet velocity are responsible for producing enough oxygen on a molar bases. **Figure 43** shows the relationship between the adsorption pressure, P_{AD}, and the total amount of oxygen that is produced within the corresponding cycle time.
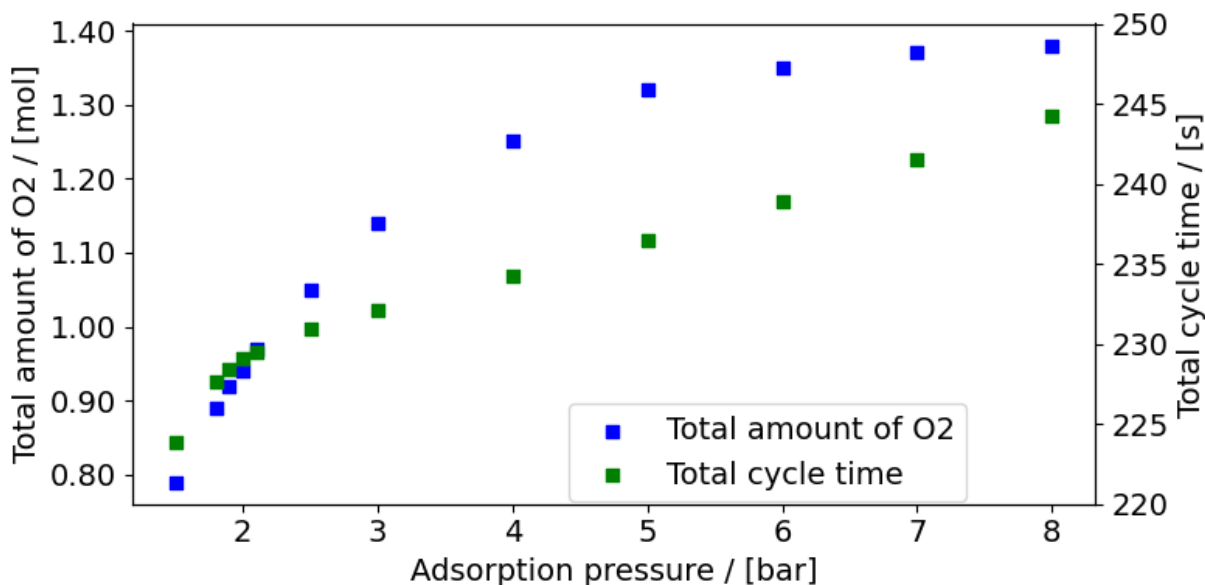
Figure 43: Oxygen production and cycle time for different adsorption pressures.
P_{DP} *= 1.05 bar and* P_{VC} *= 0.1 bar.*

When the adsorption pressure is increased, both the produced amount of oxygen and the cycle time increase. **Figure 44** shows the amount of oxygen that is produced per second, indicating an optimum at an adsorption pressure of 6 bar.
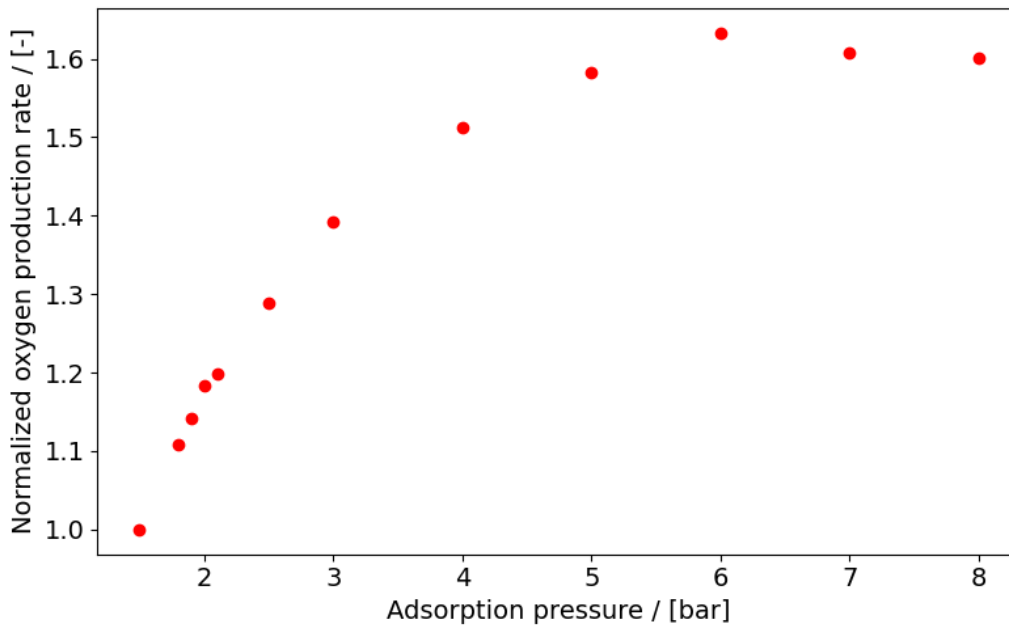
Figure 44*: Normalized oxygen production rate for different adsorption pressures. P_{DP} = 1.05 bar and P_{VC} = 0.1 bar.*

Figure 45 shows that the increase in cycle time is caused by the increased total vacuum time, even though the window for adsorption is decreasing. The maximum difference in total adsorption time is only 53.7 seconds whereas the maximum difference in total vacuum time is 74 seconds.
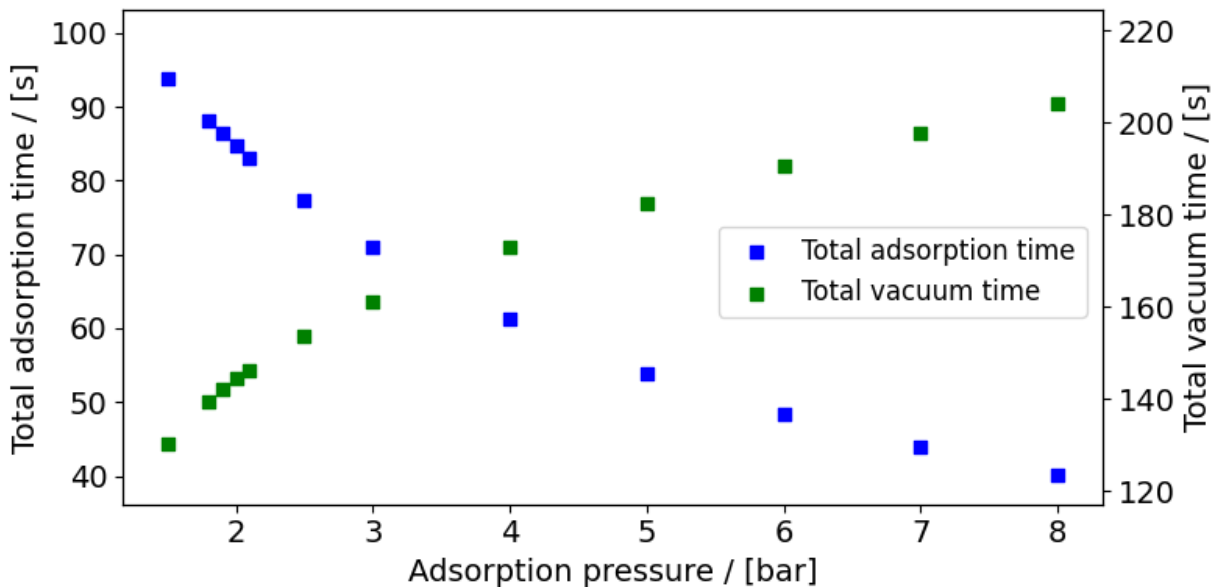
Figure 45*: Total vacuum and adsorption time for different adsorption pressures. P_{DP} = 1.05 bar and P_{VC} = 0.1 bar.*

One could argue for decreasing the vacuum pressure even further. **Figure 46** shows however that when going below 0.2 bar, there is no increase in production, but only an increase in the cycle time due to a longer vacuum time. Therefore 0.2 bar is actually chosen as the final vacuum pressure within the test setup.
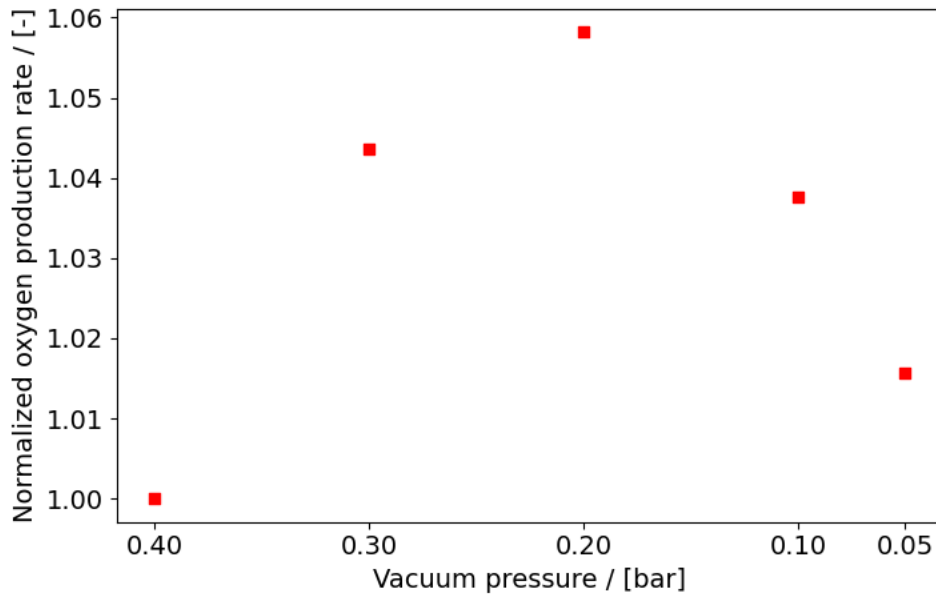
Figure 46: *Choosing the optimal vacuum pressure to maximize the oxygen production rate.*
P_{AD} = 6 bar and P_{DP} = 1.05 bar.

As already mentioned also the column geometry and gas inlet velocity play an important role for the process performance. The geometry can be simplified by taking the ratio between the column diameter and length, while keeping the volume and inlet velocity constant. Perhaps a certain ratio increases the oxygen production compared to alternative shapes while having the same amount of zeolite.
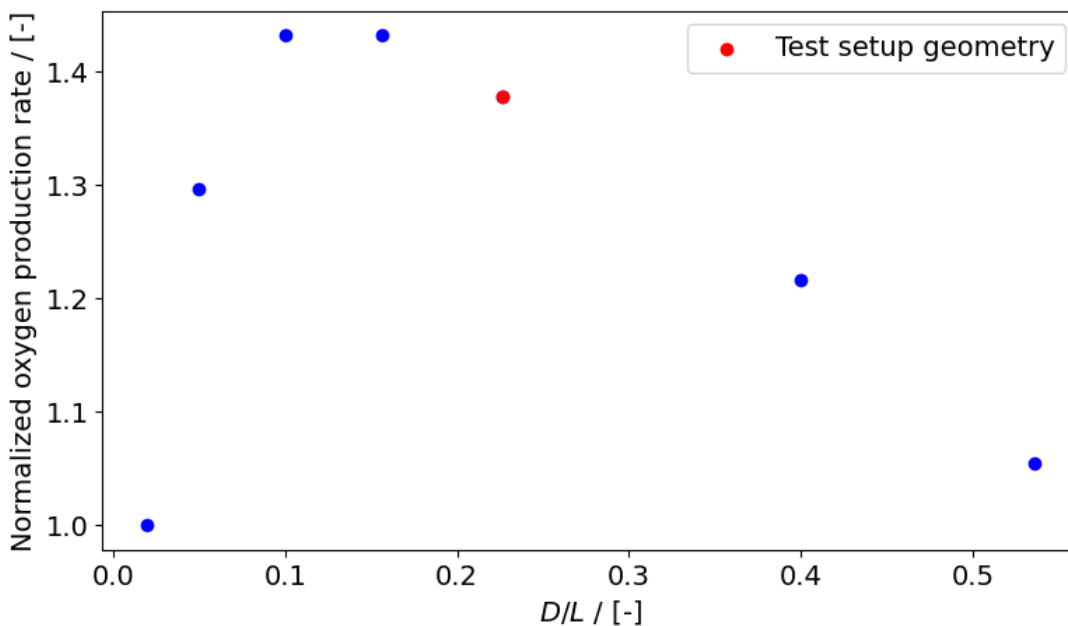
Figure 47: *Effect of the column geometry on the oxygen production rate.*
P_{AD} = 6 bar, P_{DP} = 1.05 bar, P_{VC} = 0.2 bar and V = 5 L.

Figure 47 shows the normalized oxygen production for different ratios between the diameter and column length. Of course these ratios should only contain realistic column shapes and therefore range between D/L = 0.02 and D/L = 0.55. In red is the current geometry of the test setup plotted. The figure shows that there is an optimal D/L ratio of around 0.1. Compared to the current setup this would increase the oxygen production rate by 5.4%. For a cylindrical column of 5L this would require L = 0.86 m and D = 0.086 m. When the ratio is either below or above this optimal ratio, the oxygen production rate starts to decrease. This can be explained

by looking at the adsorption times and total production from a single cycle. **Figure 48** clearly indicates that for long and thin columns, so a low D/L ratio, the adsorption time is too large compared to the total production. For thick and short columns the adsorption time is short, but after a ratio of D/L = 0.3 the adsorption time and oxygen production both flatten at a rate which is lower than for D/L = 0.1. Leading to decreased oxygen production rates.
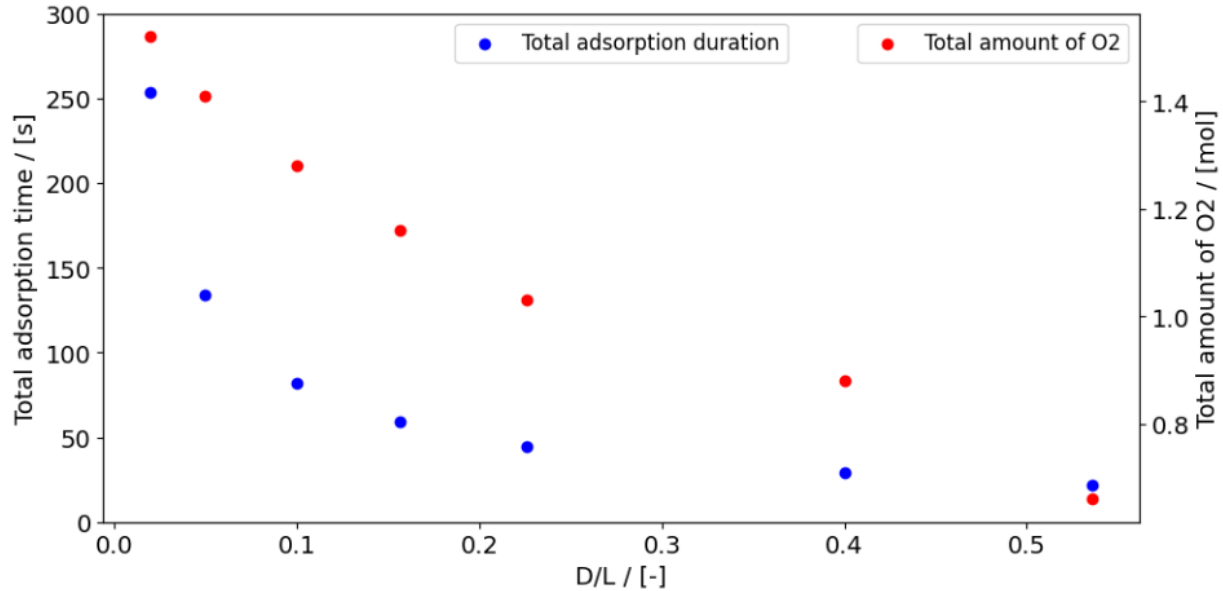
***Figure 48**: Effect of the column geometry on the total adsorption time and oxygen production. P_{AD} = 6 bar, P_{DP} = 1.05 bar, P_{VC} = 0.2 bar and V = 5 L.*

Then the ratio between the column length and inlet velocity, which will be called the dimensionless time t_c, was analysed. In the base setup with an inlet velocity of 0.09 m/s and a column length of 0.5 m, the dimensionless time equalled 5.55 s. **Figure 49** shows the effect of changing the inlet velocity, thereby creating a new dimensionless time value. Tests were also done for $t_c = 1\,s$, but then the setup is not able to produce oxygen with a concentration of at least 70%. An optimum is found for $t_c = 9.56\,s$. Meaning that the inlet velocity of 0.09 m/s for a 5 L column with a D/L ratio of 0.1 (L = 0.86 m) optimizes the oxygen production rate. For high inlet velocities the operating window for enriched enough oxygen becomes too small. For low inlet velocities the cycle time is increased a lot since it takes the gas too much time to move through the entire column.
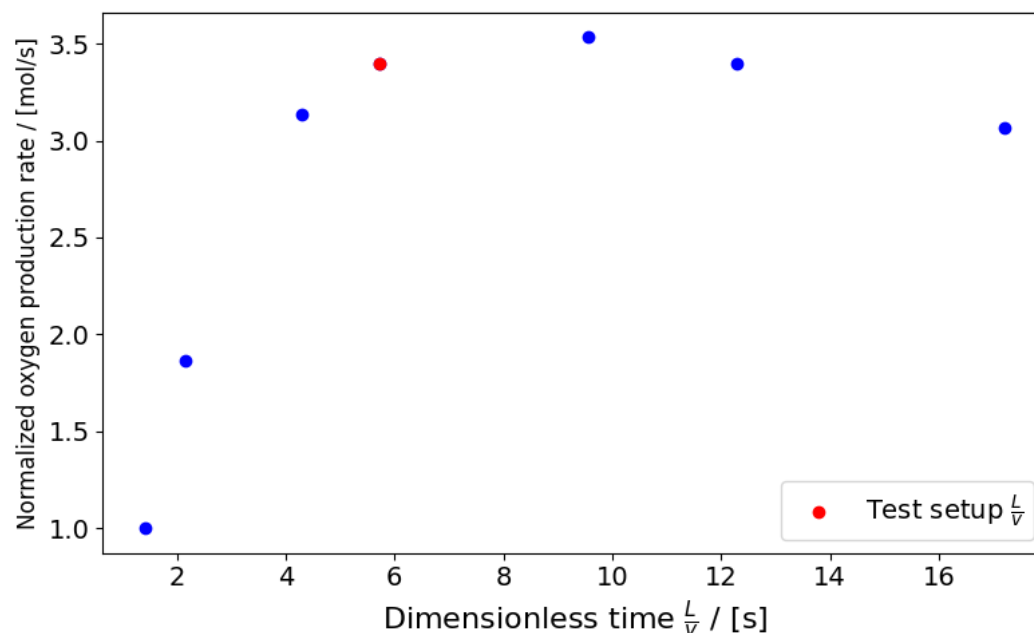
***Figure 49**: Effect of the dimensionless time on the oxygen adsorption rate. P_{AD} = 6 bar, P_{DP} = 1.05 bar, P_{VC} = 0.2 bar, V = 5 L and D/L = 0.1.*

Having analysed the pressure levels, column geometry and the dimensionless time t_c the following can be concluded. For the system to reach at least a 70% oxygen concentration the vacuum pressure should never be above 0.4 bar. When exceeding this pressure the initial partial pressure of nitrogen is too high as well as the amount of nitrogen which is already adsorbed on to the zeolite at the beginning of the adsorption step. Decreasing the vacuum pressure below 0.2 bar turned out to have a negative effect on the adsorption rate due to the large increase in vacuum time. The optimum adsorption pressure to maximize the oxygen production rate was found at 6 bar. It was also found that the decrease in total cycle time by turning the compressor on early within the vacuumizing process only had a small effect on the total cycle time. For that reason it is best to turn it on when the column is already close to the atmospheric pressure, e.g. at 1.05 bar. By optimizing the column geometry, while keeping the volume and amount of zeolite the same, a 5.4% increase in production rate can be accomplished. The optimal value for the ratio between the column diameter and length was found to be at D/L = 0.1. Finally the dimensionless time which represent the ratio between the column length and the inlet velocity was found to have an optimum for the adsorption rate at L/v = 9.56 s. When running the model with all optimized variables the oxygen production rate turned out to be 0.0053 mol/s. The goal for this test setup was to produce an oxygen flow of 30 Nl/min at 2 bar with a minimum oxygen concentration of 70%. When converting this to moles, this would require an oxygen flow rate of $n_{O_2}^{\cdot} = \frac{0.7 \cdot 2 \cdot 10^5 \cdot 30}{60 \cdot 1000 \cdot 2 \cdot 8.314 \cdot 293.15} = 0.0144 \, mol/s$. The current setup made use of 2 columns which could be operated in parallel, therefore resulting in a total oxygen production of $2 \cdot 0.0053 = 0.0106 \, mol/s$. Reaching the requirements would require a larger setup or one where 3 columns could run in parallel. Working with 3 columns would lead to a total production of 0.0159 mol/s, which meets the setup requirements. For the current setup this would require a second vacuum pump and the ability to feed more than one column at once. This enables to run two of the current processes in parallel.

7.2 Scaling the setup to hospital size

With the model for the test setup providing valuable insights, it is now time to scale the setup to meet the requirements of a hospital like RdGG. Such hospitals typically have normal oxygen demands of 10 Nm³/h. In addition to the increased demand, there are three significant differences to consider. Due to the variable demand, the setup must be capable of handling peak loads for certain periods rather than just the normal demand. Therefore, this section will also focus on the air and oxygen storage tanks, as these tanks allow for variations in demand. Secondly, the supply pressure during normal operation ranges from 4.5 to 5 bar, with the minimum and maximum supply pressures being 4 and 6 bar, respectively. Lastly, the purity of the current hospital systems is approximately 99% oxygen concentration, compared to the original setup which had an oxygen threshold of 70%. As described earlier in this thesis, the theoretical maximum for a PSA setup lies around 95%. Barely any hospital equipment makes constant use of 99% or even 95% pure oxygen. The new threshold is set at 93%. The reason for this value is extensively described in 6. Regulatory frameworks regarding a PSA-unit as this comes from Dutch regulatory frameworks. This chapter also showed that the absolute minimal oxygen purity lies at 90%. The goal for this setup is for it to be able to always carry the normal demand and on top of that it should be capable of handling peak demand for a period of three consecutive days. Generally oxygen storages for PSA-units come in the form of cylinder packages which store oxygen at 200 bar. These packages consist of 16 cylinders with a volume of 50L/cylinder. The required storage for the above mentioned duty should not be more than 5 cylinder packages, equating to a total storage capacity of 4 m³. For the PSA-units to also fit indoors within the hospital the maximum dimensions of a single column are: W x D x H: 50 x 50 x 350 cm. Ideally the amount of columns needed is kept as low as possible.

A lower amount of columns means less system parts which could potentially fail and require a smaller capital investment. The optimum production would be when all columns can run in parallel, such that the total production is equal to the amount of columns ($N_{columns}$) times the production rate per column (p_{column}) ; $p_{total,ideal} = p_{column} \cdot N_{columns}$. When using only one vacuum pump plus air supply and the full process only containing three different steps, the amount of columns should either be two or three.

During normal operation a flow of 10 Nm³/h at 4.5 bar pressure and an oxygen concentration of 93% would equate to a molar flow rate of $\dot{n}_{O_2} = \frac{0.93 \cdot 4.5 \cdot 10^5 \cdot 10}{4.5 \cdot 3600 \cdot 8.314 \cdot 293.15} = 0.11 \; mol/s$ which is 7.6 times larger than the test setup requirements. Peak loads can be up to 8 times higher than normal operation, therefore requiring oxygen flow rates of 0.88 mol/s. The hospital is assumed to have an oxygen demand for 11 hours per day and the PSA-unit can produce concentrated oxygen for 24 hours per day. When assuming that the oxygen can both be stored inside the cylinder packages and supplied to the hospital at the same time the following equation holds:

$$n(t) = S_0 - \left(t_{peak} \cdot 11 \cdot 3600 \cdot d\right) + \left(t_{peak} \cdot 24 \cdot 3600 \cdot p\right)$$

$$n(t) = S_0 - (t_d \cdot d) + (t_p \cdot p)$$

With,

n :	The amount of moles inside the oxygen storage after time t	[s]
S :	The storage capacity	[mol]
t_{peak}:	Peak load period	[days]
t_d:	Oxygen demand period	[s]
d :	The oxygen demand	[mol/s]
t_p:	Oxygen production period	[s]
p :	The oxygen production	[mol/s]

Table 10: Storage capacities and required production rates for an increasing number of cylinder packages with a three day peak load period.

Number of cylinder packages	Storage capacity S [mol]	Required production to carry peak load [mol/s]	Refill time [hours]
1	6427	0.38	4.7
2	12853	0.35	10.1
3	19280	0.33	16.3
4	25706	0.30	23.5
5	32132	0.28	32.0

Current hospital systems like the one at RdGG have a second and third oxygen source. The second source, which consists of a 3160 liters LOX storge, is able to carry the full normal demand for a maximum period of 26 days, considering 11 hours within a day. Which results in the capability to carry the peak demand for a little over three days. The third source, which are two cylinder packages with 99% oxygen at 200 bar, is smaller and can only supply the total normal demand for about three days. Meaning that this third source can only carry the peak demand for about 9 hours, which comes down to 4.5 hours/cylinder package. This period is from now on called t_{vital} = 9 hours.

For a hospital it is crucial to always have sufficient oxygen supply. In case the PSA-unit oxygen storage has completely been depleted and failure of the second source occurs, the refill time of the PSA-unit storage should be shorter than $t_{crucial}$. When achieving this the hospital is given enough time to change the cylinder packages each 4.5 hours and at the same time repair the second source. Of course, switching to the PSA-unit is also possible when its storage has not been filled completely yet, however wide margins make sure no exceptional situations cause an oxygen shortage. A refill time of t_{vital} requires an oxygen production rate of 0.40 mol/s for an oxygen storage with two cylinder packages (1.6 m^3).

As an initial estimate the model was run with the optimized parameters so, P_{AD} = 6 bar, P_{DP} = 1.05 bar, P_{VC} = 0.2 bar, L/v = 9.56 s, D/L = 0.1, but a volume which is 8 times larger (40 L). A setup with such a size would require a stronger vacuum pump and faster venting. For now both the venting and vacuum flow have been scaled with a factor of 8 as well. Just like for the test setup the vacuum pressure is determined first. A lower pressure is required since the concentration threshold is much higher. **Figure 50** shows the operating window for which the oxygen concentration is 93% or higher. The figure shows that a vacuum pressure of 0.1 bar is already too high in order to reach 93% oxygen production. Pressures below 0.045 bar pose mathematical limits within the IAST-calculations and are therefore not tested.
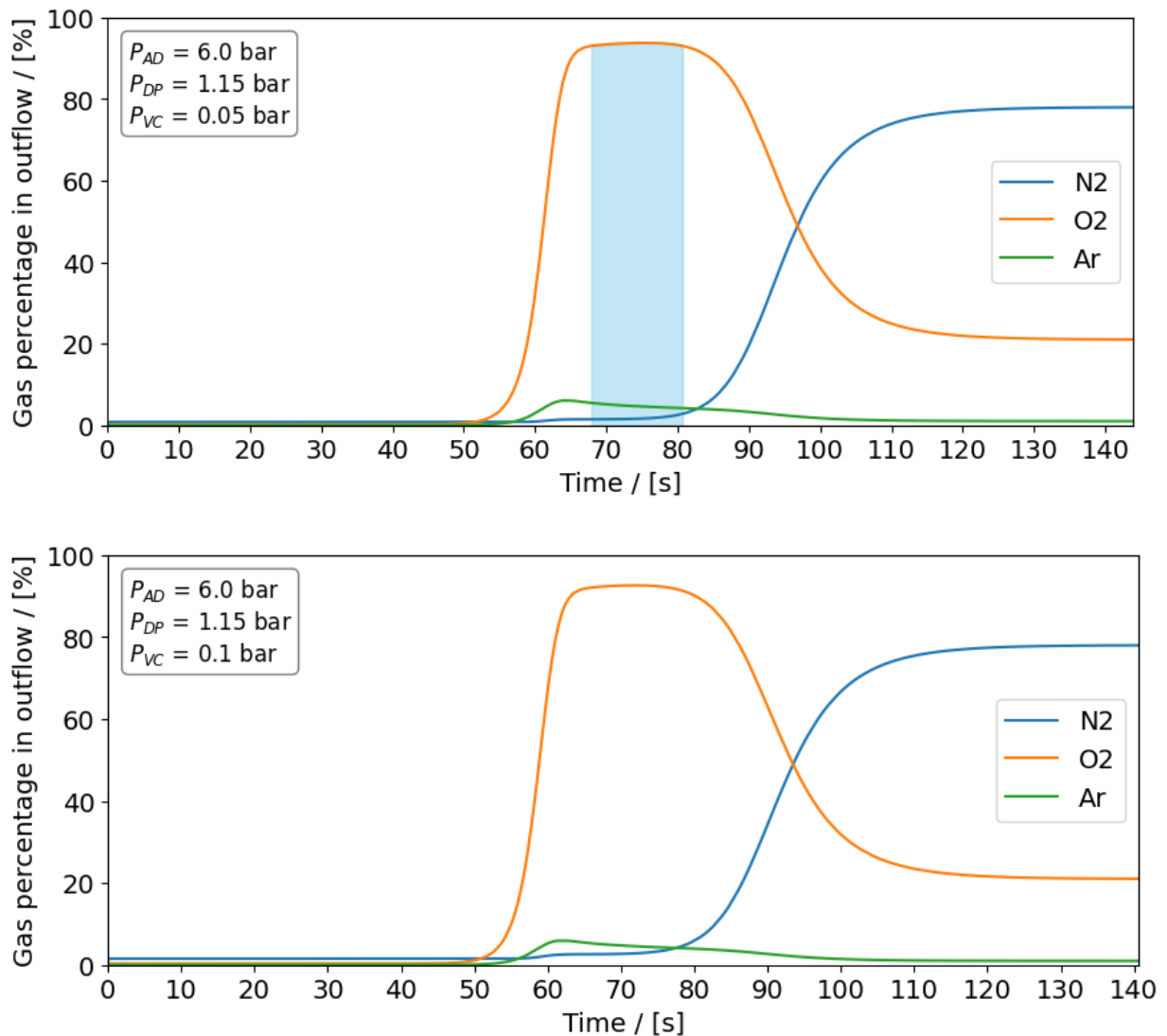
Figure 50: *Breakthrough curves for increasing vacuum pressures. Blue area indicating an oxygen concentration of 93% or higher. V = 40 L, D/L = 0.1 & t_c = 9.56 s.*

Figure 51 shows that if the threshold is set to 90%, which is also allowed, the operating window becomes much larger and even a vacuum pressure of 0.2 bar is still low enough to produce 90% oxygen.
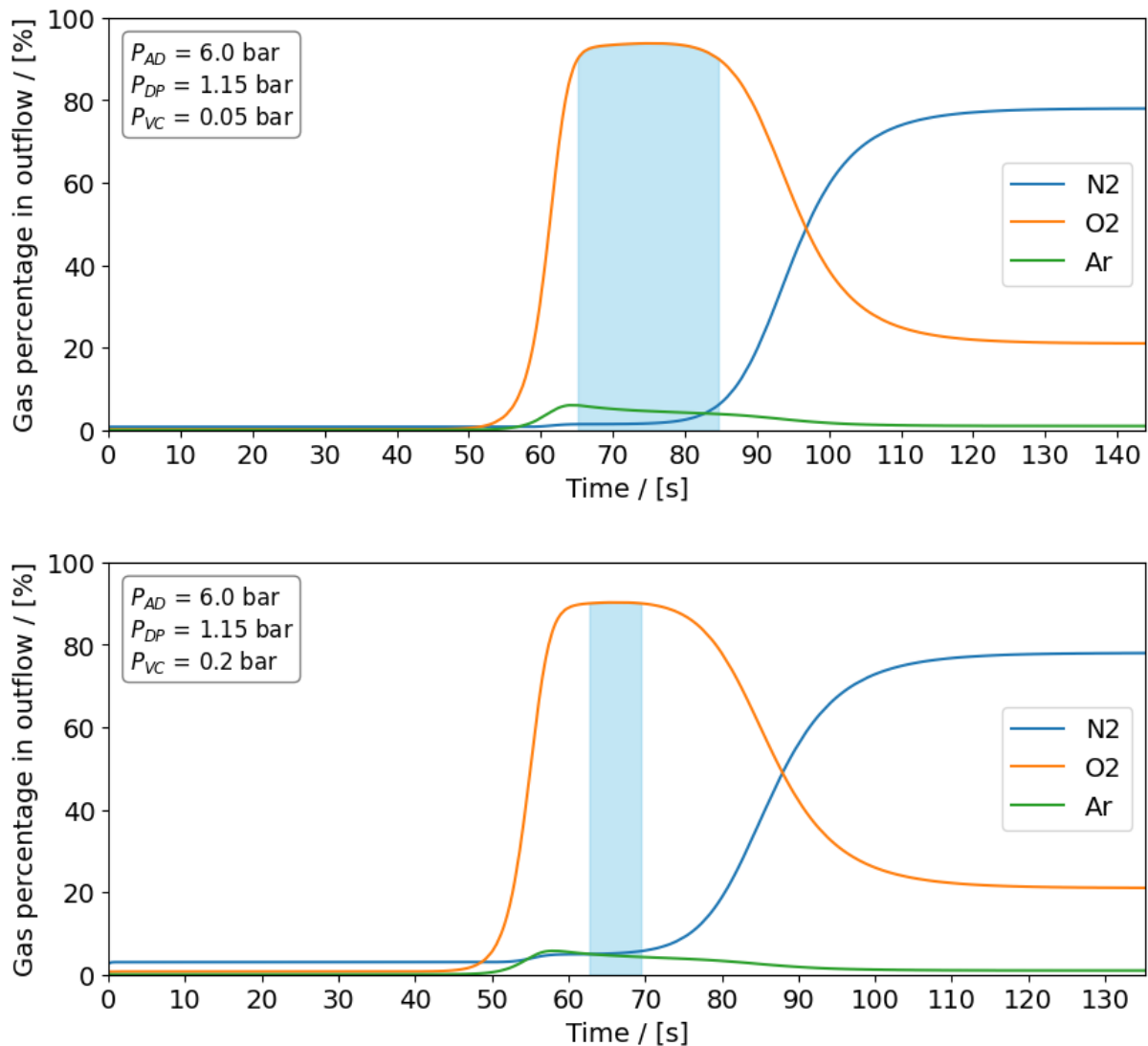
Figure 51: Breakthrough curves for increasing vacuum pressures. Blue area indicating an oxygen concentration of 90% or higher. V = 40 L, D/L = 0.1 & tc = 9.56 s.

With the optimized column of 40L the production per column comes down to only 0.0208 mol/s with the following step times: t_{AD} = 80.69 s, t_{DP} = 68.3 s, t_{VC} = 144.7 s. **Figure 49** already indicated that increasing the inlet velocity does lead to a reduced adsorption time, but decreases the overall oxygen production rate. For that reason there are two options to increase the total oxygen production rate:

1. Increase the volume of the column and thereby increase the amount of zeolite and oxygen production capacity.
2. Decrease the cycle time by decreasing the total vacuum time (t_{DP} + t_{VC}).

Figure 52 shows the effect of increasing the total volume of the column up to the maximum specified size from the requirements. For now the vacuum pump and valve performance have been scaled with the same ratio as the volume when comparing to the test setup (V_{test} = 5 L).
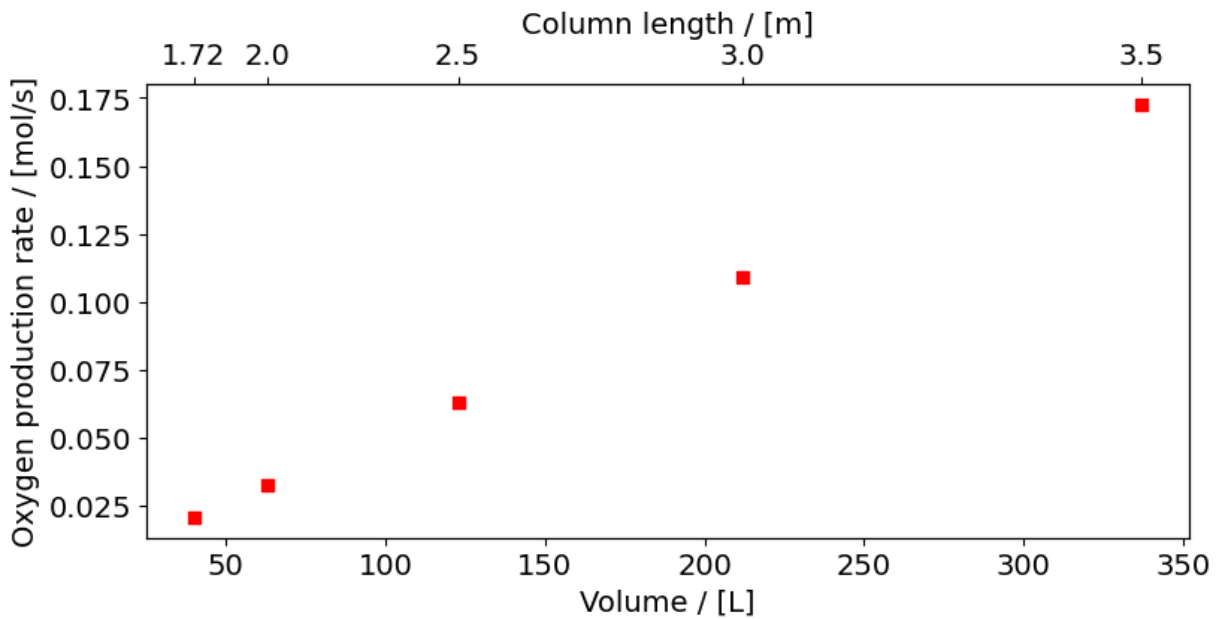
Figure 52: *93% Oxygen production rate per column for different column sizes. P_{AD} = 6 bar, P_{DP} = 1.05 bar, P_{VC} = 0.05 bar, D/L = 0.1, t_c = 9.56 s.*

The figure clearly shows a linear trend as one might expect with the made assumptions. It does however give some valuable insights in what minimum size the columns would require when the goal is to reach a production of 0.40 mol/s with only 2 or 3 columns. It shows that for a 40 L column a total of 20 columns is required and that for the maximum size column, with volume V_{max} = 337 L, a total of 3 columns is required which meets the requirements. The current total cycle time is 291 seconds. The scaling assumption for the valve performance does not cause any problems and can be realised by simply choosing a valve with a K_v which is V_{max}/V_{test} = 8.4 times larger. Resulting in a new $K_{v,DP}$ $\left(\frac{l\sqrt{K}}{min \cdot bar}\right) = 25.56 \cdot 8.4 = 214.70$. Looking back at the vacuum performance equation in **Table 9**, it becomes clear that when this equation is scaled by a factor 8.4, too high flows are estimated at low pressures. For this reason a new, larger vacuum pump has to be selected with correct flow behaviour at low pressures. With the current adsorption time of t_{AD} = 78.67 s and depressurization time of t_{DP} = 68.3 s one would ideally find a vacuum pump which leads to a vacuum pump time at a maximum of t_{VC} = 80 s. This way all three columns can work in parallel with only one vacuum pump and air supply. **Figure 53** shows the performance of four different vacuum pumps originating from the R5-line by Busch Vacuum Solutions.
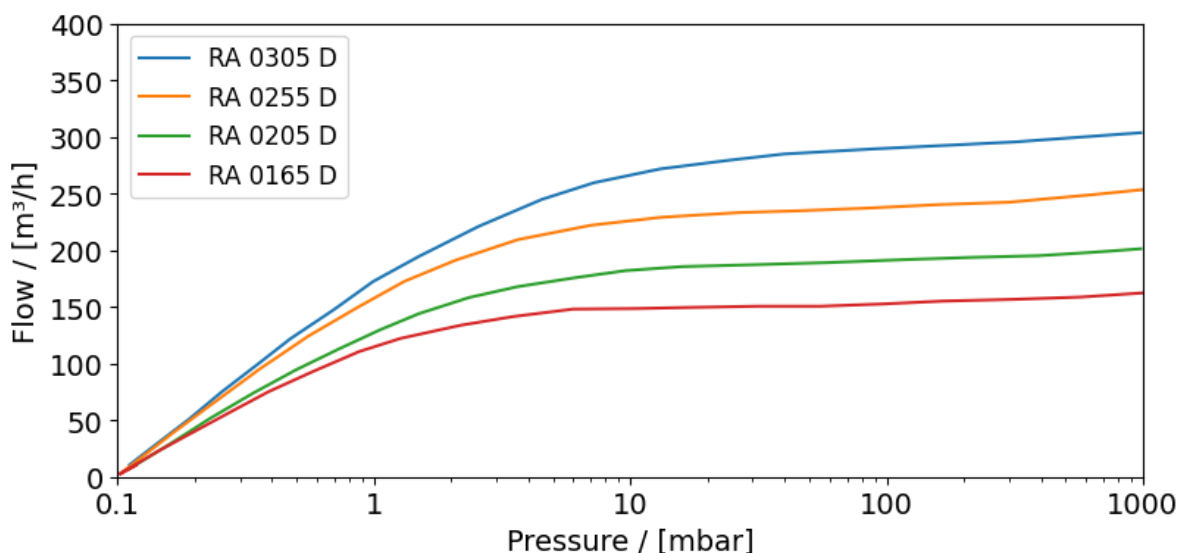
Figure 53: *Vacuum pump performance of four R5-type compressors by Busch Vacuum Solutions.*

These are oil lubricated rotary disc vacuum pumps which have enough capacity to vacuumize a 200-350 L column in a matter of minutes **Table 11** shows the new vacuum pump time and oxygen production rate for each edition.

Table 11: *Vacuum time and oxygen production rate for different R5-type vacuum pumps. P_{AD} = 6 bar, P_{DP} = 1.05 bar, P_{VC} = 0.2 bar, D/L = 0.1, t_c = 9.56 s, V = 336 L.*

Vacuum pump	Vacuum time [s]	Total cycle time [s]	Oxygen production rate [mol/s]
RA 0305 D	77.9	225.9	0.2526
RA 0255 D	92.3	238.53	0.2142
RA 0205 D	112.1	258.74	0.2031
RA 0165 D	136.6	283.58	0.1891

The table shows that when the vacuum pump time almost equals the adsorption time oxygen production rates of around 0.20 mol/s can be achieved. Meaning that with the current volume size two columns would also be able to deliver the required amount of oxygen while using the RA 0205 D. These columns could have the repeating cycle-sequence which is shown in **Figure 54**. The RA 0205 D has a nominal motor rating of 5.5 kW, a power consumption of 4.2 kW at 100 mbar and 3.3 kW at the ultimate pressure which is 0.1 mbar.
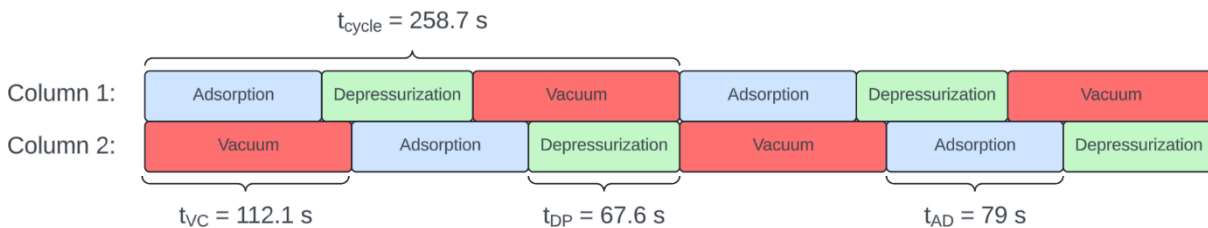
Figure 54: *Proposed cycle-sequence for a two column system with a total oxygen production rate of 0.41 mol/s.*

Due to the fact that only one vacuum pump is used, the vacuum steps should not overlap. This also holds for the adsorption steps. All other steps can occur at the same time. Even the vacuum step and depressurization step can occur simultaneously when the depressurization happens through the top of the column and the vacuum pump is installed at the bottom.

Now that the column size, number of columns, required valve flow coefficient and vacuum pump performance have been analysed there is only one equipment left which is the compressor. The compressor is responsible for the supply of sufficient air to the air storage in front of the PSA-unit. Considering that the oxygen storage tank has enough oxygen to supply a three day peak demand period, the air storage is not required to store large amounts of air at high pressure. The main purpose of this air storage is to have a small buffer which allows for a constant pressure when supplying the air to the PSA-unit. With an adsorption pressure of 6 bar it makes sense to store air at a slight overpressure. With the current diameter of d = 0.35 m, inlet velocity v_{in} = 0.366 m/s an adsorption pressure of 6 bar, the column inlet flow equals to 127 m^3/hr. Such conditions can easily be met by compressors by for instance Atlas Copco. This brand is already installed for the current compressed air facilities at RdGG. **Table 12** shows the technical specifications of the GA 37L VSD$^+$ edition. This is a premium compressor which complies with al standards and also has an integrated refrigerant dryer which make sure the gas temperature is managed.

The VSD allows for efficient electric usage of the compressor. As can be seen in the table, the operating range for the compressor with a maximum working pressure of 10.5 bara is 89-418 m³/h. The VSD allows the setup to run at the lower side of the operating range while using less electricity.

Table 12: *Technical specifications for the GA 37L VSD⁺.*

Compressor Type	Max. working pressure	Capacity (min-max)		Motor power (min-max)
	barg	l/s	m³/h	kW
	7	26-132	93-475	11.4-45
GA 37L VSD⁺	9.5	25-116	89-418	13.3-47.1
	12.5	38-99	138-355	22.6-48.2

To maintain some margin for system pressure drop and valve controllability, but still be able to reach sufficient flows, the air should be stored at 10 bar. This would require a valve with the following flow coefficient:

$$K_v = \frac{Q_g}{21.76 \cdot \sqrt{\frac{(P_{storage}^2 - P_W^2)}{T}}} = \frac{212}{21.76 \cdot \sqrt{\frac{(10^2 - 6^2)}{293.15}}} = 20.85 \ \frac{l\sqrt{K}}{min \cdot bar}$$

Since the air storage mainly serves as a stabiliser during small disturbances it should be able to accommodate the PSA-unit for 3 minutes at normal operating conditions when the compressor fails. This allows for alarms to be triggered and switch to using only stored oxygen or even switching to another source. With the current demand of the hospital this would require a 3 m³ vessel. With the columns having a height of 3.5 m, the air storage vessel would be 1.04 m in width in order to reach the desired volume. In case of complete depletion of the air storage vessel it would take the compressor around a minute and a half to refill the tank. This time is probably even shorter since the compressor reaches higher flow rates when the vessel pressure is low.

With all equipment specifications and process performances it's time to look at the performance metrics which were described in 2.2.4 Performance Metrics for Oxygen Adsorption-based Seperation Processes. When designing the system to purge product with an oxygen concentration of less than 93 % the current process is able to reach an average oxygen concentration of 93.61%. The oxygen recovery can be calculated by taking the ratio between the produced amount of oxygen in moles divided by the amount of moles which is fed into the PSA unit. During an adsorption time of 79.38 s and a flow of 35 l/s a total of 132 moles of oxygen if fed into the column. During this period 53.75 moles of oxygen 93 leaves the column. Resulting in a recovery of 41%. If the bottom range for the oxygen concentration is allowed i.e. 90%, the recovery already rises to 58%. The current setup would require 127 kg of zeolite which means a production of 5.75 mol O_2 kg⁻¹h⁻¹ which at the adsorption pressure translates to 0.66 m³ O_2 kg⁻¹ h⁻¹. The energy consumption requires a breakdown. Two steps of the total cycle require energy, these are the adsorption and the vacuum step. During the vacuum step the power of the vacuum pump decreases with pressure as mentioned earlier. For the compressor the power increases with its generated flow. For now the power behaviour is assumed to behave linear between the earlier mentioned pressure levels. When adding this up a single cycle requires 484 kJ of energy during the vacuum step and 1095 kJ for the adsorption step. Resulting in a total energy consumption of 29.38 kJ/mol which equals to 255 kWh/tO_2.

8. PSA adaptability

In order for a PSA plant to succeed it should fit into the current healthcare infrastructure as seamlessly as possible but never pose a danger to the security of supply and comply with all regulations from 6. Regulatory frameworks regarding a PSA-unit. This chapter examines the supply pressure and purity requirements as critical factors, addressing the required control system integration, and safety measures. The aim is to outline a practical strategy for the effective adoption of PSA technology in the current healthcare settings with a focus on reliability and operational efficiency.

8.1 Supply pressure

At the moment the RdGG makes use of two LOX installations as primary and secondary source and a cylinder package as backup source. Simply speaking the liquid oxygen is stored at 12 bar and is then decreased to 5 bar in several steps before being supplied to the hospital. The cylinder package stores oxygen at 200 bar which can be brought down to 5 bar in two pressure decreasing steps. This supply pressure has two important aspects , namely consistency and stability. Consistency refers to the fact that the supply pressure always needs to enter the hospital at around 5 bar, with a minimum of 4 bar and an absolute maximum of 6 bar. Stability refers to the fact that this supply needs to be constant in time and is also able to increase during higher demand. The oxygen supply system of hospital needs to be able to produce anywhere between 10 Nm^3/h and 100 Nm^3/h. In essence, consistent and stable pressure is a guarantee of an uninterrupted oxygen flow. A loss of pressure signifies an interruption in the supply. Maintaining a consistent supply pressure is crucial because medical devices, such as ventilators and anaesthesia machines, are calibrated to operate at specific pressures. Variations can lead to device malfunction, endangering patient care and safety. Stable pressures ensure that patients receive a reliable flow of oxygen for safe and effective treatment.

At the moment there are four general ways of maintaining the right supply pressure i.e. system redundancy, pneumatic FO (fail open) pressure controllers, pressure relief valves, alarm and monitoring systems. System redundancy is for example the usage of dual evaporators for a single storage tank and two final pressure regulation paths also shown in **Figure 22**. Such a setup ensures the system to still run if one of the two fails. Pneumatic FO pressure controllers build down the pressure in gradual steps, from 12 bar tot 10 bar and from 10 bar to 5 bar for the LOX installation. For the cylinder package pressure is reduced from 200 bar to 9 bar and then from 9 bar to 5 bar. Gradual pressure adjustments avoid sudden shocks to the system, allow for more control at each stage, increase safety as each step can have safety mechanisms and avoid heat formation due to large pressure drops. In a fail open configuration, the valve's default position is open when there is a failure in the control system, such as a power outage or loss of control signal. This way when a valve fails the oxygen is still provided to the hospital. Pressure relief valves would in such case reduce the pressure in the system to a certain set point by venting to the surrounding. Operational alarms are installed and go off when the liquid storage tank pressure drops below 6 bar. Urgent alarms indicate line pressures to the hospital either exceeding 5.8 bar or dropping below 4.2 bar.

When using a PSA setup, new measures need to be taken to control the supply pressure. **Figure 55** is a schematic overview of how a medical oxygen delivery system with a PSA-plant as primary source should look like according to NEN-EN-ISO 7396-1+A1:2019.
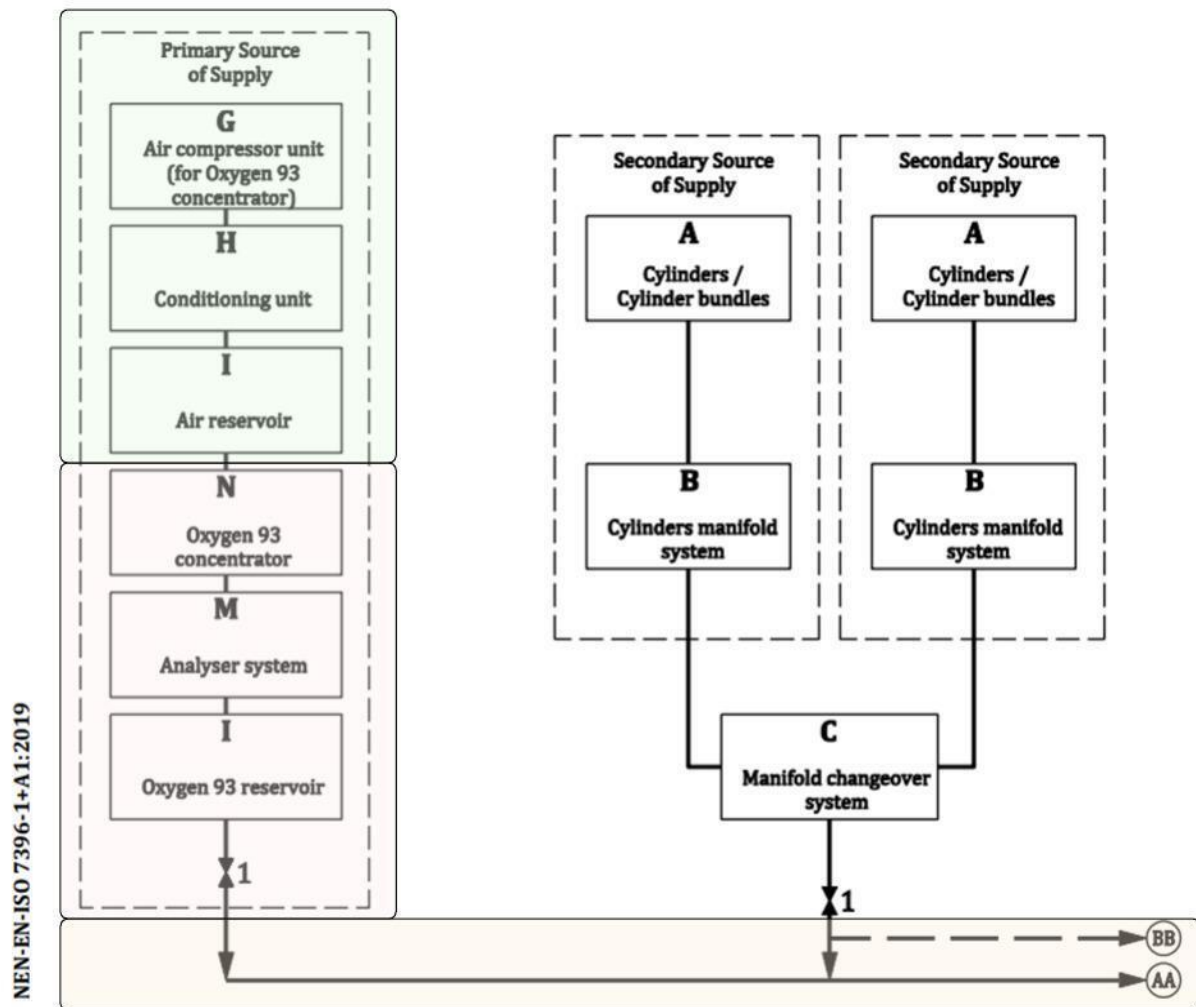
Figure 55: *Schematic supply system with an oxygen concentrator as primary source. Colours indicating the correspondence to the proposed PSA-plant in* ***Figure 56***.

This schematic and the regulatory frameworks in the previous chapter form the basis of the proposed adoption of a PSA-plant which will be extensively detailed within this chapter and which is shown in **Figure 56**. The setup is divided into three parts: 1) Air supply and pre-treatment (green), 2) Oxygen generation through PSA (red), 3) Supply to hospital (orange). **Figure 55** also shows how these parts correspond to the obligated components from the norm. **Figure 56** contains the most crucial elements. Obviously a more in depth P&ID should be made once the implementation of PSA is found feasible.
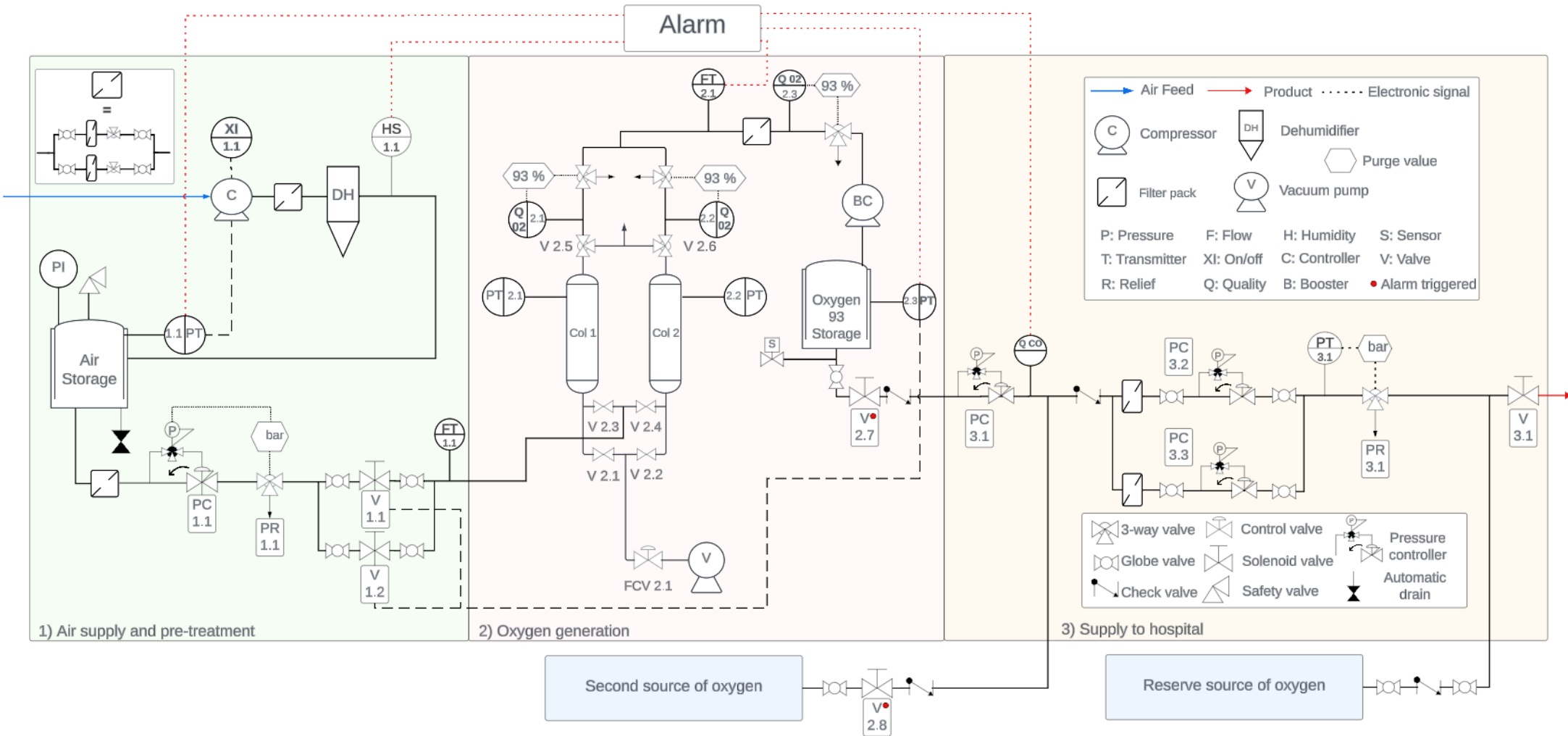
Figure 56: *Proposed adoption of a PSA-plant as a primary source onto the current infrastructure at RdGG. Complying to regulatory frameworks and focussing on certainty of supply and operational efficiency.*

The PSA system has quite some similarities with the current system but also some significant differences. Fresh air is compressed into the air storage tank which is being monitored on its pressure. Once the pressure reaches the desired upper set point, the compressor is turned off. As soon as it later drops below the lower set point, it is turned back on. This way the supply pressure of the air is maintained within the right range. In case the compressor fails, the pressure in the air storage tank will drop further below its lower set point, triggering an alarm. On top of the air storage tank both a safety relief valve and local manometer need to be installed. After the PSA unit the concentrated oxygen is stored in the oxygen storage cylinders after going through the booster compressor (BC). The pressure inside these cylinders is being monitored as well. When pressures exceed the upper set point, FO valve 1.1 (V1.1) is closed and the PSA unit is stopped as well as the booster compressor. The other way around, when the pressure drops below the lower set point, valve 1.1 is opened and the PSA unit and booster compressor are started. FO pressure controller 1.1 (PC 1.1) makes sure the PSA unit receives air at the right pressure. Once this controller would fail the relief valve (PR 1.1) behind it makes sure that the inlet pressure of the PSA unit is not receiving air with a too high pressure as this could damage the zeolite. In case of failure of the V1.1 the flow is switched to V1.2 avoiding air being fed into the PSA unit while the oxygen storage tank is already at its upper set point. The valves around V1.1 and V1.2 enable to block them in for maintenance during operation. Pressure transmitter 2.3 is linked to an alarm which indicates when the pressure drops too low, indicating that no new oxygen is coming into the oxygen storage. This would be the moment to automatically shut the PSA unit supply FO valve (V2.7) and open the FO supply valve (V2.8) of the second oxygen source with help of the pressure alarm on PT2.3. The valves before V2.7/2.8 enable to shut the supply of the system down if any of the two valves fail. The second source, which is the smaller LOX installation, has two pressure regulators to bring down the pressure before it is led into the final pressure controllers in the yellow part of the figure. For the oxygen coming from the oxygen storage tank the pressure is already reduced due to PC 3.1. Eventually the oxygen is supplied at the desired supply pressure to the hospital through valve PC 3.2/3.3. Here we see the redundancy again, allowing for one valve to fail. For the time in which the pressure controller is not switched yet, a pressure relief valve (PR 3.1) will avoid the entrance of gas at excess pressure. The third and final source, which is the package of cylinders, is connected to the system after the pressure controllers. This is the same situation as in the current layout. Valve 3.1 enables to shut off the complete oxygen supply to the hospital. Throughout the system 4 different check valves avoid backflow of oxygen from one source to another.

8.2 Purity requirements

Besides a stable and consistent flow of oxygen it is also crucial to supply oxygen which has the right purity. The hospital's pharmacist is responsible for the purity of the supplied oxygen as described in 2.5.3 Regulatory Frameworks. When using a PSA plant, the responsibility for oxygen purity shifts more directly to the hospital since the oxygen is produced on-site rather than supplied by a manufacturer. Unlike pre-tested gas from manufacturers, PSA systems require continuous, real-time monitoring to ensure that the produced oxygen consistently meets medical standards. The hospital pharmacist, as the end responsible party, must implement robust monitoring systems to track oxygen purity, manage any deviations promptly, and ensure compliance with health regulations. Maintaining high oxygen purity is crucial because medical applications require oxygen at specific purity levels to ensure patient safety and effective treatment. Even though most applications mix pure oxygen with air, so the slightly lower purity from PSA systems does not pose a significant problem, some hospital equipment is now calibrated for nearly 100% pure oxygen.

Unlike real-time measurement devices, like modern ventilators in intensive care units, assumption based devices have no knowledge about the incoming oxygen purity. This would have to be revised as reaching the same purity of LOX-installations with PSA is physically extremely challenging.

One thing to also consider is that the purity between the three sources now has a slight deviation i.e. 93% for PSA and 99% for LOX. Switching between the different sources should not pose problems for hospital equipment, therefore requiring more real-time measurement devices. The focus within this paragraph will be solely on the production side i.e. how to make sure that the PSA oxygen purity is maintained at 93%. Besides purity measures also measures which avoid contamination of the product will be addressed.

Even though high purity oxygen is fed into the current LOX-system, there are still some measures within the system to maintain the product quality. The most notable one are the filters which are installed after the evaporator and before the final pressure controllers to remove particulate matter and contaminants. These particles not only pose a danger to patient treatment, but could also lead to ignition under these high oxygen concentrations. The focus will however be on maintaining product purity during on-site oxygen production as the scope of this research would otherwise become too large. Obviously material selection, electrostatic charge prevention and filter housing should always be considered in a broader perspective. The current LOX-installation has some valves that allow for taking test samples. These allow for the verification of quality on arrival, enabling to take independent samples. Provide ongoing quality assurance as quality can be compromised by contamination or changes in purity during storage, or in the event of suspected contamination. Finally, some regulatory bodies might require test sampling.

PSA systems require different techniques to ensure product purity. Looking at **Figure 56** again, there are some important measures to be found. A filter after the compressor removes particles which were in the air or ended up in the air after the compressor. Note that the filter icon represents a filter pack who's content is shown in the top left of the figure. Each pack consists of two parallel filters, allowing to switch between them during continuous operation. The block vales around the filters make sure they can be blocked in when the filter is cleaned or repaired. The pressure relief valve downstream the filter is installed for safe venting during maintenance. The dehumidifier after the compressor removes moisture from the air. Water has a detrimental effect on the zeolite performance as described in 2.2.3 Adsorbent Materials, this could cause the PSA unit to not reach sufficient levels of purity. The humidity sensor after the dehumidifier triggers an alarm when the moisture concentration starts increasing. Indicating that the dehumidifier is failing or needs replacement. At the bottom of the air storage tank an automatic condensation drain makes sure that any liquid that came past the dehumidifier (DH) is carried away. A filter pack after the air storage removes any contaminants that entered the air during storage. As oxygen leaves one of the two columns the oxygen concentration is directly measured by an oxygen analyser or oxygen quality sensor QO2 2.1/2.2. If this drops below 93%, it will be vented to the surroundings. In case that this oxygen quality sensor fails, there is a second sensor, QO2 2.3, after a filter pack before entering the air storage. This filter pack removes contaminants, potentially really small zeolite particles, which entered during the oxygen generation. An alarm on the flow transmitter FT2.1 notices when insufficient flow is coming from the PSA unit, indicating that the unit is not working or venting all of its product due to low concentrations. If the product is vented after QO2 2.3, the alarm from PT2.3 will notice that the oxygen storage pressure is dropping. A sampling point is installed directly downstream of the oxygen storage tank. At last, the carbon monoxide alarm sensor after PC 3.1 makes sure no product with excess carbon monoxide is led into the hospital.

9. Economic viability

The aim of this chapter is to address the economic factors that come with implementing a PSA plant. For a hospital like RdGG its important to know how this new method compares to the current oxygen delivery system. A distinction will be made between operational costs and capital investments. Additionally the analysis will be conducted over a 20-year period to account for depreciation, providing a long-term perspective on the financial implications of transitioning to a PSA plant.

9.1 Capital investments

Online research and provided information on equipment prices by RdGG will be used to estimate capital investments. Looking back at **Figure 55** a list of new required equipment can be made which is shown in **Table 13** along with an estimate of the price. As mentioned in 7.2 Scaling the setup to hospital size each column contains 127 kg of zeolite which is at a price of 35 EUR/kg, resulting in a total cost of 8890 EUR for two columns.

Table 13: Fixed capital investment estimation for the complete proposed PSA-system at RdGG.

Equipment	Estimated price [EUR]	
Air compressor	32,000	
Dehumidifier	5,700	
Air storage	6,600	
PSA-unit	100,000	
Vacuum pump	5,500	
2 x Oxygen 93 cylinder packages	2,000	
Booster compressor	10,000	
5 x filter kit	15,000	+
Total Fixed Equipment Costs	176,800	
Zeolite	8,890	
Piping	17,500[*1]	
Control system	8,500[*2]	
Engineering costs	8.500[*3]	
Alarm- and monitoring system	3,500[*4]	+
Total Investment Costs	215,190	

[*1] The costs for piping are assumed to be 10% of the total fixed equipment costs.

[*2] The costs for the complete control system is assumed to be 5% of the total fixed equipment costs.

[*3] The engineering costs are assumed to be 5% of the total fixed equipment costs.

[*4] The costs for the alarm- and monitoring system is assumed to be 2% of the total fixed equipment costs.

When excluding the engineering costs and using a straight-line depreciation method over 20 years, the yearly depreciation of the total setup comes down to 9890 EUR/y. The equipment is not assumed to have any residual value after this period.

9.2 Operational costs

The results from the numerical modelling gave an estimate for the energy consumption of the PSA-unit per weight amount of Oxygen 93. Energy consumption estimations will be done for the latest available yearly oxygen consumption provided by RdGG, which was 234,000 kg. The price per kWh of electricity is 9.5 EUR ct. Besides the energy consumption there is also costs for maintenance. Both the estimation for the maintenance costs and the electricity price were provided by RdGG as well. **Table 14** shows all costs for the PSA-unit on a yearly basis.

Table 14: Annual estimated PSA-unit costs for the RdGG with a yearly oxygen demand of 234,00 kg and an electricity price of 9.5 ct per kWh.

Cost type	Yearly costs [EUR/y]	
Energy consumption	5,700	
Depreciation	9,890	
Maintenance[*1]	10,000	+
Total annual costs	25,590	

[*1] Estimation provided by RdGG.

Current prices for liquefied oxygen lie around 26 EUR ct/kg. At a total consumption of 234 tO_2 this totals to yearly annual raw material costs of 60,840 EUR. This already shows the potential of the PSA-unit since there are also extra costs for the current system e.g. maintenance, electricity, depreciation, transportation. **Figure 57** shows the development of the yearly oxygen consumption by RdGG.
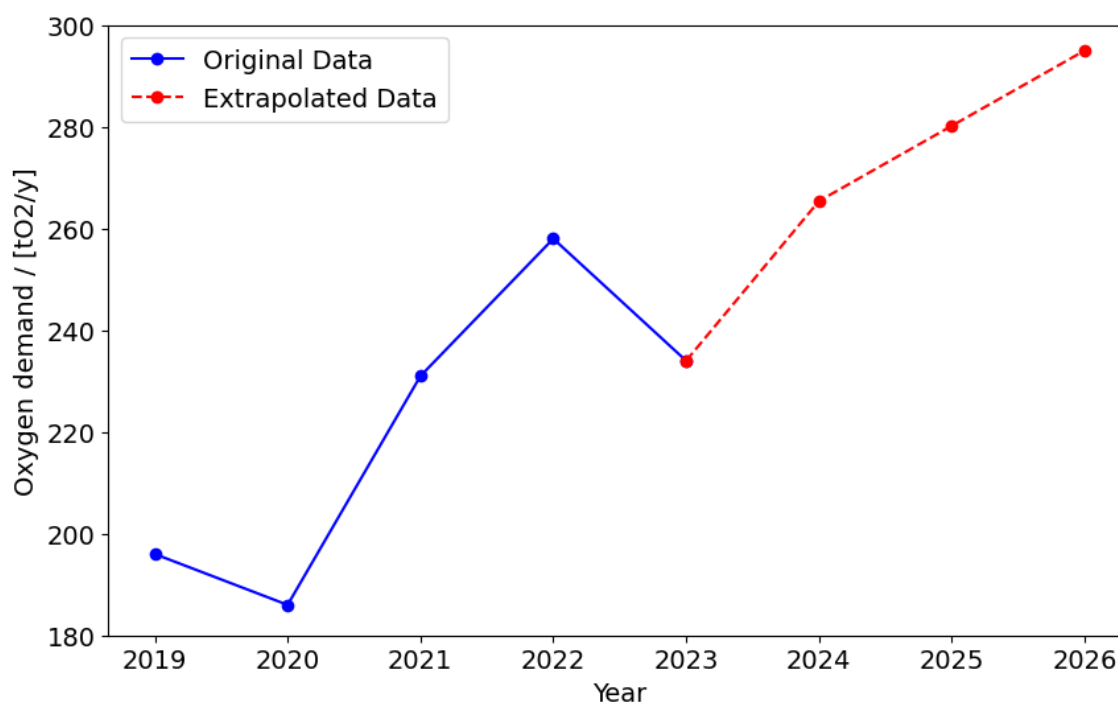
Figure 57: Development and future estimation of the oxygen demand for the RdGG.

The figure shows a general increase in oxygen demand which emphasizes on the importance of potentially having a cheaper alternative. When extrapolating this trend the oxygen demand in 2026 could already be as high as 295 tO_2/y. This would make the current installation 2.8 times more expensive on an annual cost basis. The calculation does not even take into account potential increases in liquefied oxygen which has happened during the past years.

Having all of the information on the CAPEX, OPEX and an estimation on the required future production; it is possible to compare the levelized cost of oxygen (LCOO) of PSA with the LCOO of LOX. The LCOO can be thought of as the average total cost of building and operating an asset per unit of oxygen produced over the assumed lifetime. During this calculation the net present value (NPV) of both the costs and production are calculated. This way the economic feasibility of a project considers the time value of money.

$$LCOO = \frac{NPV\ of\ total\ costs\ over\ lifetime}{NPV\ of\ oxygen\ produced\ over\ lifetime} = \frac{\sum_{t=0}^{LT} \frac{(I_t + M_t + E_t)}{(1 + r)^t}}{\sum_{t=0}^{LT} \frac{O_t}{(1 + r)^t}} \qquad 9.1$$

LT	:	total lifespan of the installation	y
t	:	time index	y
I	:	initial investment	EUR
M	:	maintenance costs	EUR
E	:	electricity costs	EUR
r	:	discount rate	%
O	:	oxygen production	tons

Table 15: Levelized costs of oxygen calculation when using PSA.

Assumptions (in 1000's for EUR amounts)		
Total Initial Investment	(EUR)	215
Maintenance Costs, MC	(EUR)	10
MC Growth Rate[1]	(%)	2
Annual Electricity Costs	(EUR)	5.7
Electricity Price Growth Rate[2]	(%)	2.2
Annual Oxygen Demand	(t/y)	234
Growth Annual Oxygen Demand[3] t = 0,…,5	(%)	5
Growth Annual Oxygen Demand[3] t > 5	(%)	2
Project Lifespan	(years)	20
Discount Rate	(%)	8

Total Costs (in 1000's for EUR amounts)		Entry	5	10	15	20
Initial Investment	(EUR)	215	-	-	-	-
Maintenance Costs	(EUR)	-	10.8	12.0	13.2	14.6
Electricity Costs	(EUR)	-	6.22	6.93	7.73	8.62
Discount Factor		-	68.1%	46.3%	31.5%	21.5%
Present Value of Costs	(EUR)	215	11.6	8.75	6.60	4.97
NPV of Total Costs	(EUR)	394.23				

Total Oxygen Demand		Entry	5	10	15	20
Yearly Oxygen Demand	(tons)	-	298.65	329.73	364.05	401.94
Discount Factor		-	68.1%	46.3%	31.5%	21.5%
Present Value of Demand	(tons)	-	203.26	152.73	114.76	86.24
NPV of Total Demand		3065.37				

LCOO	(EUR/ton)	128.61

[1]Maintenance costs assumed to increase with the average Dutch inflation over the past 30 years [55].
[2]Dutch electricity prices had an average coumpounding annual growth rate of 2.2% for 30 years [56].
[3]The growth on the annual oxygen production is estimated by the Piecewise Linear Growth model which assumes an increase in demand of 5% during the first 5 years (average of past 4 years) and a 2% growth during the last 15 years. Increasing the total oxygen demand by a factor of 1.72. In case the LOX installation is kept as oxygen source this would mean that the maximum flow of the system is being approached. The current average hourly flow is 58.8 Nm3/h with the system maximum at 100 Nm3/h.

Table 16: Levelized costs of oxygen calculation when using LOX.

Assumptions (in 1000's for EUR amounts)		
Total Initial Investment	(EUR)	0
Maintenance Costs, MC	(EUR)	10
MC Growth Rate	(%)	2
Annual LOX Costs	(EUR)	60.84
LOX Price Growth Rate[1]	(%)	4.5
Annual Oxygen Demand	(t/y)	234
Growth Annual Oxygen Demand t = 0,…,5	(%)	5
Growth Annual Oxygen Demand t > 5	(%)	2
Project Lifespan	(years)	20
Discount Rate	(%)	8

Total Costs (in 1000's for EUR amounts)		Entry	5	10	15	20
Initial Investment	(EUR)	0	-	-	-	-
Maintenance Costs	(EUR)	-	10.8	12.0	13.2	14.6
LOX Costs	(EUR)	-	67.87	75.67	84.37	94.06
Discount Factor		-	68.1%	46.3%	31.5%	21.5%
Present Value of Costs	(EUR)	0	53.56	40.58	30.76	23.31
NPV of Total Costs	(EUR)	829.23				

Total Oxygen Demand		Entry	5	10	15	20
Yearly Oxygen Demand	(tons)	-	298.65	329.73	364.05	401.94
Discount Factor		-	68.1%	46.3%	31.5%	21.5%
Present Value of Demand	(tons)	-	203.26	152.73	114.76	86.24
NPV of Total Demand		3065.37				

LCOO	(EUR/ton)	270.52

[1]Online data shows a compounding annual growth rate in the LOX price of 4.5% [57].

Table 15 and **Table 16** respectively show the LCOO-calculation for using PSA and LOX. Obviously the LOX-case would not require an initial investment since the installation is already there. The LCOO for PSA turns out to be 128.61 EUR/ton which is 2.1 times lower than that of LOX, which is 270.52 EUR/ton. This is caused by the high price for liquid oxygen which also on average grows 4.5% each year. The calculations confirm the possible cost-effectiveness and efficiency of using a PSA-plant over the LOX-installation. Making the PSA-plant preferable choise for investment and implementation.

10.   Conclusions & Recommendations

This chapter will present the key conclusions which were drawn from the research and what can be learned from it. Answers will be given to research question and the sub questions. Also limitations of the research will be discussed to highlight what further research needs to be done. This will come in the form of recommendations.

10.1   Conclusions

Dutch regulations obligate hospitals to have at least three oxygen sources. Each source needs to be able to provide the design flow if both other sources fail. This then obviously also holds for a potential PSA-unit as primary source. Regulations force the PSA-unit to be able to reach a 93% oxygen concentration, which is allowed to deviate ± 3%. It should also comply with strict limits on impurities such as carbon monoxide, carbon dioxide, oil, water vapor, nitrous gases, and sulfur dioxide. When storing the oxygen locally the storage needs to have a sampling point to assure quality while oxygen analysers and filter packages aim to guarantee the right quality. Filling of the storage, which is a package of 12x50 L cylinders at high pressure (200 bar), should not interfere with the supply of oxygen to the hospital. Compressed air storage for feed regulation is allowed as long as the storage is equipped with safety valves, an automatic condensation drain, a manometer and a pressure regulator or transmitter. Control mechanisms need to make sure that once the PSA-unit does not meet its concentration requirements an automatic switch to another source takes place.

In order to reach the required oxygen purity a vacuum pressure of 0.05 bar is required. With the current zeolite (Oxysiv MDX) the optimal oxygen production rate was found at an adsorption pressure of 6 bar. Switching on the vacuum pump early when decreasing the column pressure instead of venting through the valve turns out to only slightly decrease the vacuum pump time. Having the compressor on for 14.1% longer only caused a vacuum pump time reduction of 4.1% For that reason, the depressurization pressure, which is the pressure at the vacuum pump is switched on, should be close to atsmopheric pressure i.e. 1.05 bar. The same amount of zeolite is most effectively used for an adsorption column which has a diameter over length ratio of $D/L = 0.1$. The dimensionless time t_c, which expresses the time it takes the gas to travel the length of the column, which had the highest oxygen production was 9.56 s.

As a primary oxygen source for RdGG the PSA-unit should always be able to carry normal demand, 10 Nm^3/h, but also be able to supply the peak demand, 80 Nm^3/h, for three consecutive days. This peak demand can be carried by using the oxygen storage after the PSA-unit. The current second source at RdGG can carry the peak demand for three days and the backup source can only carry peak demand for 9 hours. This latter period is called $t_{vital} = 9$ hours. In a situation where the PSA-storage is completely depleted and the second source fails, t_{vital} is the time it should take the PSA-storage to be filled again. A refill time of t_{vital} turns out to require an oxygen production rate of 0.40 mol/s and two cylinder packages for storage (1.6 m^3). To reach this rate two 336L adsorption columns are required with a height of 3.5m. Meaning a diameter of 0.35 m and an inlet velocity of 0.36 m/s which equates to an air inlet flow of 126 m^3/hr. A vacuum pump like the RA 0205 D and a compressor like the GA 37 L VSD$^+$ allow for the following step times: $t_{AD} = 79$ s, $t_{DP} = 67.$ s and $t_{VC} = 112.1$ s adding up to a total cycle time of $t_{cycle} = 258.7$ s. With three cycle steps and the mentioned step times, two columns can be ran in parallel with only requiring one vacuum pump and air supply. Having a 3 m^3 pressure vessel storing air at 10 bar allows the PSA-unit to still run for three minutes in case of compressor disturbances.

The described setup is able to reach oxygen purities of 93.61% with a total recovery of 41%. This recovery is for oxygen with a minimum concentration of 93%. If oxygen at 90% is stored, which is allowed according to the standards, the recovery rises to 58%. Two columns require 127 kg each to be filled with zeolite, resulting in a production of 5.75 mol O_2 $kg^{-1}h^{-1}$ which at the adsorption pressure translates to 0.66 m^3 O_2 kg^{-1} h^{-1}. Each mole of oxygen requires an energy consumption of 29.38 kJ which means a total of 255 kWh/tO_2.

For a hospital to use a PSA-unit as a primary source it does require some large modifications. The technique requires quite some equipment which is not required and therefore not present in the current oxygen supply system. Some of the equipment are: air compressor, air storage tank, PSA-unit, booster compressor and oxygen storage tank. Since we are now always dealing with gases different control mechanisms and monitoring systems are required. Also the piping has to be redone completely. However when correctly controlling the flow and pressure to the current levels, the second and backup sources can be connected to the PSA-unit in the same way they are now connected to the large liquid oxygen source. The final pressure regulation can even be kept completely the same as in the current situation, allowing for easier integration.

The economics of a PSA-unit consist of two main components: fixed capital investments as indicated in the previous paragraph and operational costs. The total investment costs for a complete PSA-plant was estimated at 215,190 EUR. Total fixed equipment costs make up 176,800 EUR of this total amount. The rest comes from costs like piping, control systems, alarm systems and engineering. When using a straight line depreciation method for 20 years yearly depreciation ends up to be 9890 EUR. Other annual costs are energy consumption and maintenance costs. With an oxygen demand of 234 tons in 2023, this would require an annual cost basis of 25,590 EUR, compared to the actual costs of 60,840 EUR with the current LOX installation. The LCOO for PSA is 128.61 EUR/ton which is 2.1 times lower than LOX at 270.52 EUR/ton. This is driven by the high price of liquid oxygen growing at 4.5% annually, making the PSA-plant a more cost-effective and efficient investment.

10.2   Recommendations

In light of the conducted analyses, multiple key recommendations can improve the feasibility study on using PSA in Dutch hospitals. This would eventually lead to an even more realistic overview on the requirements and performances.

- The mentioned regulatory frameworks should be approved or new ones should be suggested by a party with extensive knowledge on the regulation of medical oxygen production.
- To better simulate the lifecycle of a PSA-unit, potential degradation of the zeolite should be analysed. Also the current zeolite should be analysed on whether it reaches the performance according to the specifications.
- Instead of modelling the column as a CSTR during the depressurization and vacuum step, it should be discretized just like the adsorption step. This way the model would approach reality even more. Adsorption times where now sufficiently large enough to take the average loadings at the final timestep within the adsorption step as a good estimate for the column loadings at the beginning of the depressurization step. However, if the adsorption time would decrease, this could not be the case anymore.
- Due to the large vacuum time the loadings at the beginning of the adsorption step were assumed to equal the equilibrium loadings. This only holds when the vacuum step is long due to the high purity requirement, like for the RdGG system. For lower purity requirements this assumption might not hold and should be researched in further detail.

- Due to mathematical limitations within the adsorption equilibrium model the vacuum pressure needed to be at least 0.045 bar. Adjusting the root finding algorithm would allow for running the model with even lower pressures.
- The current model assumes a constant temperature. This assumption should be validated by doing more temperature measurements within the setup since the performance is temperature dependent in reality.
- The current experimental setup did not allow for slow passing of the gas and allowed backflow. This caused air to pass quickly through the column once it was opened. Resulting in high concentration measurements for only a short period of time. This is the reason why no concentration validation could be done.
- The proposed PSA-setup should be validated by looking at industry practices or manufacturers of this kind of setups. This way any missing or redundant equipment can be notified.
- The economic analysis is now based on online prices. Requesting quotes or checking hospital bills should give a more accurate price estimation.

References

[1] Ismail, J., & Bansal, A. (2022). Medical Oxygen: a Lifesaving Drug during the COVID-19
Pandemic—Source and Distribution. *Indian Journal of Pediatrics*, *89*(6), 607–615.
https://doi.org/10.1007/s12098-021-03978-0

[2] *Global Oxygen Alliance launched to boost access to life saving oxygen*. (2023). PAHO/WHO |
Pan American Health Organization. https://www.paho.org/en/news/25-5-2023-global-oxygen-
alliance-launched-boost-access-life-saving-oxygen

[3] *Strengthening Medical Oxygen Ecosystems*. (n.d.). USAID. Retrieved January 28, 2024, from
https://www.fhi360.org/sites/default/files/media/documents/resource-epic-covid-19-oxygen-
synthesis-brief.pdf

[4] White, H. D., Danesh, V., Ogola, G. O., Jimenez, E. J., & Arroliga, A. C. (2023). Quantifying
oxygen supply and demand during the COVID-19 pandemic: An integrated health system
perspective. *Intensive & Critical Care Nursing/Intensive and Critical Care Nursing*, *75*,
103374. https://doi.org/10.1016/j.iccn.2022.103374

[5] Holloway-Phillips, M. (2018). Photosynthetic oxygen Production: New method brings to light
forgotten flux. *Plant Physiology*, *177*(1), 7–9. https://doi.org/10.1104/pp.18.00344

[6] Asghari, E., Abdullah, M., Foroughi, F., Lamb, J. J., & Pollet, B. G. (2022). Advances,
opportunities, and challenges of hydrogen and oxygen production from seawater electrolysis:
An electrocatalysis perspective. *Current Opinion in Electrochemistry*, *31*, 100879.
https://doi.org/10.1016/j.coelec.2021.100879

[7] P. Rao, M. Muller, Industrial oxygen: its generation and use, ACEEE Summer Study on
Energy Efficiency in Ind. 6 (2007) 124–135.

[8] Smith, A. R., & Klosek, J. (2001). A review of air separation technologies and their integration
with energy conversion processes. *Fuel Processing Technology*, *70*(2), 115–134.
https://doi.org/10.1016/s0378-3820(01)00131-x

[9] Headquarters, W. (2020, April 4). *Oxygen sources and distribution for COVID-19 treatment
centres*. https://www.who.int/publications/i/item/oxygen-sources-and-distribution-for-covid-
19-treatment-centres

[10] Aneke, M., & Wang, M. (2015). Potential for improving the energy efficiency of cryogenic air separation unit (ASU) using binary heat recovery cycles. *Applied Thermal Engineering*, *81*, 223–231. https://doi.org/10.1016/j.applthermaleng.2015.02.034

[11] Banaszkiewicz, T., Chorowski, M., & Gizicki, W. (2014). Comparative analysis of cryogenic and PTSA technologies for systems of oxygen production. *Nucleation and Atmospheric Aerosols*. https://doi.org/10.1063/1.4860866

[12] *Medical Oxygen Cylinders Market Size, Share & Trends Analysis Report by product type (Fixed, Portable), by application (Home-care, Non Home-care), by technology, by region, and segment Forecasts, 2023 - 2030*. (2022, April 26). https://www.grandviewresearch.com/industry-analysis/medical-oxygen-cylinders-market-report

[13] Guenot, M. (2021, April 23). India's COVID-19 surge is highlighting a ruthless, global black market for oxygen, where sellers jack prices up to 1,000%. *Business Insider*. https://www.businessinsider.com/india-covid-19-black-market-oxygen-crisis-1000-markup-2021-4?international=true&r=US&IR=T

[14] Industrial Oxygen Generation, https://www.zeochem.com/our-applications/ industrial-oxygen-generation (accessed: January 22 2024).

[15] Benkirane, L., Metyouy, K., & Chafik, T. (2024b). Integration of Large-Scale pressure swing adsorption units in local hospitals in Morocco: Design, simulation and performance evaluation. *Separation and Purification Technology*, *333*, 125886. https://doi.org/10.1016/j.seppur.2023.125886

[16] Smith, V., Changoor, A., McDonald, C. R., Barash, D., Olayo, B., Adudans, S., Nelson, T. J., Reynolds, C., Cainer, M., & Stunkel, J. (2022). A Comprehensive Approach to Medical Oxygen Ecosystem Building: An implementation case study in Kenya, Rwanda, and Ethiopia. *Global Health, Science and Practice*, *10*(6), e2100781. https://doi.org/10.9745/ghsp-d-21-00781

[17] *WHO and EU hand over life-saving medical oxygen plant to Somalia: a landmark achievement in bridging gaps in oxygen supply in the country - Somalia*. (2022, March 20).

ReliefWeb. https://reliefweb.int/report/somalia/who-and-eu-hand-over-life-saving-medical-oxygen-plant-somalia-landmark-achievement

[18] Oxygen Plant Find & Fix Map. Updated September 9, 2022. Accessed Januari 3, 2024. https://experience.arcgis.com/experience/c3584c0ebcba4833a0159ffff17c2c89

[19] Holloway-Phillips, M. (2018b). Photosynthetic oxygen Production: New method brings to light forgotten flux. *Plant Physiology*, *177*(1), 7–9. https://doi.org/10.1104/pp.18.00344

[20] *You may be surprised where most of Earth's oxygen comes from*. (n.d.). https://www.thomasnet.com/insights/you-may-be-surprised-where-most-of-earth-s-oxygen-comes-from/

[21] Katebah, M., Al-Rawashdeh, M., & Linke, P. (2022). Analysis of hydrogen production costs in Steam-Methane Reforming considering integration with electrolysis and CO2 capture. *Cleaner Engineering and Technology*, *10*, 100552. https://doi.org/10.1016/j.clet.2022.100552

[22] Hu, K., Fang, J., Ai, X., Huang, D., Zhong, Z., Yang, X., & Wang, L. (2022). Comparative study of alkaline water electrolysis, proton exchange membrane water electrolysis and solid oxide electrolysis through multiphysics modeling. *Applied Energy*, *312*, 118788. https://doi.org/10.1016/j.apenergy.2022.118788

[23] Kato, T., Kubota, M., Kobayashi, N., & Suzuoki, Y. (2005). Effective utilization of by-product oxygen from electrolysis hydrogen production. *Energy*, *30*(14), 2580–2595. https://doi.org/10.1016/j.energy.2004.07.004

[24] García-Luna, S., Ortíz, C., Chacartegui, R., & Pérez-Maqueda, L. A. (2023). Large-scale oxygen-enriched air (OEA) production from polymeric membranes for partial oxycombustion processes. *Energy*, *268*, 126697. https://doi.org/10.1016/j.energy.2023.126697

[25] Valappil, R. S. K., Ghasem, N., & Al-Marzouqi, M. (2021). Current and future trends in polymer membrane-based gas separation technology: A comprehensive review. *Journal of Industrial and Engineering Chemistry*, *98*, 103–129. https://doi.org/10.1016/j.jiec.2021.03.030

[26] Wind, J. D., Paul, D. R., & Koros, W. J. (2004). Natural gas permeation in polyimide membranes. *Journal of Membrane Science*, *228*(2), 227–236. https://doi.org/10.1016/j.memsci.2003.10.011

[27] Robeson, L. M. (2008). The upper bound revisited. *Journal of Membrane Science*, *320*(1–2), 390–400. https://doi.org/10.1016/j.memsci.2008.04.030

[28] Introduction to adsorption. (2019). In *Elsevier eBooks*. https://doi.org/10.1016/c2018-0-00297-2

[29] Skarstrom, C. W. U.S. Patent 2,944,627, 1960

[30] Sircar, S. Adsorption 2000, 6 , 359.

[31] Quaranta, I. C. C., Pinheiro, L. S., Gonçalves, D. V., Peixoto, H. R., & Lucena, S. M. P. (2021). Multiscale design of a pressure swing adsorption process for natural gas purification. *Adsorption*, *27*(7), 1055–1066. https://doi.org/10.1007/s10450-021-00330-y

[32] Zheng, Y., Li, Q., Yuan, C., Tao, Q., Zhao, Y., Zhang, G., & Liu, J. (2019). Influence of temperature on adsorption selectivity: Coal-based activated carbon for CH4 enrichment from coal mine methane. Powder Technology, 347, 42–49. https://doi.org/10.1016/j.powtec.2019.02.042

[33] Dubbeldam, D., Calero, S., & Vlugt, T. J. (2018). iRASPA: GPU-accelerated visualization software for materials scientists. Molecular Simulation, 44(8), 653–676. https://doi.org/10.1080/08927022.2018.1426855

[34] Wu, C. W., Vemula, R. R., Kothare, M. V., & Sircar, S. (2016). Experimental Study of a Novel Rapid Pressure-Swing Adsorption Based Medical Oxygen Concentrator: Effect of the Adsorbent Selectivity of N2 over O2. *Industrial & Engineering Chemistry Research*, *55*(16), 4676–4681. https://doi.org/10.1021/acs.iecr.5b04570

[35] Fu, Y., Liu, Y., Yang, X., Li, Z., Jiang, L., Zhang, C., Wang, H., & Yang, R. T. (2019). Thermodynamic analysis of molecular simulations of N2 and O2 adsorption on zeolites under plateau special conditions. *Applied Surface Science*, *480*, 868–875. https://doi.org/10.1016/j.apsusc.2019.03.011

[36] Santos, J. C., Magalhães, F. D., & Mendes, A. (2008). Contamination of zeolites used in oxygen production by PSA: Effects of water and carbon dioxide. Industrial & Engineering Chemistry Research, 47(16), 6197–6203. https://doi.org/10.1021/ie800024c

[37] Ahn, H., Lee, C. H., Seo, B., Yang, J., & Baek, K. (1999). Backfill Cycle of a Layered Bed H2 PSA Process. *Adsorption*, *5*(4), 419–433. https://doi.org/10.1023/a:1008973118852

[38] Mehrotra, A., Ebner, A. D., & Ritter, J. A. (2011). Simplified graphical approach for complex PSA cycle scheduling. *Adsorption*, *17*(2), 337–345. https://doi.org/10.1007/s10450-011-9326-6

[39] Yuan, P., Qiu, Z., & Liu, J. (2017). Recent enlightening strategies for co2capture: a review. *International Symposium on Resource Exploration and Environmental Science*, *64*, 012046. https://doi.org/10.1088/1755-1315/64/1/012046

[40] Ferreira, D., Da Silva Bárcia, P., Whitley, R. D., & Mendes, A. (2015). Single-Stage Vacuum Pressure Swing Adsorption for Producing High-Purity Oxygen from Air. *Industrial & Engineering Chemistry Research*, *54*(39), 9591–9604. https://doi.org/10.1021/acs.iecr.5b02151

[41] Zhu, X., Sun, Y., Zhou, S., Feng, F., Liu, J., Ma, J., Li, S., & Niu, Z. (2023). Comparative performance of industrial-scale oxygen production by pressure swing adsorption and vacuum pressure swing adsorption under plateau environment. *Adsorption*. https://doi.org/10.1007/s10450-023-00391-1

[42] Zhang, R., Shen, Y., Tang, Z., Li, W., & Zhang, D. (2022). A review of numerical research on the pressure swing adsorption process. *Processes*, *10*(5), 812. https://doi.org/10.3390/pr10050812

[43] Zhou, L., Qu, Z., Chen, L., & Tao, W. (2015). Lattice Boltzmann simulation of gas–solid adsorption processes at pore scale level. *Journal of Computational Physics*, *300*, 800–813. https://doi.org/10.1016/j.jcp.2015.08.014

[44] Myers, T., Font, F., & Hennessy, M. G. (2020). Mathematical modelling of carbon capture in a packed column by adsorption. *Applied Energy*, *278*, 115565. https://doi.org/10.1016/j.apenergy.2020.115565

[45] Ma, Q., Chen, Z., & Liu, H. (2017). Multiple-relaxation-time lattice Boltzmann simulation for flow, mass transfer, and adsorption in porous media. *Physical Review*, *96*(1). https://doi.org/10.1103/physreve.96.013313

[46] Li, Z., Liu, Y., Wang, H., Tsai, C., Yang, X., Xing, Y., Zhang, C., Xiao, P., & Webley, P. A. (2018). A numerical modelling study of SO2 adsorption on activated carbons with new rate equations. *Chemical Engineering Journal*, *353*, 858–866. https://doi.org/10.1016/j.cej.2018.07.119

[47] Ali, A., Othman, M. R., & Helwani, Z. (2021). Evaluation of thermal effects on carbon dioxide breakthrough curve for biogas upgrading using pressure swing adsorption. *Energy Conversion and Management*, *247*, 114752. https://doi.org/10.1016/j.enconman.2021.114752

[48] Zhang, R., Shen, Y., Tang, Z., Li, W., & Zhang, D. (2022b). A review of numerical research on the pressure swing adsorption process. *Processes*, *10*(5), 812. https://doi.org/10.3390/pr10050812

[49] Šulc, R., & Ditl, P. (2021). A technical and economic evaluation of two different oxygen sources for a small oxy-combustion unit. *Journal of Cleaner Production*, *309*, 127427. https://doi.org/10.1016/j.jclepro.2021.127427

[50] Bancroft, M. L., Du Moulin, G. C., & Hedley-Whyte, J. (1980). Hazards of hospital bulk oxygen delivery systems. *Anesthesiology*, *52*(6), 504–510. https://doi.org/10.1097/00000542-198006000-00010

[51] Love-Jones, S., & Magee, P. (2007). Medical gases, their storage and delivery. *Anaesthesia & Intensive Care Medicine*, *8*(1), 2–6. https://doi.org/10.1053/j.mpaic.2006.10.006

[52] Nikhil, S., & Sharma, N. (2023). Medical oxygen: Sources and regulatory guidelines. *Pharmaspire*, *15*(03), 189–196. https://doi.org/10.56933/pharmaspire.2023.15130

[53] Peterson, T. J., & Weisend, J. G., II. (2019). *Cryogenic safety: A Guide to Best Practice in the Lab and Workplace*. Springer.

[54] Sharma, S., Balestra, S. R. G., Baur, R., Agarwal, U., Zuidema, E., Rigutto, M. S., Calero, S., Vlugt, T. J. H., & Dubbeldam, D. (2023). RUPTURA: simulation code for breakthrough, ideal adsorption solution theory computations, and fitting of isotherm models. *Molecular Simulation*, *49*(9), 893–953. https://doi.org/10.1080/08927022.2023.2202757

[55] Centraal Bureau voor de Statistiek. (n.d.). *Inflatie*. Centraal Bureau Voor De Statistiek.

https://www.cbs.nl/nl-nl/onze-diensten/leren-met-het-cbs/evenementen/te-voorspellen-

indicatoren/inflatie

[56] Centraal Bureau voor de Statistiek. (n.d.-a). *Aardgas en elektriciteit*. Centraal Bureau Voor

De Statistiek. https://www.cbs.nl/nl-nl/dossier/energieprijzen/aardgas-en-elektriciteit

[57] *US Producer price Index: Industrial Gas Manufacturing: Oxygen yearly analysis: Producer

price Index | YCharts*. (n.d.). YCharts.

https://ycharts.com/indicators/us_producer_price_index_industrial_gas_manufacturing_oxyge

n_yearly